Spring 2012

Development and application of a mechanistic model to predict juvenile salmon swim paths

Antonio Arenas Amado
University of Iowa

DEVELOPMENT AND APPLICATION OF A MECHANISTIC MODEL TO PREDICT JUVENILE SALMON SWIM PATHS

by

Antonio Arenas Amado

An Abstract

Of a thesis submitted in partial fulfillment
of the requirements for the Doctor of
Philosophy degree in Civil and Environmental Engineering
in the Graduate College of
The University of Iowa

May 2012

Thesis Supervisors: Adjunct Associate Professor Marcela Politano
Professor Larry Weber

ABSTRACT

Utility companies and regulatory agencies are interested in understanding juvenile salmon swimming patterns as they approach hydropower dams because it can allow them to assess fish bypass efficiency and conduct fish survival studies. A model capable of predicting juvenile salmon swim paths can assist in the design of fish bypasses and diversion structures.

This thesis presents a mechanistic model tailored to simulate swimming patterns of juvenile salmon swimming in forebays, tailraces, and free-flowing rivers. The model integrates information on juvenile salmon behavior at both field and laboratory scale and literature on juvenile salmon swimming capabilities.

Simulated fish swim paths are determined by solving Newton's Second Law. Most of the model parameters are represented by probability distributions. Behavioral responses are triggered for the most part by the flow acceleration and pressure. The model uses conditional probability distributions of thrust magnitude and direction, given flow acceleration. Simulated fish select a swimming direction referenced to the flow velocity vector. To consider juvenile salmon's tendency to coast with the flow, the model intersperses periods of active swimming and gliding.

Chinook salmon measured swim paths were analyzed. The flow variables at the fish locations were obtained from CFD simulations. Juvenile salmon mean thrust was determined from solving Newton's Second Law at every measured location. Results show that as flow acceleration increases, the juvenile salmon average thrust increases and the probability of gliding decreases. Chinook salmon tend to migrate tail-first as flow acceleration increases. For the flow accelerations of $5x10^{-4}$ m/s^2 and $1x10^{-2}$ m/s^2, approximately 85% and 95% of the analyzed fish migrated tail-first, respectively.

The model capacity to predict fish migration route selection, fish-like trajectories, and residence times was tested at two hydropower dams. On average, migration routes were predicted with 17 percent of relative error. Model predictions for fish average residence times were within 10 percent of measured values.

Abstract Approved: _____
Thesis Supervisor

_____
Title and Department

_____
Date

_____
Thesis Supervisor

_____
Title and Department

_____
Date

DEVELOPMENT AND APPLICATION OF A MECHANISTIC MODEL TO PREDICT JUVENILE SALMON SWIM PATHS

by

Antonio Arenas Amado

A thesis submitted in partial fulfillment
of the requirements for the Doctor of
Philosophy degree in Civil and Environmental Engineering
in the Graduate College of
The University of Iowa

May 2012

Thesis Supervisors: Adjunct Associate Professor Marcela Politano
Professor Larry Weber

Graduate College
The University of Iowa
Iowa City, Iowa

CERTIFICATE OF APPROVAL

_____

PH.D. THESIS

_____

This is to certify that the Ph.D. thesis of

Antonio Arenas Amado

has been approved by the Examining Committee
for the thesis requirement for the Doctor of Philosophy
degree in Civil and Environmental Engineering at the May 2012 graduation.

Thesis Committee: _____
Marcela Politano, Thesis Supervisor

_____
Larry Weber, Thesis Supervisor

_____
William Eichinger

_____
Pablo Carrica

_____
George Constantinescu

ACKNOWLEDGMENTS

First and foremost, I would like to express my deepest gratitude to my supervisors Drs. Marcela Politano and Larry Weber. This dissertation could not have been done without their encouragement and support. One simply could not wish for better and more supportive supervisors.

Drs. Alejandro Castro and Pablo Carrica made valuable suggestions to improve this dissertation. Their help is greatly appreciated. Dr. Eva Enders also deserves a big thank you for her willingness to share with me the findings of her research and knowledge.

I am also indebted to my wife Laura and my daughter Isabella who tolerated my long hours at the lab.

TABLE OF CONTENTS

LIST OF TABLES

LIST OF FIGURES

CHAPTER I

INTRODUCTION

1.1 Background and Motivation

The economy of every nation is deeply intertwined with the availability of energy. Depletion of fossil fuel energy sources, geopolitical reasons, and growing concerns about the effect of fossil fuels on the environment have led many countries around the world to aggressively promote the use of renewable energies. The most important renewable energy sources are biomass, geothermal, hydropower, solar, and wind (Yuksel 2010).

Many countries that are members of the Organisation for Economic Co-operation and Development (OECD) have developed most of the economically feasible hydroelectric projects. Wind is expected to have the biggest share of growth of renewable energy in OECD countries whereas in non-OECD countries hydropower will play that role (EIA 2010). The International Energy Agency projects, by the year 2035, hydropower to generate 50.6% and 79.7% of the renewable electricity in OECD and non-OECD countries, respectively.

According to the U.S. Department of Energy (DOE), water power is the largest source of domestic renewable energy in the United States and in the year 2009 hydropower covered almost 7% of the U.S. electricity demand.

Hydropower electricity generation does not release carbon dioxide to the atmosphere and therefore it is considered a cleaner energy source than fossil fuels. Hydroelectricity constitutes a reliable source of energy, which is not always the case with wind and solar. In addition, hydropower facilities can assist in flood mitigation, facilitate navigation, and increase reliability of water supply.

In spite of its many advantages, hydropower is not free of negative impacts on the environment. Throughout history, human action has significantly modified freshwater

ecosystems and the construction of dams is arguably one of the greatest modifications (Williams 2008). Dams may block historic fish migration pathways and alter flow conditions, which could delay and/or hinder fish migration. Many countries have written legislation intended to mitigate the impact of dams on fish migration due to dams (e.g. Endangered Species Act (United States), EU Water Framework Directive (European Union) and Species at Risk Act (Canada)).

Downstream migrating fish can move past a dam through the spillway or turbines. These migration routes can potentially expose fish to mechanical injury and/or high levels of total dissolved gas (TDG). Some hydroelectric facilities have built fish bypass systems to provide an alternative route. The efficiency rate of these systems varies considerably from one project to the other. The interaction between hydraulic and biological variables dictates the effectiveness of a fish bypass design.

The temperature of the water impounded in the reservoir upstream of a dam does not follow the seasonal temperature cycle present before building the dam. As this water flows into the river, it can result in unnatural temperature conditions that have the potential of disrupting the life-cycle of aquatic creatures.

A natural free-flowing river carries sediments with it. A dam can block almost entirely the flow of sediments creating a sediment imbalance in the river downstream, which is likely to lead to erosion of downstream riverbanks. Dissolved oxygen (DO) content in the river is a key water quality indicator. Reservoirs are prone to decreasing water DO amounts making it potentially unfit to drink and unable to sustain aquatic life.

Another important environmental impact of dams is the gas supersaturation downstream of spillways. The air entrained by spillway releases can be forced into solution when transported to deeper regions, elevating the levels of TDG downstream of dams. High levels of TDG are detrimental to fish life and can induce the phenomenon known as gas bubble disease (GBD), which is the creation of gas bubbles in body cavities of fish.

1.2 Goals and Objectives

Utility companies and regulatory agencies have great interest in knowing fish behavior as they approach hydropower dams because it allows them to assess fish bypass efficiency and conduct fish survival studies. A juvenile salmon swimming behavior model can assist in the design of fish bypasses and diversion structures. Juvenile salmon exposure to TDG downstream of dams is highly dependent on the fish swim path. A juvenile salmon swimming behavior model could also help in estimating fish TDG exposure.

The main goals of this thesis are to:

1) Develop a mechanistic model to simulate swimming patterns of downstream migrating juvenile salmon. The model is based on observed juvenile salmon behavior at field and laboratory scale. Model parameters are represented by probability distributions.

2) Determine fish swimming thrust through a comprehensive analysis of Chinook salmon measured trajectories at a hydropower forebay and CFD data.

3) Reproduce laboratory studies on juvenile salmon behavior, through CFD simulations, to determine the flow acceleration that elicits avoidance behavior in juvenile salmon.

4) Apply the model at two hydropower dams to test the model ability to predict fish migration paths, fish-like trajectories, and residence times.

Figure 1.1 shows a conceptual model of the work presented in this thesis. This figure presents the interconnection between the four objectives stated above.

Literature reports two types of individual based models used to simulate fish swimming patterns. The dynamic models predict fish swimming trajectories by analyzing the forces acting on the fish. The kinematic models do not apply Newton's Second Law to study fish movement; they add a model parameter to the flow velocity to determine the fish trajectory. An approach that does not consider forces and imposes the fish velocity could lead to unphysical results. Dynamic models have been applied to geometries with small (~ 10 m) length scales (e.g. Haefner and Bowen 2002, Matuda and Sannomiya

1980, Matuda and Sannomiya 1985, and Sannomiya and Matuda 1987). Kinematic models have been applied at river and hydroelectric facility scales (e.g. Scheibe and Marshall 2002 and Goodwin et al. 2006). This thesis presents the first dynamic model tailored to simulate swimming patterns of juvenile salmon at hydroelectric facilities scale.

Some fish behavior models (e.g. Scheibe and Marshall 2002 and Goodwin et al. 2006) are based on particle tracking algorithms that use, as input data, the flow and water quality data obtained with separate CFD models. This decoupled approach may hinder studies on juvenile salmon movements under unsteady flow conditions, as the data management requirements of unsteady CFD models may be prohibitive. The model developed in this thesis is implemented on the same platform as the hydrodynamics model.

Hydroacoustic and radiotelemetry techniques have been extensively used to better understand juvenile salmon behavior and determine migration routes and times. CFD simulations are used at hydroelectric facilities to study a broad range of applications. The combination of CFD and hydroacoustic telemetry provides the means for evaluating juvenile salmon responses to hydrodynamic conditions.

To date, studies on juvenile salmon measured trajectories and CFD data have focused on the relative velocity of fish with respect to water and on determining flow variables thresholds that could aid in the design of fish passage structures (e.g. Johnson et al. 2009 and Johnson et al. 2000). An objective of this thesis is to perform a comprehensive analysis of measured juvenile salmon trajectories and CFD data through Newton's Second Law. The thrust force that juvenile salmon generated to swim is one of the outcomes of this analysis.

Two different individuals of the same species, age, and size could react differently when exposed to the same flow conditions. A way to simulate different fish responses to the same stimulus is to build a fish swimming behavior model based on probability distributions instead of single-valued parameters. Based on the analysis of juvenile

salmon trajectories and CFD data, this thesis aims at developing probability distributions that describe juvenile salmon swimming thrust and direction as a function of the flow field variables. To the best knowledge of the author, a study that determines juvenile salmon swimming thrust and direction probability distributions from measured trajectories has not been performed at hydroelectric project scale.

Laboratory studies determined juvenile salmon maximum swimming thrust force by forcing fish to swim against the water current (Tang and Wardle 1992). That thrust is not likely to be regularly used by fish when migrating downstream. The analysis of juvenile salmon trajectories and CFD data of this thesis offers insight into natural swimming tendencies and thrust production of juvenile salmon.

The lateral line system allows fish to detect the motion of the water surrounding them and thus plays an important role in orientation and obstacle, prey, and predator detection. Studies have demonstrated that the fish lateral line is capable of detecting flow acceleration, relative velocity, and pressure gradients (Denton and Gray 1983, Denton and Gray 1988, Denton and Gray 1989, and van Netten 2006). Laboratory studies investigated the response of juvenile salmon to rapidly accelerating flows (Enders et al. 2009, Kemp et al. 2006, and Haro et al. 1998). These studies did not report values of instantaneous flow acceleration that elicited avoidance behavior in juvenile salmon. By building CFD models of the aforementioned laboratory studies, this thesis attempts to establish the values of flow acceleration that trigger avoidance behavior in juvenile salmon.

1.3 Contribution of this Thesis

The main contribution of this thesis is twofold: 1) It develops the first mechanistic model of juvenile salmon swimming patterns based on the fish swimming thrust. Fish behavior and swimming capacity are represented through probability distributions. 2) It introduces a methodology to study juvenile salmon behavior through analyses of

measured swim paths and CFD data. Probability distributions are generated to represent the relation between fish swimming variables (e.g. thrust) and the flow field instead of looking for single-value thresholds of hydrodynamic variables that trigger fish behavioral responses.

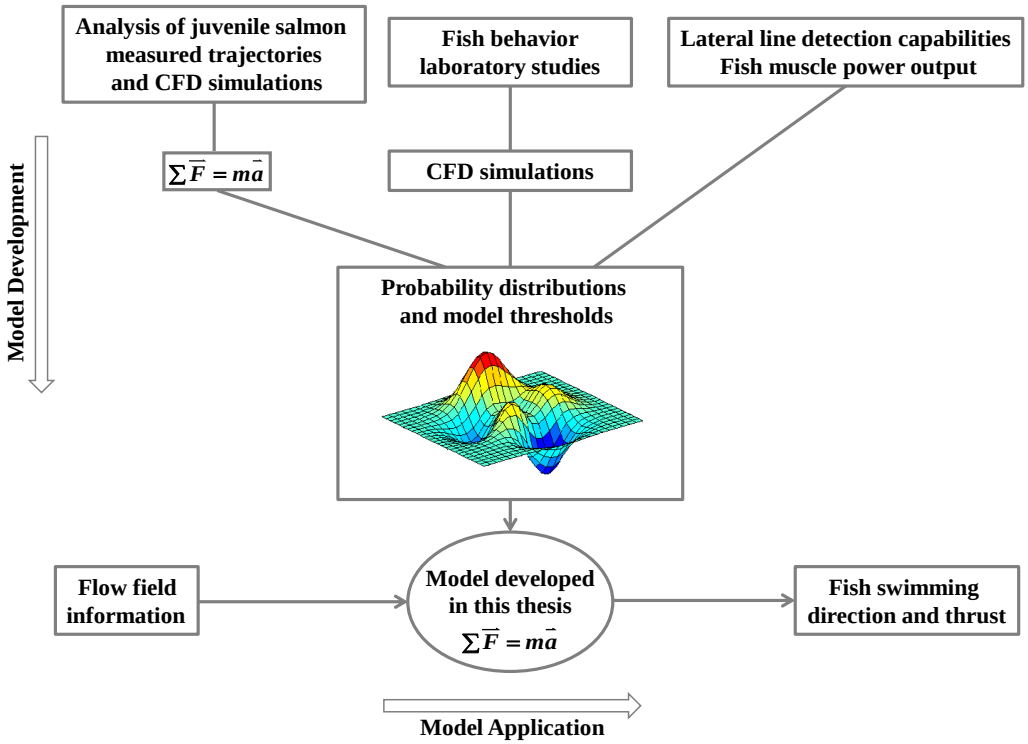

Figure 1.1 Conceptual model.

1.4 Thesis Overview

The outline of this thesis is at follows. After stating the objectives and the contributions of this thesis, chapter I provides a review of field, laboratory, and theoretical studies related to juvenile salmon migration and swimming behavior. Chapter II describes the formulation and mathematical expressions of the model developed in this thesis. Chapter III presents the results of CFD simulations at two hydropower dams. A

comprehensive analysis of Chinook trajectories measured at a hydropower forebay is presented in chapter IV. The linkage between the results discussed in Chapter IV and model parameters is presented in Chapter V. Chapter VI discusses the results of applying the model developed in this thesis to simulate swim paths of juvenile salmon at two hydropower dams. Chapter VII summarizes the main findings of this thesis and offers recommendations for future work.

1.5 Literature Review

1.5.1 Fish Lateral Line System

Most aquatic organisms are able to perceive and analyze the pressure and velocity fields of the surrounding water using a unique sensory system called the lateral line system (Sichert et al. 2010). The lateral line, like the inner ear, is part of the acoustico-lateralis system.

Fish use the lateral line in a variety of activities namely, schooling, prey detection, courtship, spawning, rheotaxis, and obstacle detection (Coombs and van Netten 2005). The lateral line is divided into two main submodalities, superficial neuromasts placed on the surface of the skin and canal neuromasts, which are underneath the skin (Montgomery et al. 1995). Both types of neuromast include a group of hair cells embedded within the epithelium. Kinocilia from these cells extend into a gelatinous matrix that forms the cupula of the neuromast (McHenry et al. 2008). The cupula is believed to be driven by viscous forces and therefore superficial neuromasts are deemed to act as relative velocity detectors and better at processing low-frequency or slow events (Coombs and van Netten 2005, Montogomery et al. 2000). Studies (e.g. Montgomery et al. 1997) found that superficial neuromasts are linked to rheotactic behavior too.

Lateral line canals are usually distributed along the fish trunk, above and below the eye, across the top of the head, and along the edge of the pre-opercle and lower jaw. In most species, canal neuromasts are connected to the flow via canal pores. Nearly

equally spaced neuromasts are located between the pores (Coombs and van Netten 2005). Denton and Gray (1983), Denton and Gray (1988), and Denton and Gray (1989) measured and modeled the flow field within the lateral line canal and arrived at the conclusion that the flow velocity within the canal is proportional to the acceleration of the adjacent medium. Canal neuromasts are better at detecting high-frequency rapidly-changing events (Coombs and van Netten 2005).

van Netten (2006) estimated the lateral line canal hydrodynamic detection thresholds. Values of 1-10 μm/s, 0.1-1.0 mm/s^2, and 0.1-1.0 mPa are the thresholds for relative velocity, fluid acceleration, and pressure difference, respectively. These thresholds were calculated by solving the force balance equation on the neuromast cupula. Forces considered were stiffness force and forces caused by the fluid. The stiffness force was assumed proportional to the neuromast cupula displacement. Fluid forces were estimated assuming that the convective acceleration term in the Navier-Stokes equations was negligible (linear fluid). The detection thresholds reported by van Netten (2006) may be affected by the abovementioned simplifications.

1.5.2 Juvenile Salmon Movements Macro Scale Studies

1.5.2.1 Dam Forebays

Dams may block or delay migrations of fish. Seaward migrating fish pass a dam mainly through turbines, spillways or a structure built to help fish migrate downstream (e.g. surface bypass). Mortality is generally higher for fish passing through turbines (Muir et al. 2001). Altering hydraulic conditions upstream of the dam can guide downstream migrating fish towards a desirable passage route. Application of a stimulus (e.g. light, sound, and electric current) can sometimes accomplish the same goal (OTA 1995).

Downstream migrating smolts are prone to occupying the first part of the water column when approaching dams (Dauble et al. 1999, Johnson et al. 2000). Studies on fish

movements measured via telemetry allow one to record swimming tracks when fish are approaching dams. Khan et al. (2011) carried out an investigation intended to enhance smolts downstream passage at Lookout Point Dam. Fish vertical distribution displayed a diel periodicity, spanned the first 20 m of the water column, and was skewed towards the free surface with an average value of 10 m approximately. No species apportionment of the hydroacoustic data was presented but the bulk of fish detected were believed to be Chinook salmon.

At The Dalles Dam, hydroacustic measurements at the powerhouse intakes reported that approximately half of downstream migrants, mainly Chinook, swam at depths of approximately 9 meters with fish swimming deeper during night than day in spring. In summer, that diel pattern was reversed. The same technique was employed to study the sluiceway nearfield fish movements and put forth modifications to enhance sluiceway efficiency at diverting salmonids from turbines intakes. A gradual increment in the approaching velocity (< 1 m/s per meter) and velocities above 3 m/s at the entrance can help in accomplishing this task (Johnson et al. 2006).

Steig and Johnston (2010) presented swimming patterns of migrating sockeye smolts approaching Rocky Reach Dam. Most of the fish (> 90%) were detected swimming on the west and center portion of the river about 300 m upstream of the dam. Fish density plots for the area close to the powerhouse showed the highest concentration of sockeyes at a depth of roughly 10 meters. At Rocky Reach Dam the powerhouse and surface collector are located on the west side of the river. For the days Steig and Johnston (2010) reported fish passages, most of the river flow was passing through the turbines. For these specific conditions, downstream migrating sockeye smolts detected and oriented themselves with the bulk of the river flow at least 300 meters upstream of the dam, which played an important role in the final migration route selection.

Dams build surface collectors or surface bypasses to take advantage of smolts swimming tendencies when approaching dams. Johnson et al. (2000) and Evans et al.

(2008) used radiotelemetry to evaluate performance and efficiency of that type of structures at Lower Granite Dam and Bonneville Dam, respectively. Both studies concluded that upstream from the dam (> 30 m) smolts followed the bulk of the flow, which agrees with the fish horizontal distribution upstream from the Rocky Reach Dam mentioned in Steig and Johnston (2010). The change in hydraulic conditions in the zone immediately upstream (< 10 m) from a surface collector heavily influences the effectiveness of the structure. Telemetry studies found that smolts followed the bulk of the flow and only start swimming against the flow near surface collectors (Faber et al. 2001, Johnson et al. 2000).

At Priest Rapids Dam there are three different paths downstream migrants can select powerhouse, top-spill, and spillway. Timko et al. (2007) carried out an acoustic tag study to assess the passage behavior of salmonids through this dam. Histograms of approach elevation for Chinook, sockeye, and steelhead showed that approximately 60% of migrants swam within the first 13 meters of the water column. Most fish (~75%) used the powerhouse as migration route. Fish 3D tracks observation suggested that fish did not reject the top-spill but rather did not find the hydrodynamic cues associated to it. Of all fish swimming within 15 m from the top-spill, 97% chose that route. This finding highlights the importance of the far field hydrodynamics in migration route selection.

1.5.2.2 Free-flowing River

In contrast to the surface orientation of smolts while approaching dams there are indications that when migrating in free-flowing streams, smolts tend to vertically position themselves close to the river bed (Svendsen et al. 2007). A set of underwater cameras recorded spatial and temporal migratory behavior of wild Atlantic salmon smolts in a sub-Arctic river. The river cross-section was approximately 20 m wide and had a maximum depth of about 1.6 m. Most smolts (73%) swam in the deepest half of the water column and showed a tendency to horizontally locate themselves above the deepest part

of the river where flow velocities ranged 0.8-1.0 m/s (Davidsen et al. 2005). After analyzing four different fish habitat studies, Beecher et al. (2002) reported that juvenile coho salmon showed preference for depths of 76-100 cm.

Tiffan et al. (2009) studied the migratory behavior of Chinook salmon, in the Snake River over a three-year period, by surgically implanting coded radio tags in subyearlings. That study argues that velocity and turbulence are the driving factors behind fish migration. In the free-flowing reach, the percentage of fish migrating faster than the average flow velocity was close to 50%. That number dropped to 3.6% for a river reach located between the free-flowing one and the Lower Granite Dam. After fish spent some time relocating, they resumed downstream migration and 48.5% of the migrants travelled faster than the water velocity in the reach immediately upstream of the dam.

1.5.2.3 Effect of Turbulence

Fish bypass efficiency seems to be affected by highly turbulent conditions. At Bishop's Falls Dam, with highly turbulent conditions, efficiencies fell within the 62-72% range and at other facilities, with close to laminar conditions, they reached 80-87% (Scruton et al. 2007). An investigation on fish guidance efficiency for downstream migrating Atlantic salmon drew the conclusion that the bypass entrance should be turbulence free for bypass efficiency to increase (Scruton et al. 2003). Enders et al. (2003) measured the swimming cost of juvenile Atlantic salmon in turbulent flows using respirometry experiments and found that for the same mean flow velocity the cost of swimming increased 1.3-1.6 times as turbulence increased.

On the other hand, Coutant (1998) argues that fish use turbulent flow cues to locate regions of higher velocity, which in turn speeds migration up and may assist in locating fish bypasses. Both of the findings presented above can be explained by thinking

of a turbulence level threshold beyond which turbulence stops attracting smolts and begins to elicit avoidance behavior.

1.5.3 Juvenile Salmon Fine Scale Behavioral Responses

Studies conducted at the river and dam scale provide an adequate picture of salmonids behavioral responses and migration preferences. However, they do not shed adequate light on how emigrating smolts react to flow changes that occur at a scale comparable to the fish length.

Early studies considered seaward migration of juvenile salmonids as a passive process related to a decrease in swimming ability when transformation from parr to smolt occurs (Thorpe and Morgan 1978, Smith 1982, Flagg et al. 1983). When migrating downstream, salmonids can clearly find energetic savings by associating themselves to accelerating flows. At the same time, swimming in high-velocity flows could increase the risk of predation since reaction capacity is diminished.

Chinook salmon smolts avoid areas with decelerating flows (William and Gessel 1993). This behavior prevents migration delay, being trapped in recirculation zones, and increasing predations risks (Enders et al. 2009). The above statements suggest the existence of a range of flow accelerations preferred by downstream migrants.

Atlantic smolts with fork length (FL) 155-240 mm were given the option of passing over two different weirs. A sharp crested weir and a weir that produced an almost uniform spatial velocity increase of 1 m/s/m (NU-Alden weir). After ten minutes an average of 38.3% of Atlantic salmon smolts passed the NU-Alden weir whereas only 0.7% did so for the sharp-crested weir. After 30 minutes, the percent of fish passed was 64.3% and 16.7% for the NU-Alden weir and the sharp-crested weir, respectively. Smolts tried to escape, using burst swimming, swimming against the flow from velocities above 1 m/s. Velocities above 2 m/s rarely allowed fish to escape (Haro et al. 1998).

Enders et al. (2009) studied Chinook salmon smolts (FL 97 ± 19 mm) to determine the velocity gradient that elicits fish avoidance reaction. The test flume had a wall with an opening at the bottom. When trying to pass through the opening, smolts reacted to velocity gradients in the range of 0.5 to 0.9 cm/s/cm. The paper by Enders et al. (2009) provides the basis to determine the flow conditions juvenile salmon try to avoid. Smolts were given just one passage route and they decided to either pass it or reject it. Studies that present juvenile salmon with more than one migration route help in understanding the process juveniles use to select migration routes.

Kemp et al. (2005) observed fine-scale behavioral responses of salmonid smolts as they encountered accelerating flows. Different species (Chinook, steelhead, coho, and sockeye) of migrants, with different fork lengths ranging 87.8-213.2 mm, chose between two different flumes with different hydraulic conditions. One flume had a structure that constrained its width. Mean linear flow accelerations in the constricted channel are in the range of 1.27-1.84 m/s^2. The percentage of smolts that rejected the flumes after initial entry ranged from 6% to 14% for the unobstructed channel and from 22% to 44% for the constricted channel.

In a laboratory study to analyze the effect of the presence of structures within culverts, on downstream migrating Chinook salmon smolts, Kemp and Williams (2008) found that fish selected the route with less bed roughness and turbulence. Under light conditions, migrants were more prone to avoiding highly heterogeneous hydraulic conditions than under dark conditions. This is an indication of the interplay between visual stimuli and flow conditions when migrants are selecting a route.

Turbidity decreased the capacity of juvenile Atlantic cod to escape from predator attacks. The escape success went down from 73% to 21% for a fast predator attack in highly turbid water (Meager et al. 2006). These findings validate the importance of the visual ability of fish.

1.5.4 Juvenile Salmon Swimming Capacity

Velocity-time endurance curves define activity levels in fish. The muscle fiber, red or white, used to generate propulsive movement could also be used to classify fish activity levels. Blake (1983) identified three basic fish activity levels: sustained, prolonged, and burst. Sustained swimming represents a swimming behavior that can be maintained for a period longer than 200 minutes (Brett 1967). It employs red muscle fibers and metabolism is aerobic. Burst swimming encompasses fish movements with short duration (< 15 s). White muscle fibers function anaerobically and are mainly used during burst swimming. Prolonged swimming can be roughly defined as the intermediate fish activity level between sustained and burst swimming.

A study found that Atlantic salmon parr (FL 4.8-13.1 cm) could hold position for periods of at least 200 minutes at the bottom of an experimental tank against currents ranging 0.53-0.86 m/s. Atlantic salmon smolts (FL 12.4-21.1 cm) were capable of swimming for long periods of time (e.g. > 200 min) against currents up to 1.26 m/s. This indicates that swimming capacity after smoltification is not totally diminished and that downstream migration is not an entirely passive process (Peake and McKinley 1998). Tang and Wardle (1992) reported a maximum sustained swimming speed of 0.54 m/s for a smolt with FL of 15 cm. Smolts maintained a speed of 0.50 m/s for at least 200 minutes according to Virtanen and Forsman (1987). Webb and Brett (1973) reported a maximum sustained swimming speed of 0.38-0.43 m/s for juvenile sockeye salmon (FL 5.3-6.0 cm).

Most of the fish do not swim at a steady pace but rather they tend to swim in cycles of active swimming followed by a gliding phase (Blake 1983, Videler and Weihs 1982). Wu et al. (2007) estimated drag coefficients for koi carps swimming in kick-and-glide mode and found that the drag coefficient for the swimming phase (~ 0.242) was about 4 times greater than the gliding phase one. Kick-and-glide swimming mode yielded energy savings of about 45% when compared with steady swimming at the same mean

speed. Other studies have estimated comparable energy savings for fish swimming in kick-and-glide mode (Weihs 1974, Videler and Weihs 1982).

Hydrodynamic models (e.g. Lighthill 1971 and Yates 1983) can determine the power output and the thrust exerted by a fish while swimming at maximum sustained swimming speed. Many of these models are based on the slender-body theory, which assumes that the pressure force comes from the added mass accelerating sideways during fish body undulatory movement. Forces and moments balance inertial components and pressure components. Filming fish swimming helps in obtaining the parameters needed to calculate thrust and power with the hydrodynamic models.

Fish muscle power output could be measured by extracting muscle fibers from fish and subjecting them to sinusoidal movements that simulate fish swimming activities at different speeds. Altringham and Johnston (1990) built curves of maximum power output vs. tailbeat frequency from studying muscle fibers of bull trout. Fast fibers (white muscle) reached maximum power output (25-35 W/kg) with a tailbeat frequency of 5-7 Hz. A frequency of 2 Hz produced maximum power output (5-8 W/kg) for slow fibers (red muscle). Tang and Wardle (1992) obtained power outputs of 0.0059 W–0.0074 W for a salmon smolt (FL 15 cm) swimming at 0.54 m/s. The output power for the same fish and conditions using 5-8 W/kg power output is 0.007-0.019 W.

Fast starts are sudden accelerations fish use under predator-prey encounters. They are a form of burst swimming. The study of these sudden movements is performed via high-speed video-recording and subcutaneous accelerometery (Domenici and Blake 1997). Escape responses in fish could imply turns that vary from 0 to 180° (Foreman and Eaton 1993). Fast-start performance studies conducted on rainbow trout of different sizes (FL 9.6-38.7 cm) found that maximum accelerations are between 16.0 and 42.1 m/s^2 and have a duration of 65-114 ms (Weihs 1973, Webb 1975, Webb 1976, Webb 1977, Webb 1978).

1.5.5 Fish Behavior Models

Overall, there are two different approaches to model the behavior of fish. Stochastic population models that address population behavior in bulk (e.g. Crittenden 1994, Zabel and Anderson 1997) and individual or agent based models (IBMs), where the trajectories of individual fish are tracked (e.g. Goodwin et al. 2006, Scheibe and Marshall 2002, Goodwin 2004).

The IBMs found in literature could be split into two different broad categories. The dynamic models take into account forces to study fish movements. Dynamic models predict fish swimming trajectory by integrating a force balance differential equation. Forces usually considered are inertia, drag, virtual mass, pressure gradient, and fish thrust. The kinematic models add some parameter representing fish swimming capacity to the fluid velocity to predict fish swimming trajectory. The solution of an algebraic equation produces the fish trajectory. An approach that disregards forces to analyze fish movements offers the advantage of not having to solve a differential equation but could lead to unrealistic fish paths. Particularly, this approach could result in relative velocities that are impossible to obtain with the thrust fish can generate. As the fluid velocity or turbulence level increase the kinematic models are expected to have more trouble predicting physically possible fish movements.

Haefner and Bowen (2002) developed a physical-based model, intended to study fish collection facilities, which moved fish subject to fundamental forces. The fish response to barriers was the main behavioral component. An algorithm kept track of the energy consumed by fish depending on the swimming mode used to avoid obstacles. Swimming thrust was a function of the swimming mode and the energy fish had available. Obstacles were detected assuming a detection distance. Forces acting on fish were drag and thrust.

Matuda and Sannomiya (1980) developed a dynamic a model to investigate fish behavior in relation to fishing gear. The propulsive force accounts for the tendency of the

fish to swim forward. When an individual approached within a given distance from the wall, a repulsive force was active. A random force accounted for behavioral and environment random variations. Similar models were presented in Matuda and Sannomiya (1985) and Sannomiya and Matuda (1987).

Scheibe and Marshall (2002) described a particle-based model of juvenile salmonid movements that did not analyze fundamental forces. The main goal of the model was to determine fish exposure to dissolved gasses. Flow and dissolved gas fields were known prior to running particle simulations. Particles move due to four different processes. 1) Advection represents the movement of fish with flow velocity. The product of the local velocity and the time step yields the particle displacement and direction. 2) Dispersion coefficients in the longitudinal and transverse direction represent fish movements that deviate from the water velocity. 3) A correlated random-walk model represents fish swimming behavior. 4) Fish vertical movements are simulated through a preferred swimming depth model combined with a random variation model. Scheibe and Marshall (2002) did not correlate fish movements with a variable related to the flow velocity derivatives (e.g. acceleration, velocity gradient).

An IBM model is presented in Goodwin et al. (2006). The model forecasts behavior of outmigrating juvenile salmon using CFD to represent the hydrodynamics. Trajectories of individual fish and fish behavior decisions are simulated using a Lagrangian method with fish behavioral rules.

Swimming vector magnitude and direction are determined for each fish every time step. The swimming vector is added to the flow velocity vector. No forces are included in the fish movement analysis. Hydraulic strain, flow velocity magnitude and pressure are the flow variables that elicit fish behavioral response in this model. The strength of the flow stimuli and a probability-based benefit of movement model determine behavioral responses. Fish behaviors included are: follow the flow, swim toward increasing water velocity, swim towards decreasing water velocity or against the

flow vector, and swim toward acclimated depth. The model accounts for the ability of fish to acclimate to some environments. The model presented in Goodwin et al. (2006) uses as input information flow field determined by a separate CFD software and horizontal and vertical distributions of fish as initial condition.

The model has three main drawbacks. First, it does not account for the forces acting on the fish. The algorithm imposes a swimming velocity, which may lead to instantaneous changes in velocity. Any step change in swimming velocity requires an infinite acceleration and thrust, which obviously violates fish thrust generation capacities. Changes in swimming speed should be accomplished by changing the fish thrust. Second, the model assumes that juvenile salmon are constantly swimming. Swimming speeds are between approximately 10 and 2 body lengths per second. Juvenile salmon intersperse periods of active swimming and gliding (Zabel 1994, Brett 1965). By disregarding juvenile salmon tendency to glide with the flow the model may underpredict juvenile salmon migration times and overpredict juvenile salmon endurance capacity. Third, the model describes a particle tracking algorithm that uses as input information the flow field solution obtained with a separate software. This may hinder studies on juvenile salmon movements under unsteady flow conditions.

CHAPTER II

MATHEMATICAL MODEL

This chapter presents the model developed in this thesis to simulate swim paths and residence times of downstream migrating juvenile salmon.

The individual based model presented below was implemented into the ANSYS FLUENT code through User Defined Functions (UDFs). Model results were compared with results from two acoustic tag studies in two hydropower forebays.

2.1 Fish Movement Model

The fish movement model (FMM) proposed in this thesis is tailored to simulate downstream migrating juvenile salmon movements swimming in forebays and tailraces of hydroelectric facilities and free-flowing rivers. The trajectory of individual particles in three-dimensional space represents fish migration paths. FMM is developed and implemented to assess juvenile salmon migration routes at two hydropower forebays. Fish reactions are elicited by the flow field variables and obstacle detection. FMM simulations can be run under steady or unsteady flow conditions. It is not in the scope of this thesis to simulate fish undulatory locomotion. FMM focuses on the resultant thrust exerted by fish. Simulated fish are assumed to have no effect on the fluid (one-way coupling).

2.1.1 FMM Formulation

Simulated fish move subject to fundamental physical forces. The force balance equation on the fish includes a term whose magnitude and direction simulates seaward migrating juvenile salmon swimming capacity and behavior. FMM assumes that fish have two distinct activity levels, sustained mode (SM) and burst mode (BM). Depending on flow field information and fish location, fish switch from one level to the other.

Studies on juvenile salmon show heterogeneity in values of swimming depths, flow accelerations that elicit avoidance behavior and swimming direction changes, and travel times for individuals of the same age and species (i.e. Timko et al. 2007, Enders et al. 2009, Kemp et al. 2006, Johnson et al. 2009). A fish movement model based solely on single-value parameters is not capable of representing such variability. In this study, FMM parameters are defined by probability distributions obtained from measured swim paths and fish laboratory studies.

One of the basic premises of this model is that fish select, most of the time, a swimming direction referenced to the water velocity vector. Swimming direction should be understood as the direction of the fish thrust. This direction could be different from the actual fish displacement as in the case of juvenile salmon moving downstream tail-first. By referencing fish movements to the flow velocity vector, FMM results are independent of the grid orientation.

FMM considers juvenile salmon swimming in kick-and-glide mode instead of constantly. A probability distribution, P_g, is used to determine if fish are gliding. The drag coefficient of a fish actively swimming is about 3-5 times higher than that of one gliding (Wu et al. 2007, Videler and Weihs 1982). FMM includes different expressions for the drag coefficient depending on whether fish are actively swimming or gliding. The time fish actively swim is represented by t_{as}, and the time fish glide by t_g. Both times are model parameters. Fish are unlikely to maintain a constant swimming thrust while actively swimming. FMM assumes that the swimming thrust magnitude changes every τ seconds.

FMM considers two different flow acceleration thresholds. a_d is the minimum value of flow acceleration detected by the fish canal lateral line, and a_b stands for the maximum flow acceleration fish can be exposed to without exhibiting avoidance behavior.

The fish distance from an obstacle is represented by d_{ob}. Fish detect obstacles when $d_{ob} < d_d$ where d_d is the detection distance. d_a represents the distance for which fish consider collision with an obstacle imminent. For $d_a < d_{ob} < d_d$, fish use SM to maintain distance from the obstacle. If $d_{ob} \le d_a$ fish use BM to avoid impact by swimming in a direction perpendicular to the obstacle surface.

Studies at hydropower dams (Timko et al. 2007, Johnson et al. 2006, and Steig and Johnston 2010) and free flowing rivers (Svendsen et al. 2007 and Davidsen et al. 2005) show that juveniles have a clear tendency to occupy different parts of the water column. Fish swimming depth is likely to be selected as a trade-off of many factors like predator avoidance, food availability, temperature distribution, and fish capacity to withstand pressures. Based on observed data, FMM assumes that the part of the water column used by simulated fish is limited. A pressure threshold, P_m, defines that region.

The decision algorithm displayed in Figure 2.1 uses the values of the aforementioned thresholds and the parameters to select a swimming mode (SM or BM) and direction. BM always takes precedence over SM. SM is active when fish are exposed to flow accelerations below a_b and are swimming at distances greater than d_a from obstacles. If the flow acceleration is above a_b or fish distance from an obstacle is smaller than d_a, BM is active.

2.1.2 FMM Mathematical Model

The force balance equation on the fish in Lagrangian reference frame reads:

$$m_f \frac{d\vec{u}_f}{dt} = \overrightarrow{F_D} + \overrightarrow{F}_T + \overrightarrow{F_k} \tag{2.1}$$

where $\vec{u}_f$ and m_f are the fish velocity and mass, respectively. $\overrightarrow{F}_T$ represents the fish thrust force, $\overrightarrow{F_k}$ is the force acting on the fish due to the turbulence field, and $\overrightarrow{F_D}$ is the drag force. The subscript f stands for fish. The vector $\overrightarrow{F}_T$ in Eq. 2.1 is the key

component of FMM. The magnitude and direction of $\overrightarrow{F_T}$ depend on juvenile salmon swimming capacities and behavioral responses.

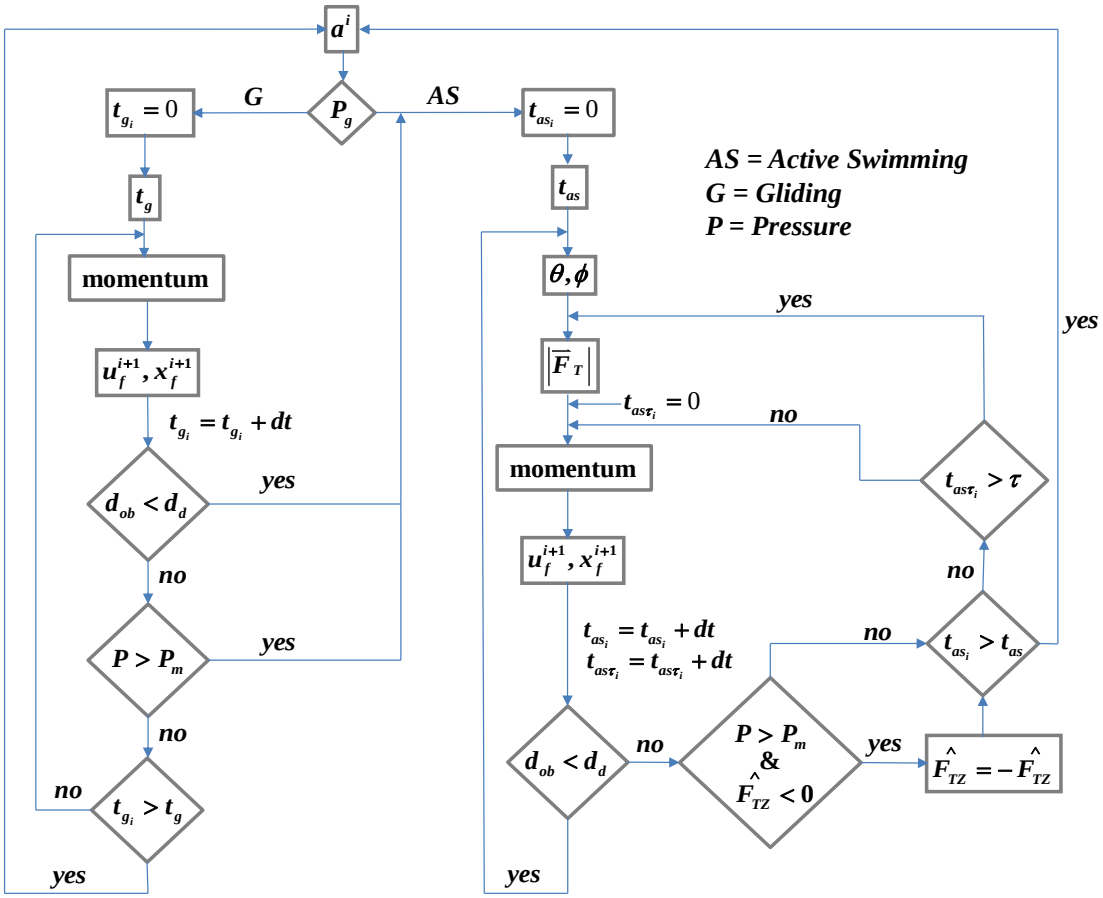

Figure 2.1 FMM flow chart.

The expression to calculate the drag force is:

$$\overrightarrow{F_D} = -0.5\rho|\vec{u}_{rf}|\vec{u}_{rf}AC_{df} \tag{2.2}$$

where $\vec{u}_{rf}$ is the relative velocity of the fish with respect to the fluid phase, A is the reference area, and C_{df} is the fish drag coefficient shown in Eq. 2.3.

Webb et al. (1984) estimated for rainbow trout, of lengths (L) between 5.0 and 56.0 cm, fish thrust power using the Lighthill's small amplitude bulk momentum model.

Fish were forced to swim against a flow current and their movements were recorded to measure kinematic variables. Webb et al. (1984) reported plots of fish Reynolds number $\mathrm{Re}_f = \rho \left|\vec{u}_{rf}\right| L \big/ \mu$ versus drag coefficient. This dissertation uses fitted curves to the plots mentioned above to calculate the drag coefficient of fish actively swimming (see Eq. 2.3a). When fish are gliding, the drag coefficient is calculated with the expression for a fully turbulent flow in a plate presented in Eq. 2.3b. Haider and Levenspiel (1998) obtained the drag coefficient correlation for non-spherical particles, presented in Eq. 2.3c, that is used to calculate the drag coefficient of fish actively swimming for low values of Re_f.

The minimum value of Re_f presented in Webb (1984) is 10^4. Here, Eq. 2.3a is extrapolated up to $\mathrm{Re}_f = 2000$ to avoid discontinuities in the drag force when transitioning from Eq. 2.3a to Eq. 2.3c.

$$C_{df} = \begin{cases} a)\ \dfrac{493.9}{\mathrm{Re}_f^{0.922}} & \text{if } \mathrm{Re}_f > 2000 \text{ and AS=1} \\ b)\ \dfrac{0.072}{\mathrm{Re}_f^{0.2}} & \text{if G (AS=0)} \\ c)\ \dfrac{24}{\mathrm{Re}_{sph}}\left(1 + b_1 \mathrm{Re}_{sph}^{b_2}\right) + \dfrac{b_3 \mathrm{Re}_{sph}}{b_4 + \mathrm{Re}_{sph}} & \text{if } \mathrm{Re}_f \le 2000 \text{ and AS=1} \end{cases} \tag{2.3}$$

In Eq. 2.3 AS stands for active swimming and G for gliding. The Reynolds number of the sphere Re_{sph} is calculated with the diameter of a sphere d_{sph} having the same volume as the fish. Fish are approximated by an ellipsoid to calculate their volume. The coefficients for Eq. 2.3c are:

$$\begin{aligned} b_1 &= \exp(2.3288 - 6.4581\gamma + 2.4486\gamma^2) \\ b_2 &= 0.0964 + 0.5565\gamma \\ b_3 &= \exp(4.905 - 13.8944\gamma + 18.4222\gamma^2 - 10.2599\gamma^3) \\ b_4 &= \exp(1.4681 + 12.2584\gamma - 20.7322\gamma^2 + 15.8855\gamma^3) \end{aligned} \tag{2.4}$$

The shape factor γ is defined as:

$$\gamma = \frac{s}{S_f} \tag{2.5}$$

where s is the surface area of a sphere having the same volume as the fish and S_f is the actual surface area of the fish.

When using Eqs. 2.3a and 2.3b to calculate fish drag coefficient, the reference area in Eq. 2.2 is $A = S_c L^{S_e}$. For salmonids, $S_c = 0.465m$ and $S_e = 2.11$ (Webb 1971). The expression for the reference area in Eq. 2.2 when using Eq. 2.3c takes the form of $A = \pi d_{sph}^2 / 4$.

For a typical juvenile salmon ($L \approx 10$cm) Eq. 2.3a is used for values of $\left|\vec{u}_{rf}\right|$ between 0.02 and 1.00 m/s. Based on Tang and Wardle (1992) the maximum sustained swimming speed for a Juvenile Atlantic salmon ($L \approx 15$cm) is in the order of 0.50 m/s thus Eq. 2.3a is used most of the time in this dissertation to calculate the drag coefficient of fish actively swimming.

2.1.3 Fish Swimming Thrust and Power Magnitude

Altringham and Johnston (1990) measured the power output of fast and slow myotomal muscle of bulltrout. Maximum power output was 25-35 W/kg and 5-8 W/kg for fast fibers (white muscle) and slow fibers (red muscle), respectively. In a study to determine the mean thrust and mean power output for large ($L \approx 45$cm) and small ($L \approx$ 15cm) Atlantic salmon swimming at maximum sustained swimming speeds, Tang and Wardle (1992) reported a power output of 0.125-0.3 W for large salmon and 0.007-0.019 W for small salmon. The same paper calculated a thrust force of about 0.006 N for small salmon swimming at 0.37 m/s, which represents about 68% of the maximum small salmon sustained swimming velocity. Assuming that the thrust force is proportional to $\left|\vec{u}_{rf}\right|^2$, the maximum thrust force a small salmon can generate when swimming in SM is approximately 0.013 N.

White muscle fibers are employed mainly when fish are swimming in BM. According to Blake (1983) white muscle comprises about 90% of fish muscle mass. The maximum power output for Juvenile salmon ($L \approx 15$cm) swimming in BM is in the range 0.315-0.74 W. The maximum thrust force for juvenile salmon swimming in BM is approximately 0.40 N.

Table 2.1 shows the scenarios included in FMM. The thrust force for simulated fish swimming in BM (scenarios S3 and S5) is 0.40 N. For fish trying to avoid obstacles and swimming in SM (scenario S4) the force is 0.013 N. For different conditions, the swimming thrust probability distributions presented in chapter IV are used to calculate $\left|\vec{F}_T\right|$.

Table 2.1 FMM scenarios.

Scenario	Acceleration	Distance from Obstacles	Swimming Mode
S1	$a < a_d$		SM
S2	$a_d < a < a_b$		SM
S3	$a_b < a$		BM
S4		$d_a < d_{ob} < d_d$	SM
S5		$d_{ob} < d_a$	BM

When migrating downstream in forebays, tailraces and free-flowing rivers, the scenarios S1 and S2 include the conditions juvenile salmon are most likely to encounter. The conditions described in scenarios S3-S5 could be found in the vicinity of a spillway gate, turbine intake or other type of hydraulic structure.

2.1.4 Force Caused by the Turbulence Field

In ANSYS FLUENT the default method to account for the effect of the turbulent field on the particle trajectory neglects the mass of the particle. Particles of different masses are displaced, by the turbulent field, the same distance as long as they are subject to the same velocity fluctuation. In order to overcome this limitation an additional force due to the turbulent field is used. The turbulent integral length scale $l = k^{3/2}/\varepsilon$ is, qualitatively, the distance that fluid elements are moved by turbulent eddies (Ni et al. 2003). Considering that the fluctuating component of the velocity can be calculated by $u' = \sqrt{2k/3}$ under isotropic conditions, the expression for the force acting on the fish due to the turbulence field is:

$$\overrightarrow{F_k} = m_f \zeta \frac{\varepsilon}{k^{1/2}} \tag{2.6}$$

where ζ is a random number between -1 and 1. Eq. 2.6 is considered in the force balance equation when l is greater than $L/2$.

2.1.5 Flow Field Information at Fish Location

FMM uses an inverse distance interpolation scheme to obtain the flow variables information at the fish actual location:

$$\beta_f = \sum_{j=0}^{j=6} \frac{\beta_{cj}\omega_j}{\sum_{j=0}^{j=6} \omega_j} \tag{2.7}$$

where β is the variable to be interpolated, the subscript cj represents the cell center of the cell j, $\omega_j = 1/d(f,cj)$, and $d(f,cj)$ is the distance between the fish location and the cell center of the cell j. The algorithm uses the cell occupied by the simulated fish and its six neighboring cells. The use of this interpolation algorithm is not to be interpreted as fish being able to detect flow information at locations fish are not occupying.

2.1.6 Fish Swimming Thrust Direction

The direction of the thrust force $\overrightarrow{F_T}$ is represented by the unit vector $\hat{F}_T$:

$$\hat{F}_T = (\sin\phi\sin\theta, \cos\phi\sin\theta, \cos\theta) = (\hat{F}_{TX}, \hat{F}_{TY}, \hat{F}_{TZ}) \tag{2.8}$$

where the angles θ and ϕ are presented in the Figure 2.2. The normalized projection of the vector $\hat{F}_T$ onto the XY plane is shown in Figure 2.3a.

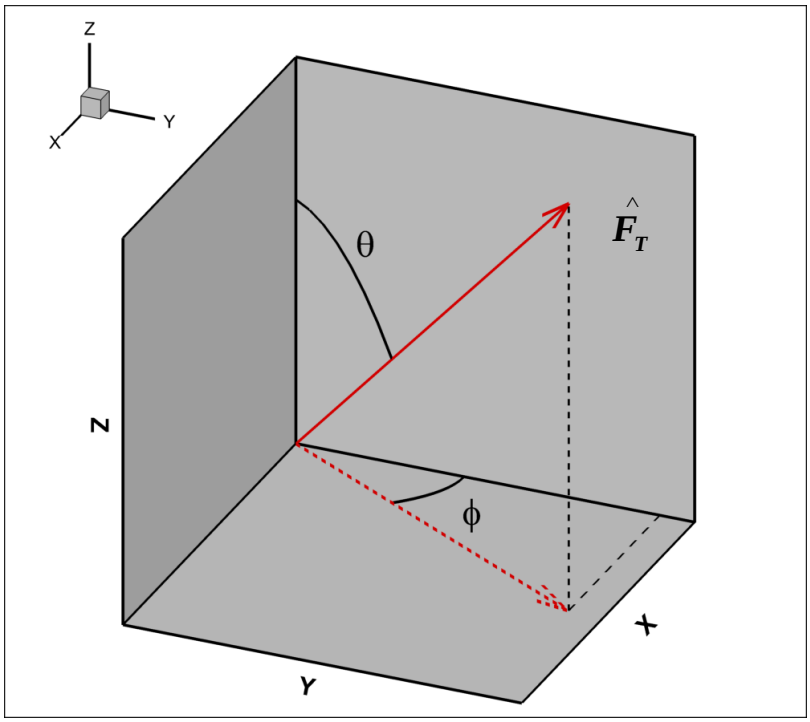

Figure 2.2 Direction of the swimming thrust force.

The direction of the thrust force is calculated using one of the unit vectors described below. The obstacle surface vector $\hat{\eta}_o$, the vector tangent to the fish swimming trajectory $\hat{\xi}$, and the flow velocity vector at the fish location $\hat{u}$. The unit vectors are displayed in Figures 2.3a and 2.3b. The normalized XY projections of the vectors $\hat{\xi}$, and $\hat{u}$ are presented in Fig. 2.3a using the subindex XY. The components of $\hat{u}$ at the fish

location are calculated using Eq. 2.7 with $\beta = u_i$. To determine $\hat{\xi}$ the current and previous fish locations are used. FMM assumes that fish, unless they try to avoid obstacles, orient themselves in the XY plane by defining a rotation angle with respect to the flow velocity vector. Vector rotations are accomplished using a 2D rotation matrix R_α:

$$R_\alpha = \begin{pmatrix} \cos\alpha & -\sin\alpha \\ \sin\alpha & \cos\alpha \end{pmatrix} \tag{2.9}$$

where α is the rotation angle. A standard right-handed coordinate system is used in this study.

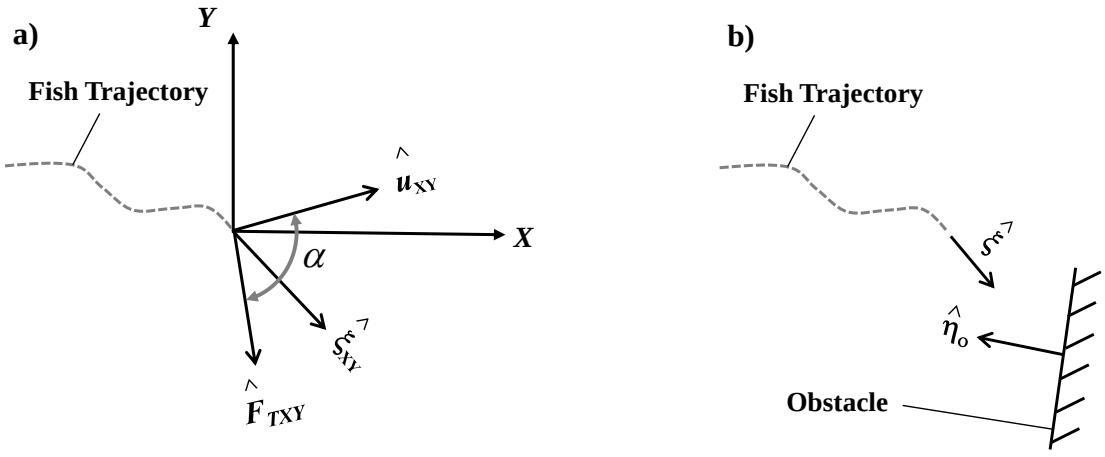

Figure 2.3 Unit vectors used to determine the direction of the thrust force.

FMM uses the probability distributions presented in chapter IV to obtain α and θ for scenarios S1-S3. The direction of the thrust swimming force is given by Eqs 2.10 and 2.11 for scenarios S4 and S5, respectively.

$$\hat{F}_T = \frac{\hat{\eta}_o + \hat{\xi}}{\left|\hat{\eta}_o + \hat{\xi}\right|} \tag{2.10}$$

$$\hat{F}_T = \hat{\eta}_o \tag{2.11}$$

2.1.7 Kick-and-glide mode

Migration is an energy-demanding endeavor. When migrating downstream, juvenile salmon are likely to glide with the current for periods of time looking for energy savings. Swimming movements of fish distort the flow conditions around them. Alternating gliding phases with swimming phases allows fish to better detect the information of their surroundings.

Chapter IV presents an extensive analysis of measured juvenile salmon trajectories together with CFD data. Fig. 2.4 presents an overview of a juvenile salmon swimming trajectory. Results show that fish change swimming direction every 5-300 seconds. FMM uses the probability distributions for P_g, t_{as}, and t_g presented in chapter IV to simulate periods of active swimming and gliding.

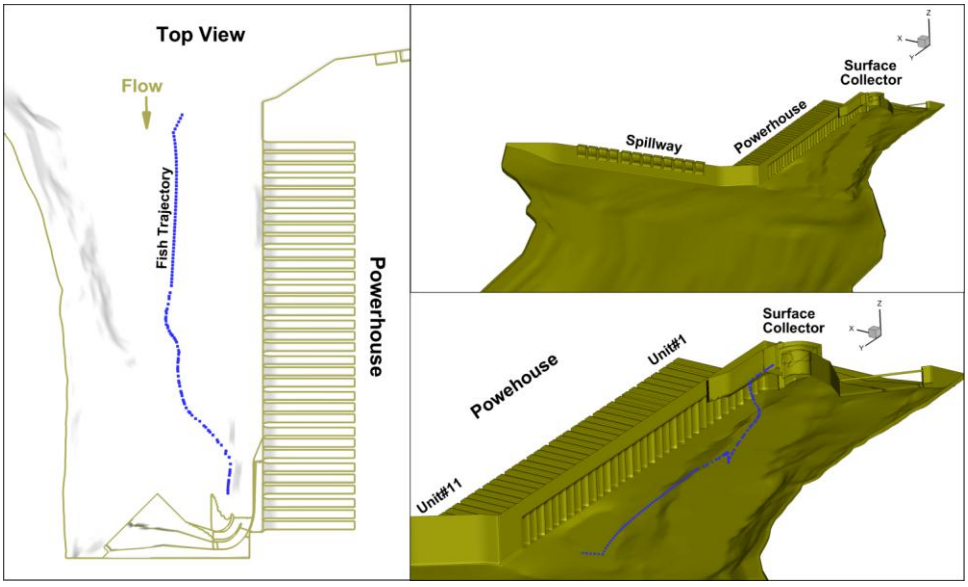

Figure 2.4 CFD model and a juvenile salmon swimming trajectory.

2.1.8 Fish Model Variables

Below the relevant variables of FMM. A list of FMM model parameters is presented in Table 2.2.

a_b	flow acceleration threshold for BM
a_d	minimum flow acceleration detected by the fish lateral line
a	flow acceleration
A	reference area to calculate drag force
C_{df}	fish drag coefficient
d_{ob}	fish distance from an obstacle
d_d	obstacle detection distance
d_a	obstacle avoidance distance
$\overrightarrow{F_T}$	fish swimming thrust force
$\overrightarrow{F_D}$	drag force
$\overrightarrow{F_k}$	force due to turbulence field
$\hat{F}_T$	direction of the thrust force
$\hat{F}_{TX}$	x-component of $\hat{F}_T$
$\hat{F}_{TY}$	y-component of $\hat{F}_T$
$\hat{F}_{TZ}$	z-component of $\hat{F}_T$
L	fish length
m_f	fish mass
P_g	probability of gliding
P	pressure
P_m	pressure threshold
Re_f	fish Reynolds number
R_α	2D rotation matrix
S_c	fish wetted surface area coefficient
S_e	fish wetted surface area exponent

t_{as}	time of active swimming
t_g	time of gliding
τ	time swimming thrust is constant
$\vec{u}_{rf}$	relative velocity of the fish respect to the fluid phase
$\vec{u}_f$	fish velocity
X	grid x axis
Y	grid y axis
$\hat{\xi}$	unit vector tangent to the fish trajectory
$\hat{\eta}_o$	unit vector normal to obstacle surface
α	angle between the fish thrust and flow velocity in the XY plane
θ	swimming inclination from the vertical axis
ϕ	swimming direction in the XY plane
ζ	random number between -1 and 1

Table 2.2 FMM parameters.

Symbol	Meaning	Modeled by
a_d	minimum flow acceleration detected by the fish lateral line	single value
a_b	flow acceleration threshold for BM	probability distribution
d_a	obstacle avoidance distance	single value
d_d	obstacle detection distance	single value
t_{as}	active swimming time	probability distribution
t_g	gliding time	probability distribution
P_g	probability of gliding	probability distribution
P_m	pressure threshold	probability distribution
$\left\|\vec{F}_T\right\|$	magnitude of the fish swimming thrust	probability distribution
α	angle between the fish thrust and flow velocity in the XY plane	probability distribution
θ	swimming inclination from the vertical axis	probability distribution

CHAPTER III

HYDRODYNAMICS

This thesis uses CFD results obtained from modeling two dam forebays under different operational scenarios. The present chapter describes the CFD results. Information from this chapter is used in chapter IV to analyze juvenile salmon measured trajectories. The results of FMM presented in chapter V are also based on the flow fields described below.

3.1 Dam 1 Forebay

Figure 3.1 shows an aerial photo of Dam 1. To provide an alternative route to turbines and spillway for downstream migrants, Dam 1 built a surface collector. Fish entering the surface collector are directed via a conduit to the tailrace. Approximately 161 m^3/s flow into the surface collector and 96.0% of that discharge is pumped back into the forebay and the remaining flow is used to transport fish to the tailrace.

Figure 3.1 Dam 1 aerial photo.

Table 3.1 summarizes the flow conditions used for the CFD simulations. Discharges were obtained by averaging flow values of selected consecutive days in 2004, 2005, and 2010. In this table FB stands for forebay and SC for surface collector. For the cases 2005_S and 2004_S, the spillway was operating with approximately 22.0% of the total river flow. No spillway flow was simulated for 2010_NS.

Table 3.1 Operating conditions.

		2010_NS	2005_S	2004_S
FB Level (m)		215.0	215.0	215.0
Powerhouse Discharge (m^3/s)	Unit 1	340.9	339.9	346.1
	Unit 2	341.0	337.1	335.8
	Unit 3	296.0	293.3	282.5
	Unit 4	293.3	277.2	267.8
	Unit 5	289.9	275.9	232.6
	Unit 6	285.1	207.6	240.3
	Unit 7	266.3	197.0	262.5
	Unit 8	332.5	216.9	216.5
	Unit 9	312.9	182.5	166.3
	Unit 10	284.3	146.7	138.1
	Unit 11	230.7	80.6	77.9
	Total	3272.9	2554.6	2566.4
Spillway Discharge (m^3/s)	Bay 1	0.0	0.0	0.0
	Bay 2	0.0	102.6	96.3
	Bay 3	0.0	0.0	10.2
	Bay 4	0.0	101.7	165.2
	Bay 5	0.0	136.4	66.0
	Bay 6	0.0	168.0	187.0
	Bay 7	0.0	135.3	94.7
	Bay 8	0.0	0.0	181.5
	Bay 9	0.0	0.0	1.6
	Bay 10	0.0	0.0	0.7
	Bay 11	0.0	0.0	0.5
	Bay 12	0.0	0.0	0.0
	Total	0.0	644.1	803.8
SC (m^3/s)	In	161.4	161.4	161.4
	Return	154.9	154.9	154.9
River (m^3/s)		3279.4	3205.2	3376.7

3.1.1 Grids and Numerical Model

Structured meshes of about 10^6 nodes were generated in GRIDGEN 15.15. The grid size for the region close to the surface collector entrance was 0.14 m, 0.19 m, and 0.30 m along the x , y , z axes, respectively. Figure. 3.2 shows an overview of the grid used for the 2005_S simulation. The SIMPLE algorithm was used to couple pressure and velocity. Turbulence closure was achieved with the $k-\varepsilon$ model. After running approximately 60,000 time steps with a fixed time step size of 120 s, statiscally converged solutions were achieved.

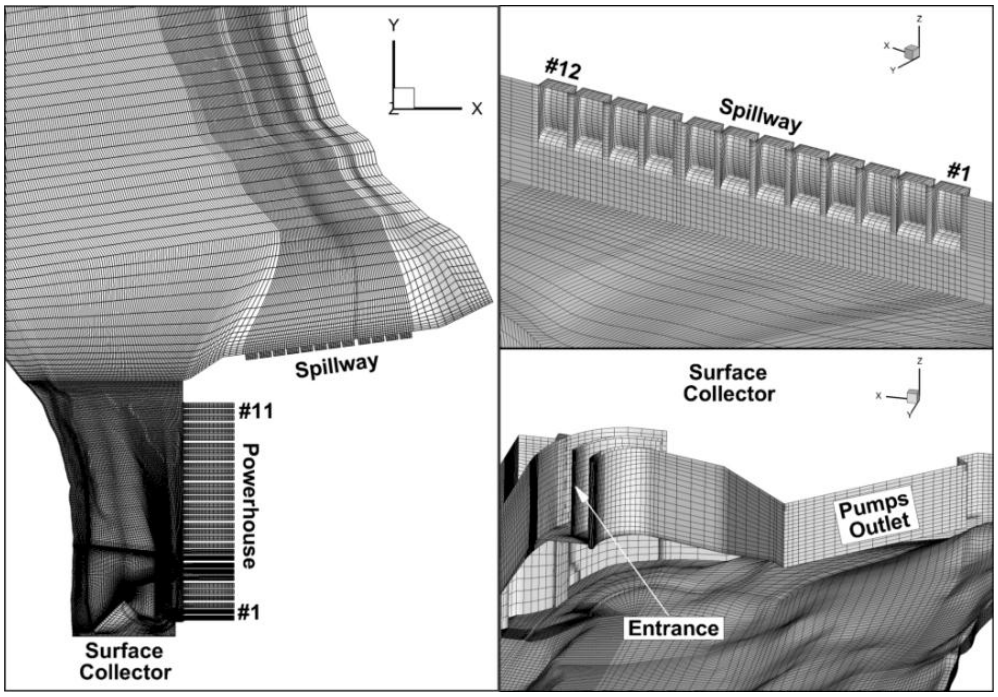

Figure 3.2 Dam 1 forebay grid.

3.1.2 Hydrodynamics

Contours of velocity and streamlines at depths of 16.6 and 5.0 m are presented in Figures 3.3, 3.4, and 3.5 for 2004_S, 2005_S, and 2010_NS, respectively. Consistent

with the flow distributions (see Table 3.1), CFD simulations for the cases 2004_S and 2005_S yielded similar results. The maximum flow velocity was in the order of 3.0 m/s for the region upstream of the open spillway gates. CFD simulations predicted a maximum velocity of about 0.8 m/s at the entrance of the surface collector. Figures 3.3a-3.5a show that inert particles moving at a depth of 16.6 m and at distances from the east bank greater than 156.0, 145.0, and 66.0 m, leave the computational domain through either the powerhouse or the surface collector for the cases 2004_S, 2005_S, and 2010_NS, respectively.

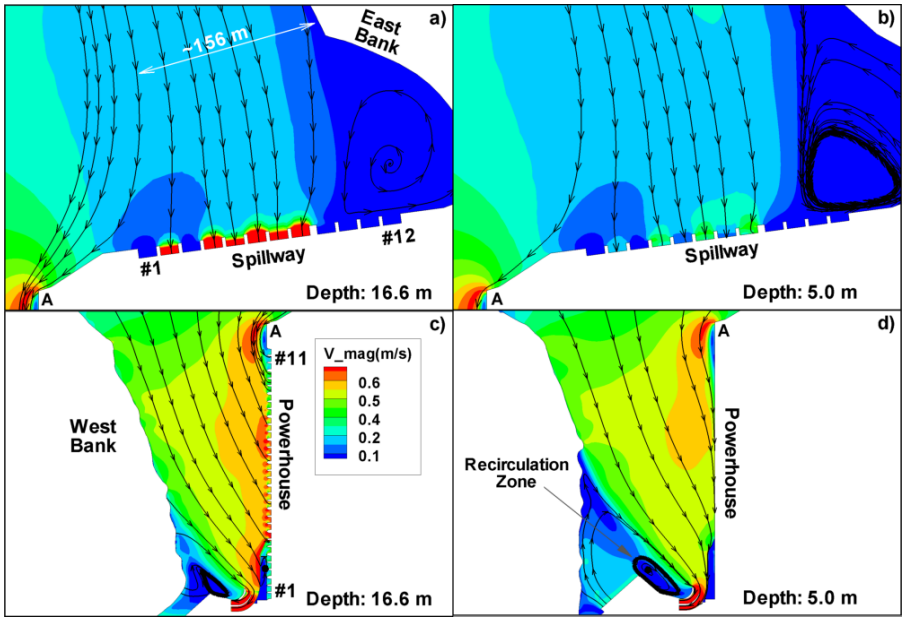

Figure 3.3 Case: 2004_S. Streamlines and velocity contours. Horizontal slices at depths of 16.6 m and 5.0 m. The point A is shown in all the frames to assist in visualization.

A recirculating flow zone was predicted by the simulations for both depths and for all the cases on the east side of the spillway. That flow pattern is depicted in Figures 3.3a-3.5a and 3.3b-3.5b.

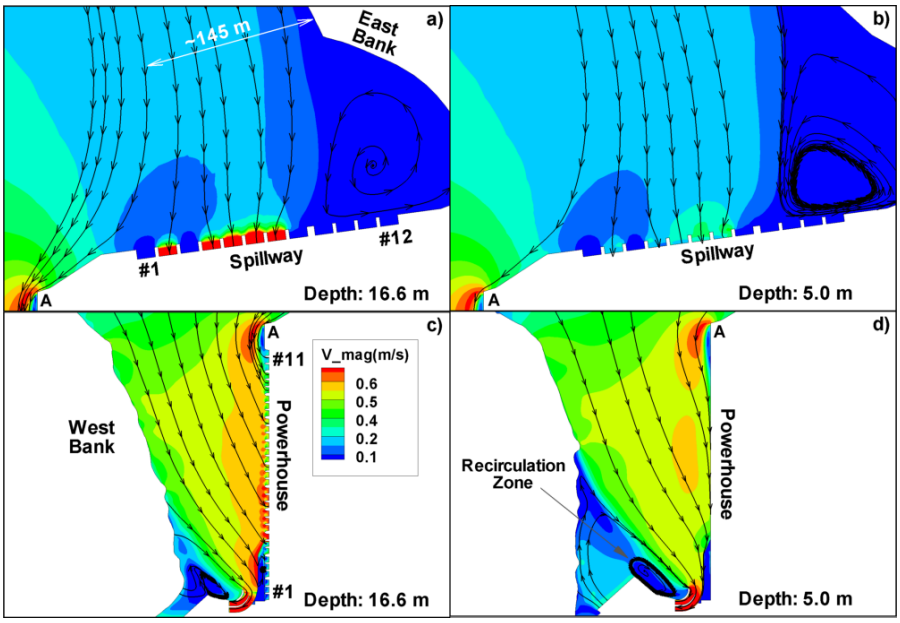

Figure 3.4 Case: 2005_S. Streamlines and velocity contours. Horizontal slices at depths of 16.6 m and 5.0 m. The point A is shown in all the frames to assist in visualization.

Streamlines in Figures 3.3c-3.5c and 3.3d-3.5d are directed mainly towards the turbine units, which is consistent with the flow rates reported in Table 3.1. These figures also show the recirculation zone created by the percent of the water drawn by the surface collector that is pumped back into the forebay.

Figures 3.6-3.8 show contours of flow acceleration for the cases 2004_S, 2005_S, and 2010_NS, respectively. The zone with values of flow acceleration above $a_d = 10^{-4} m/s^2$ extends as far as 232.0, 218.0, and 263.0 m upstream of the dam for the cases 2004_S, 2005_S, and 2010_NS, respectively as displayed by the point B in Figures 3.6a-3.8a. The total river flow for the cases 2004_S, 2005_S, and 2010_NS differed by about 3%, but the powerhouse discharge for the case 2010_NS was approximately 28.0% greater than for the other two cases, which explains why the effect of the powerhouse operation extends further upstream for the case 2010_NS.

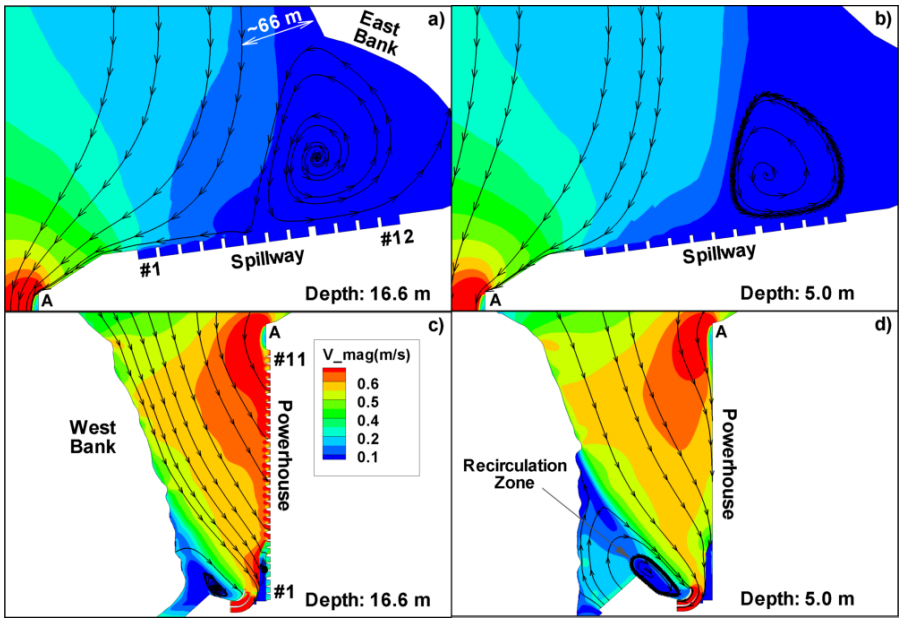

Figure 3.5 Case: 2010_NS. Streamlines and velocity contours. Horizontal slices at depths of 16.6 m and 5.0 m. The point A is shown in all the frames to assist in visualization.

CFD results predicted values of flow acceleration above $a_d = 10^{-4} m/s^2$ for the spillway region as far as 49.0 and 53.0 m upstream of the spillway for the cases 2004_S and 2005_S, respectively as displayed by the point C in Figures 3.6a and 3.7a.

Figures 3.6c-3.8c and 3.6d-3.8d show the acceleration contours for depths of 16.6 and 5.0 m for the region close to the powerhouse. Maximum flow acceleration values at the entrance of the surface collector and at the turbine intakes were about 0.015 and 0.05 m/s^2, respectively. For the simulated forebay elevations, the top of the turbine draft tubes were at a depth of approximately 11.5 m. At a depth of 5.0 m, values of flow acceleration near the turbines were considerably lower than at the entrance of the surface collector as seen in Figures 3.6d-3.8d.

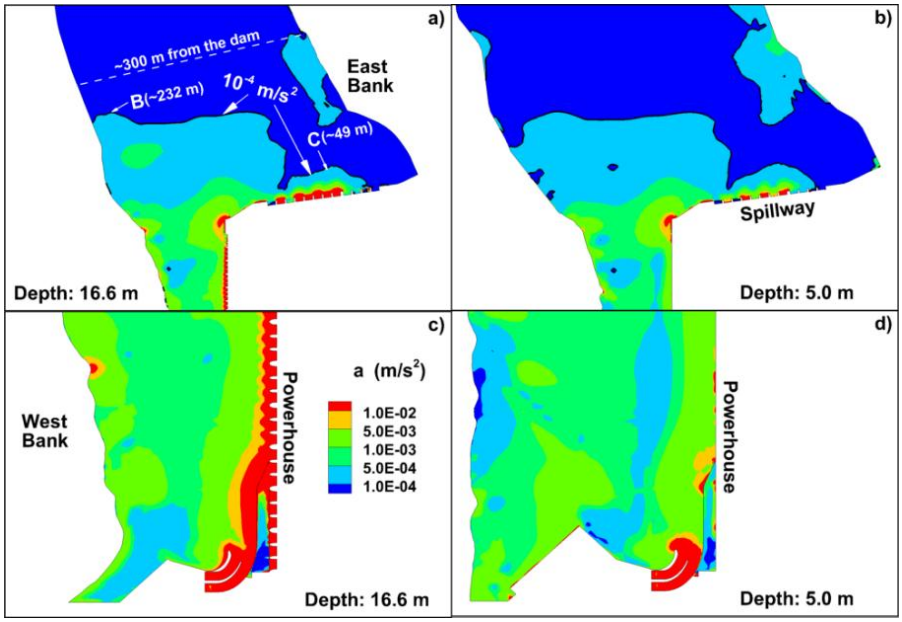

Figure 3.6 Case: 2004_S. Acceleration contours. Horizontal slices at depths of 16.6 m and 5.0 m.

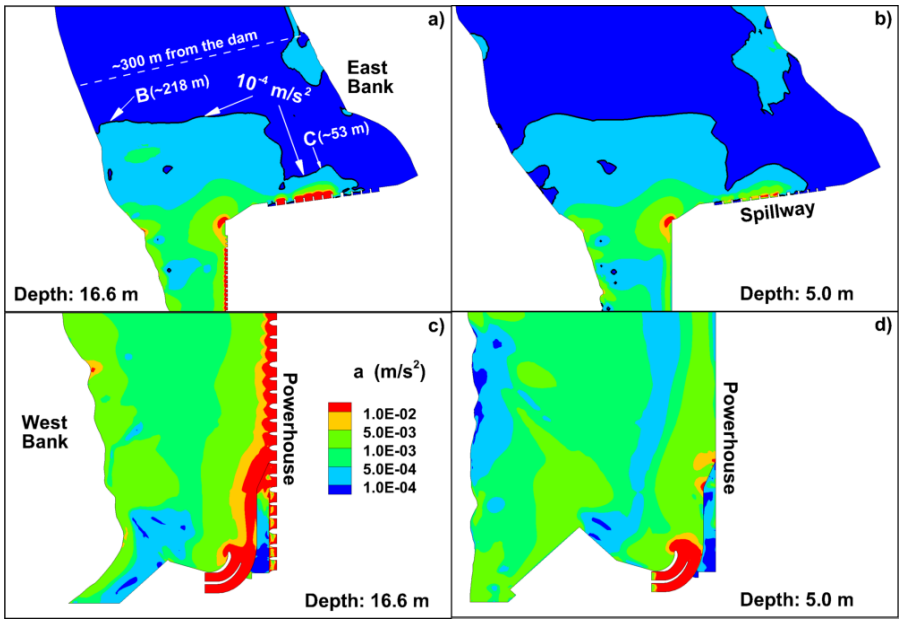

Figure 3.7 Case: 2005_S. Acceleration contours. Horizontal slices at depths of 16.6 m and 5.0 m.

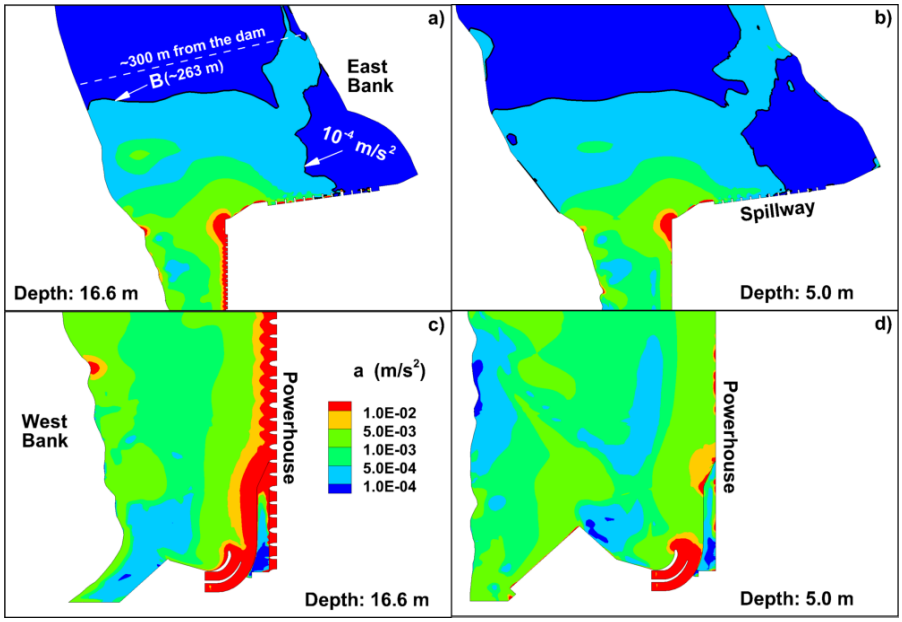

Figure 3.8 Case: 2010_NS. Acceleration contours. Horizontal slices at depths of 16.6 m and 5.0 m.

3.2 Dam 2 Forebay

Dam 2 has 10 powerhouse units and 22 spillway bays. For the simulated conditions spillway bay #22 operated as a top-spill. Figure 3.9a shows an aerial photo of the project. Table 3.2 shows the flow conditions simulated that defined in the Memorandum of Agreement (MOA) in 2002.

3.2.1 Grids and Numerical Model

A structured mesh of approximately 1.8×10^6 nodes was generated in GRIDGEN 15.15. The finest part of the grid was located nearby the top-spill with a grid element size of 2.5 m, 0.24 m, and 1.6 m along the x , y , z axes, respectively. Figures 3.9b and 3.9c display the grid for the region close to the top-spill and an overview of the grid in the powerhouse and spillway region, respectively. Continuity and turbulence closure were achieved using the SIMPLE algorithm and the $k-\varepsilon$ model, respectively. Converged solutions were achieved by running 25,000 time steps with a time step size of 80 seconds.

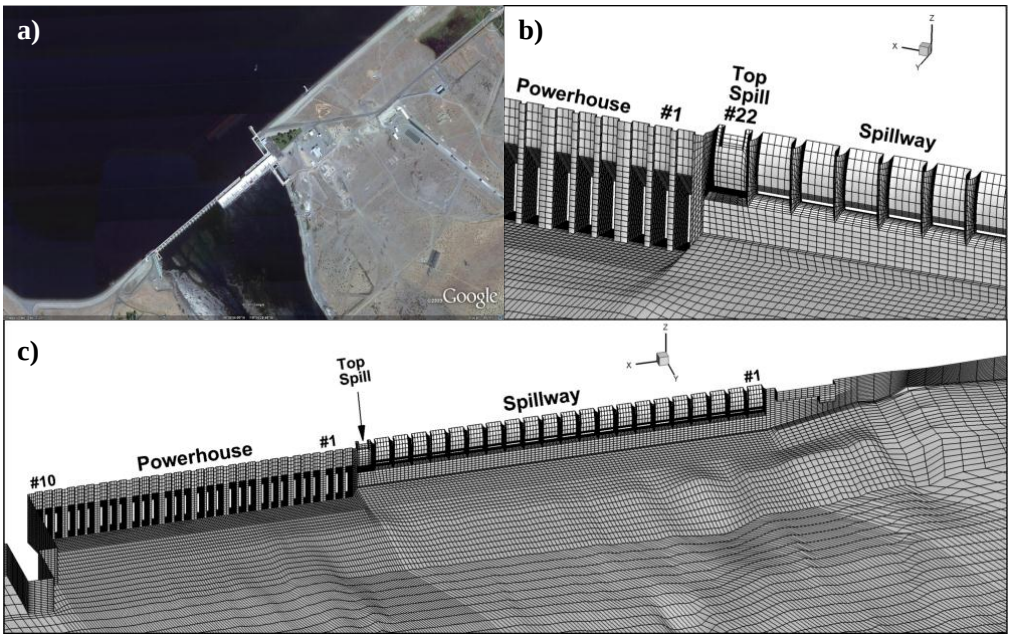

Figure 3.9 Dam 2. a) Aerial photo, b) Top spill grid, and c) Overview of the grid.

3.2.2 Hydrodynamics

Roughly, 64.0% of the total river discharge was flowing through all 22 spillway bays with 0.6% flowing through the top-spill. The maximum flow velocities immediately upstream of the top-spill and spillway bays were in the order of 3.0 and 12.0 m/s. Figures 3.10a and 3.10b depict horizontal slices at depths of 0.8 and 14.8 m, which correspond with the top-spill entrance and spillway gate entrance levels, respectively. Vertical slices through the top-spill and spillway bay #8 are shown in Figures 3.10c and 3.10d. Figure 3.10 shows significant curvatures in the streamlines for the region within 20 m from the dam. Streamlines in Figures 3.10c and 3.10d show that the drag force could cause important fish swimming depth changes in the region within 16 and 19 m upstream of the top-spill and spillway bays, respectively.

Table 3.2 Operating conditions.

		2002MOA
FB Level (m)		148.3
Powerhouse Discharge (m^3/s)	Unit 1	9.6
	Unit 2	227.1
	Unit 3	261.9
	Unit 4	167.4
	Unit 5	322.8
	Unit 6	98.8
	Unit 7	333.9
	Unit 8	167.6
	Unit 9	49.6
	Unit 10	186.9
	Total	1825.6
Spillway Discharge (m^3/s)	Bay 1	123.2
	Bay 2	131.1
	Bay 3	141.3
	Bay 4	144.7
	Bay 5	146.7
	Bay 6	162.5
	Bay 7	165.1
	Bay 8	179.0
	Bay 9	175.3
	Bay 10	167.4
	Bay 11	161.7
	Bay 12	147.8
	Bay 13	158.3
	Bay 14	154.6
	Bay 15	152.6
	Bay 16	143.0
	Bay 17	141.3
	Bay 18	136.2
	Bay 19	142.2
	Bay 20	129.1
	Bay 21	123.7
	Bay 22 (TS)	30.3
	Total	3157.0
River (m^3/s)		4982.6

Figures 3.11a, 3.11c, and 3.11d show contours of acceleration. An isoline of $a_d = 10^{-4}\ m/s^2$ is presented in Figure 3.11b. Values of 0.1 m/s^2 are displayed approximately 4.5 m upstream of the top-spill entrance in Figures 3.11a and 3.11c.

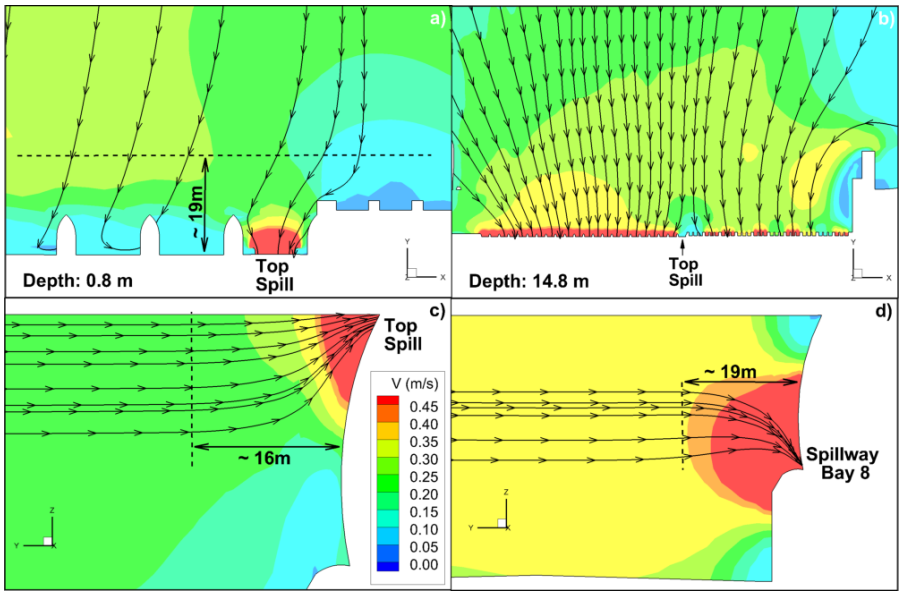

Figure 3.10 Case: 2002MOA. Streamlines and velocity contours. a) Horizontal slice at a depth of 0.8 m, b) Horizontal slice at a depth of 14.8 m, c) Slice through spillway bay 22 (top-spill), and d) Slice through spillway bay 8.

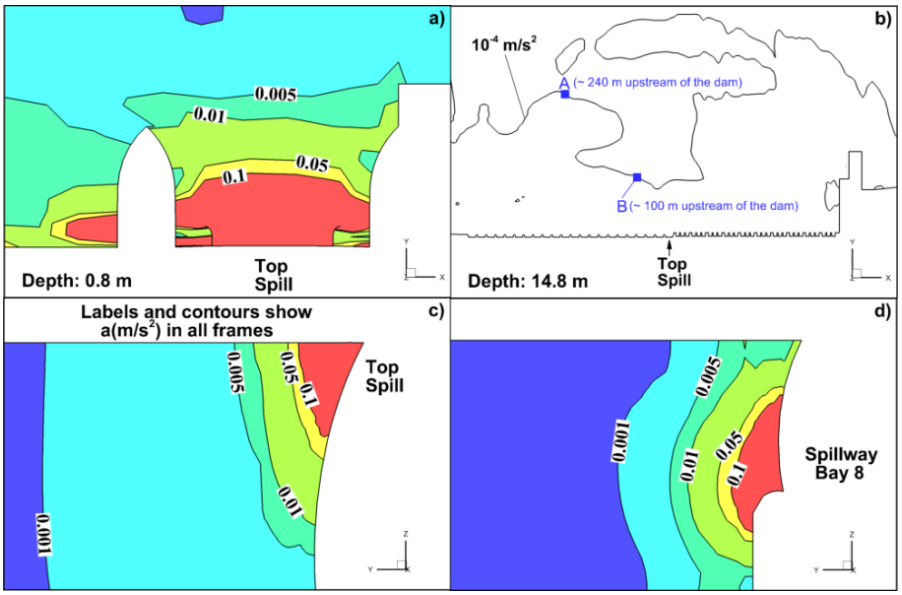

Figure 3.11 Case: 2002MOA. Acceleration contours. a) Horizontal slice at a depth of 0.8 m, b) Horizontal slice at a depth of 14.8 m, c) Slice through spillway bay 22 (top-spill), and d) Slice through spillway bay 8.

According to Figure 3.11b and van Netten (2006), fish swimming towards the spillway region could detect flow acceleration values within about 240 m from the dam (see point A in Figure 3.11b). In front of the top-spill, the zone with values of flow acceleration above $a_d = 10^{-4}\ m/s^2$ extends approximately 100 m upstream of the dam.

CHAPTER IV

JUVENILE SALMON BEHAVIOR

The first part of this chapter shows a comprehensive analysis of measured juvenile salmon swimming trajectories and CFD results. The second one describes how this thesis further analyzed fish behavior laboratory studies using CFD models.

4.1 Juvenile Salmon Measured Trajectories

Yearling Chinook salmon with implanted acoustic tags were monitored in the forebay of Dam 1 in the year 2010. Fish positions were measured on average every 5 seconds. An analysis of fish behavior in response to hydrodynamics is presented below. The flow field of the case 2010_NS (see Table 3.1) was used to determine the flow variables at the measured fish locations. Approximately 3000 fish were tagged in this year. This thesis analyzed trajectories that spanned at least 100 m. 662 trajectories were chosen. In total 333,962 fish locations were analyzed.

Figure 4.1a shows a top view of a Chinook trajectory used in this thesis. The change in fish swimming depth can be seen in Figure 4.1b. This figure also shows the vertical distance between the fish location and the riverbed (see dashed line). In Figure 4.1, trajectory time and Y coordinate are shown for points A, B, and C. This information is used below in further discussions about this particular trajectory. Twelve additional Chinook trajectories are presented in Figures 4.2-4.4.

4.1.1 Approach

Newton's Second Law was solved for every fish location. The considered forces were thrust and drag. The first and second derivatives of the measured trajectories with respect to time yielded the fish velocity and acceleration, respectively. The fish relative velocity, $\vec{u}_{rf}$, was calculated by subtracting the flow velocity from the fish velocity. The

drag coefficient was calculated using Equation 2.3. The mass of every individual fish was not available. An average mass of 30 g was used in this thesis. The results presented below did not consider fish schooling activity and trajectories of fish migrating at night and day were analyzed together.

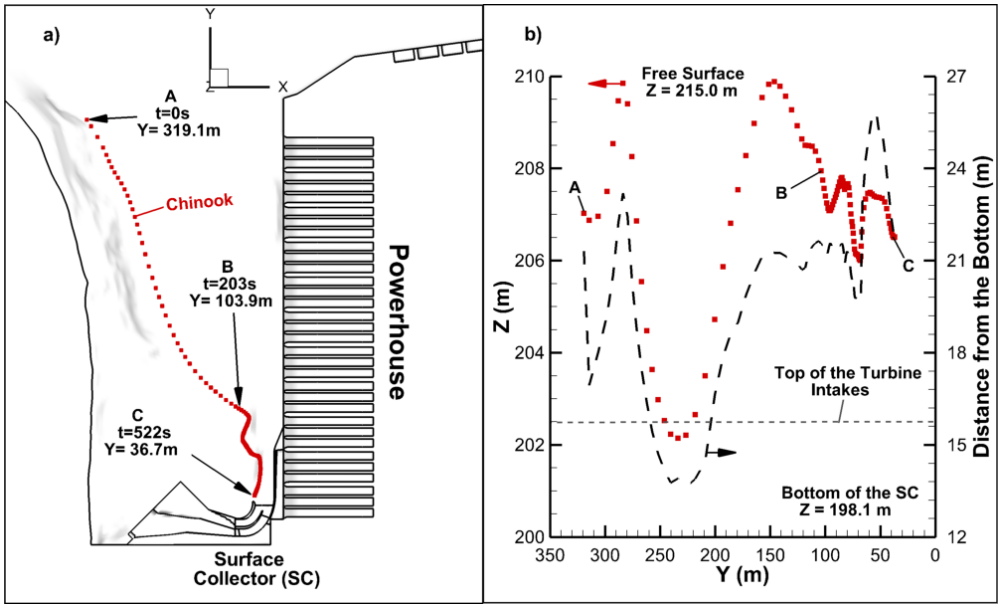

Figure 4.1 Chinook trajectory. Chinook ID=1362.

4.1.2 Smoothing

The lack of smoothness in the fish trajectory could affect the results of the first and second derivative. Fish trajectories were smoothed prior to calculating fish velocity and acceleration. Taking space as the dependent variable and time as the independent variable, second order polynomials were fitted in the X, Y and Z directions. A least squares algorithm used the given point, three points backwards in time, and three points forward in time. For the fish trajectory displayed in Figure 4.1, Figure 4.5 shows both the measured and smoothed trajectories in the Y direction. In Figures 4.6 and 4.7 symbols show information calculated with the raw data and lines with the smoothed trajectory.

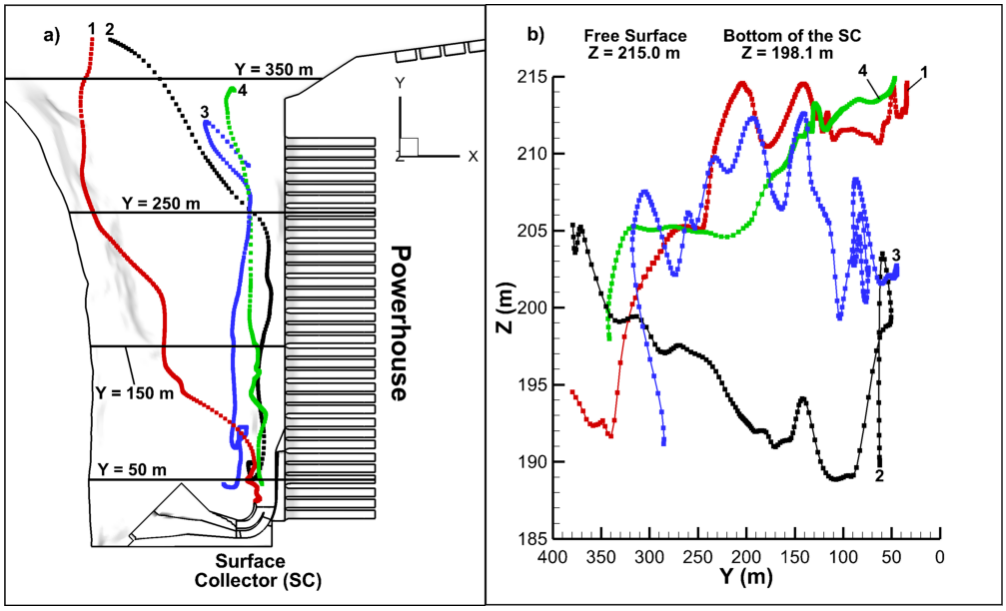

Figure 4.2 Chinook measured trajectories.

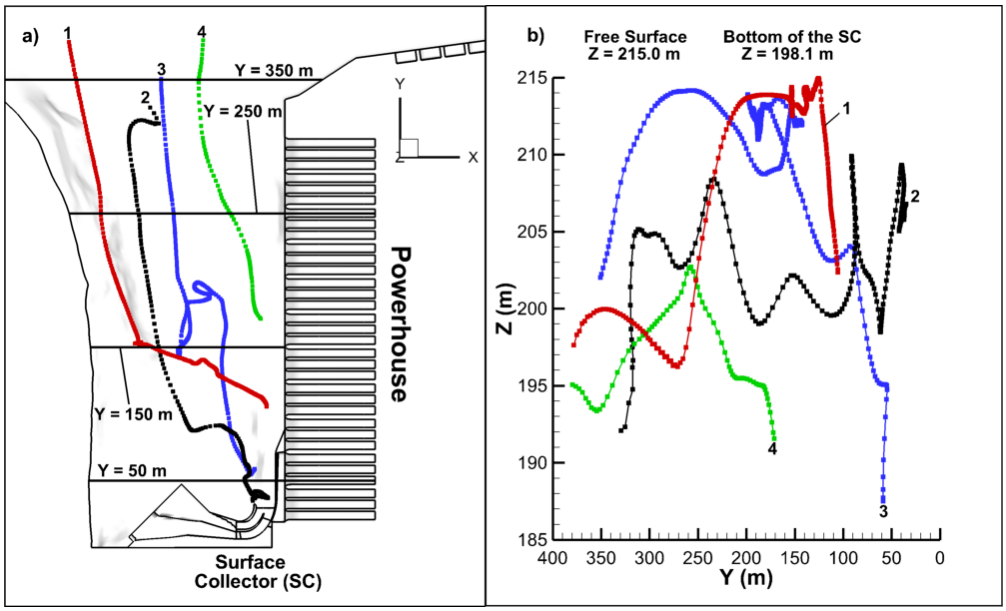

Figure 4.3 Chinook measured trajectories.

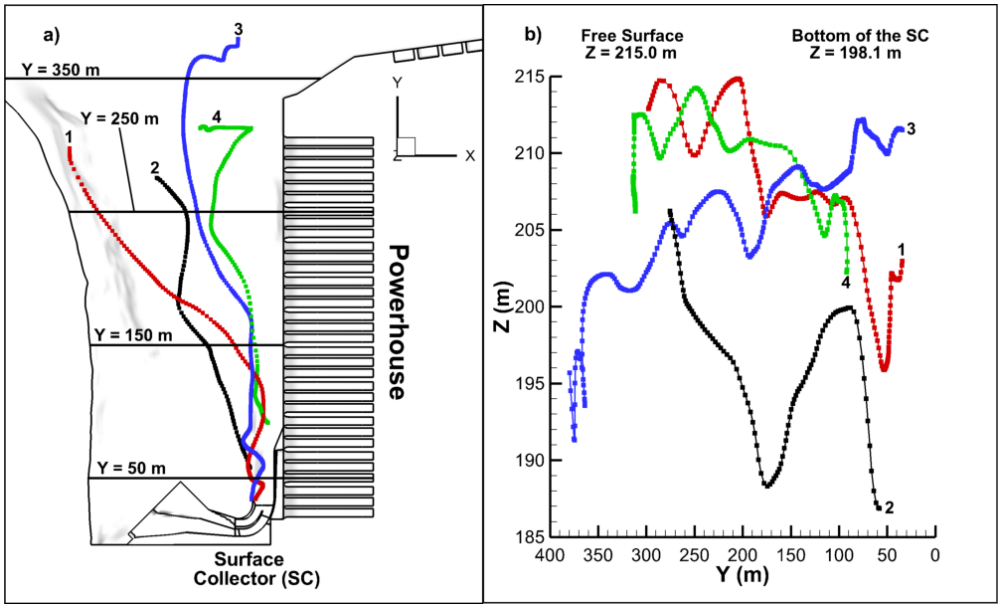

Figure 4.4 Chinook measured trajectories.

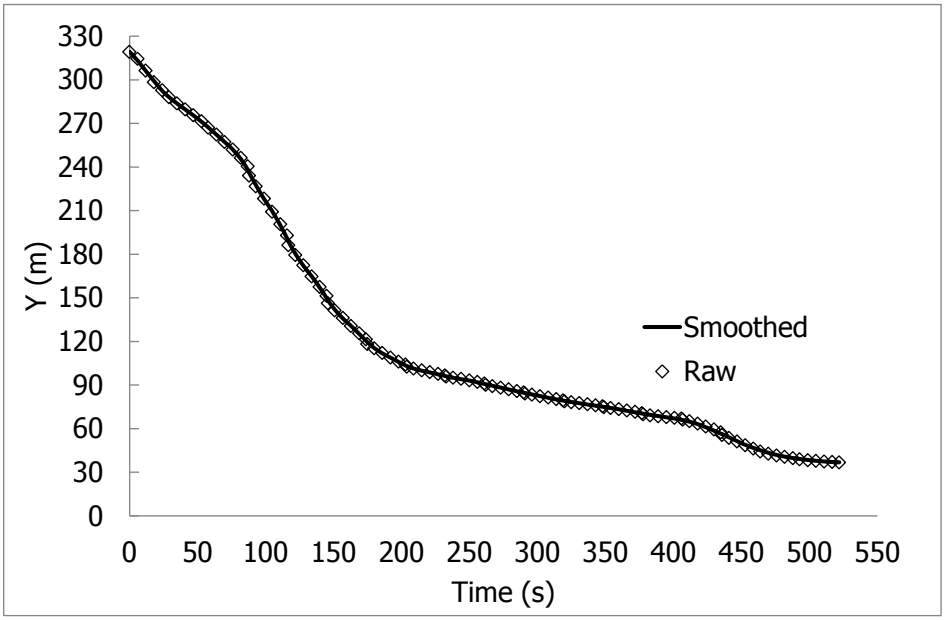

Figure 4.5 Y-direction. Chinook ID=1362.

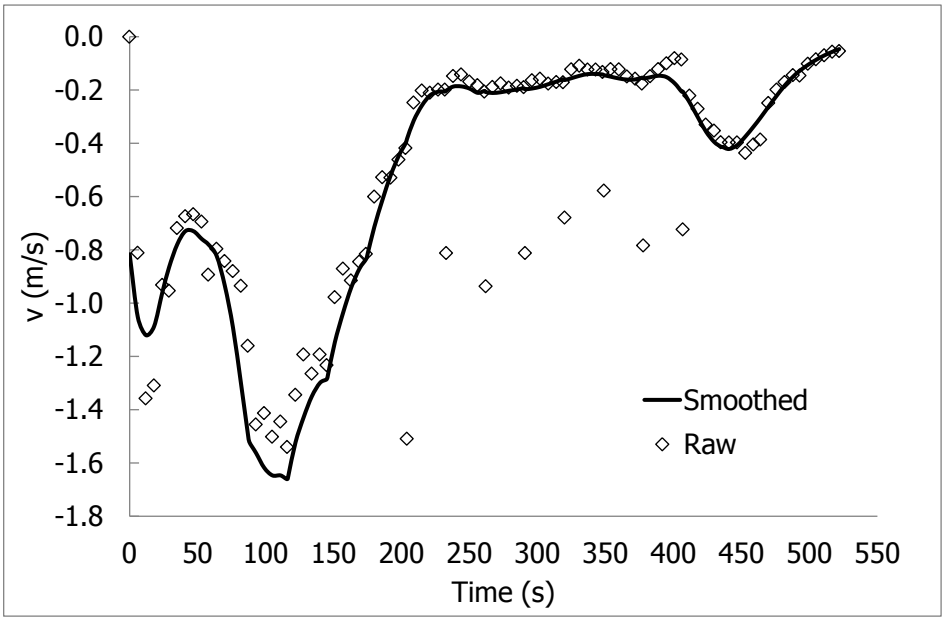

Figure 4.6 Y-velocity. Chinook ID=1362.

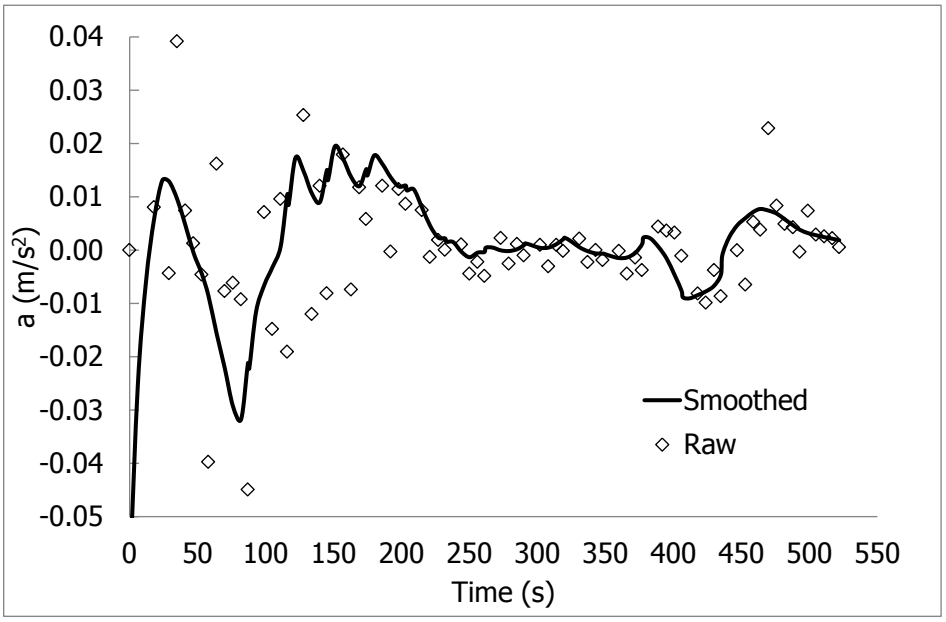

Figure 4.7 Y-acceleration. Chinook ID=1362.

Figures 4.6 and 4.7 show velocity and acceleration in the Y direction, respectively. Derivatives with the raw data presented in these figures were calculated using backwards differences.

It is worth noting that Figure 4.6 shows the fish velocity in the Y direction that an observer on the ground perceives. Peake and McKinley (1997) reported Atlantic salmon smolts swimming against currents of up to 1.26 m/s. The maximum value in Figure 4.6 of about 1.7 m/s corresponds to a relative velocity of 1.2 m/s, which is consistent with values reported in literature.

4.1.3 Swimming Thrust

By solving Newton's Second Law, it is possible to determine fish periods of gliding and active swimming, thrust magnitude, and orientation of the swimming thrust with respect to the water velocity. Figure 4.8 shows the magnitude of the fish thrust $\left|\vec{F}_T\right|$ and relative velocity $\left|\vec{u}_{rf}\right|$ for the trajectory presented in Fig. 4.1.

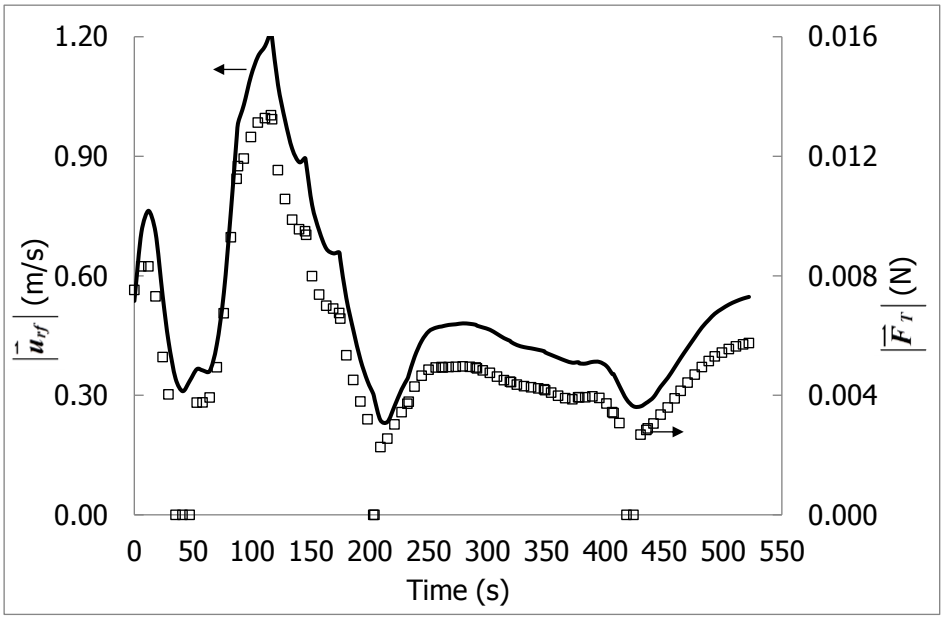

Figure 4.8 Swimming thrust and relative velocity. Chinook ID=1362.

If the thrust force calculated using the drag coefficient for gliding fish (Equation 2.3b) was smaller than 0.6×10^{-3} N, the thrust force was assumed zero. Otherwise, the thrust was calculated using the drag coefficient for fish actively swimming. This thrust threshold corresponds to approximately 5% of the maximum thrust for juvenile salmon swimming in sustained mode as reported by Tang and Wardle (1992).

As expected fish gliding activity, $\left|\vec{F}_T\right| = 0$, coincides with the minimum values of the relative velocity. The expression used in this thesis to calculate the drag coefficient of fish actively swimming (Equation 2.3a) creates a nearly linear relation between the swimming thrust and the fish relative velocity, which explains why both curves in Fig. 4.8 show similar trends. Results show that this particular fish glided for about 19 seconds, which represented about 3.6% of the total time. This thesis assumes that the maximum thrust force generated by juvenile salmon swimming in sustained mode is 0.013 N. Under the current analysis assumptions, the fish whose trajectory is displayed in Figure 4.1, was always swimming in sustained mode. Burst swimming occurs, for the most part, at a time scale smaller than 5 seconds. The measured Chinook trajectories studied in this thesis do not have the time resolution to analyze the thrust force of juvenile salmon swimming in burst mode.

Figure 4.9 shows, for the fish shown in Figure 4.1, the angle α between the fish thrust and the flow velocity in the XY plane (see Figure 2.3a). The angle θ between the swimming thrust and the vertical axis is also shown in the same figure (see Figure 2.2). Values of α of 180° or -180°, indicate that fish were swimming in the exact opposite direction of the flow in the XY plane. Fish swimming upwards have $\theta < 90^{\circ}$, and $\theta > 90^{\circ}$ represents fish swimming downwards. For fish gliding, the values of α and θ were assumed 0° and 90°, respectively. Fig. 4.10 presents the flow acceleration along the fish trajectory. The angle α is also presented in this figure to allow for comparisons between fish behavior and values of flow acceleration.

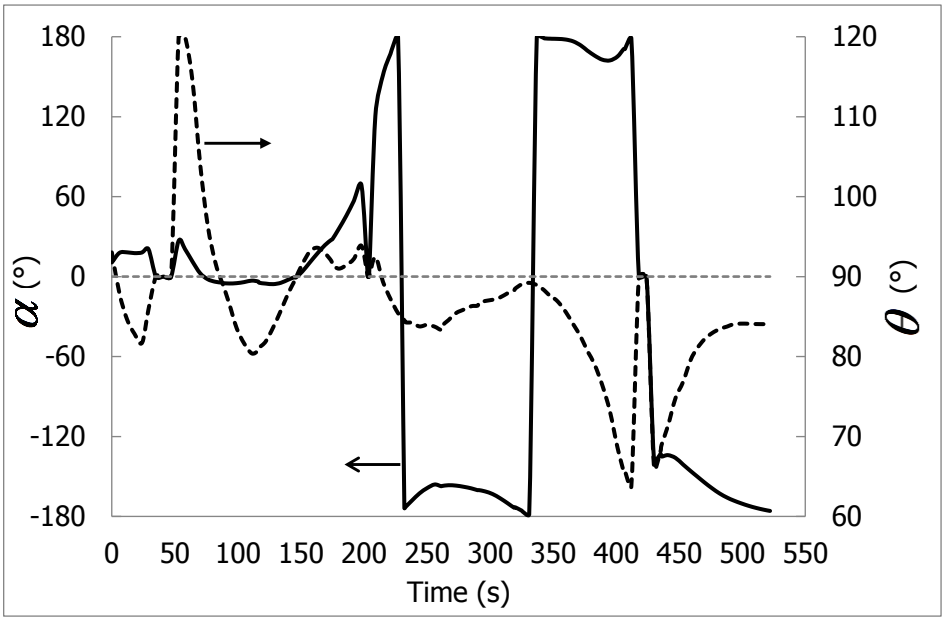

Figure 4.9 Swimming thrust angles. Chinook ID=1362.

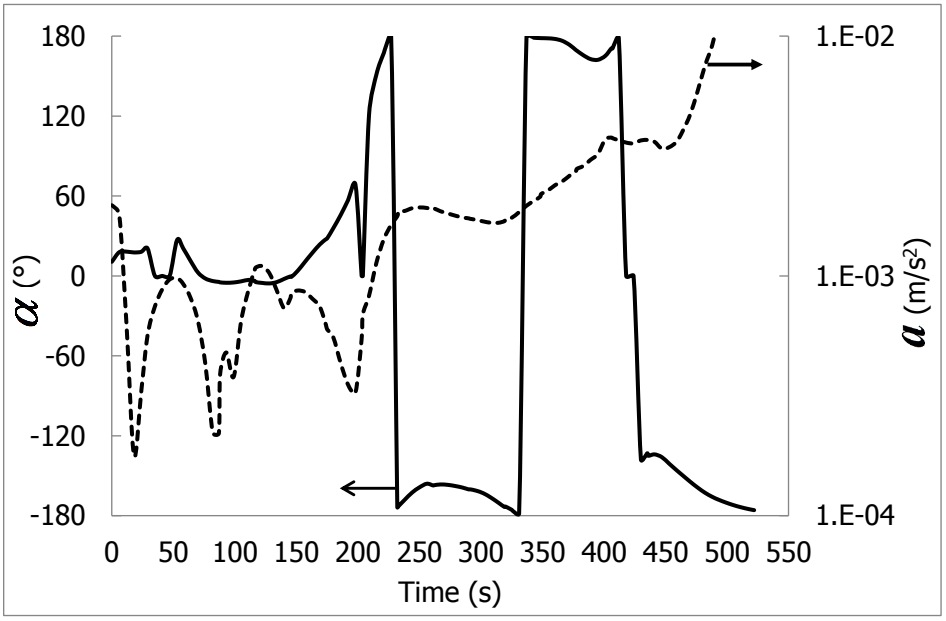

Figure 4.10 Flow acceleration and α . Chinook ID=1362.

In Figure 4.1, the points A, B, and C define specific segments of the Chinook measured trajectory. For about the first 200 seconds (segment AB), the fish swam in a similar direction as the flow in the XY plane with values of α in the ±60° range. In the vertical direction, no clear pattern was displayed and the fish swam both upwards and downwards.

In the segment BC (t > 200 s) the fish faced the flow with values of α close to either 180 or -180. It is important to note that the net movement of fish was in the downstream direction despite the fish thrust was directed in the upstream direction. In the same segment, fish swam consistently upwards. Figure 4.8 shows that the average thrust for the segment BC was about 0.005 N, which represents about 40% of the maximum thrust for juvenile salmon in sustained mode. For fish decidedly trying to move in the upstream direction, the analysis presented here should yield higher values of the thrust force. Fish switching from facing downstream to moving tail first is not necessarily an indication that fish want to move upstream. The fish desire to move downstream could still be present and the change in fish orientation could be a mechanism to increase fish readiness for escaping if needed.

Figure 4.10 shows that the fish started swimming tail first for a flow acceleration of about 2.0×10^{-3} m/s^2 (t~220 s). As the fish approached the surface collector entrance, the magnitude of the flow acceleration increased. After switching orientation, this particular fish did not go back to swim in the downstream direction.

The effect of migrating tail first on migration time is important. It took 203 s and 319 s for the fish to cover the segments AB (~247 m) and BC (~122 m), respectively.

4.1.4 Correlation Coefficients

Pearson correlation coefficients between flow variables and fish swimming thrust were calculated for different zones of the Dam 1 forebay. Results are presented for four selected zones located at different distances from the turbine intakes and surface

collector. Figure 4.11 shows the four zones. In the XY plane, the zones are viewed as 25x25 m squares. Table 4.1 shows the flow variables used in the present correlation analysis and the symbols that were used to represent them.

Table 4.1 Flow variables.

P	Hydrostatic Pressure
a_{ξ}	Flow acceleration in the flow direction (XY plane)
a_{ψ}	Flow acceleration normal to the flow direction (XY plane)
a_{z}	Flow acceleration in the vertical direction
a	Flow acceleration magnitude

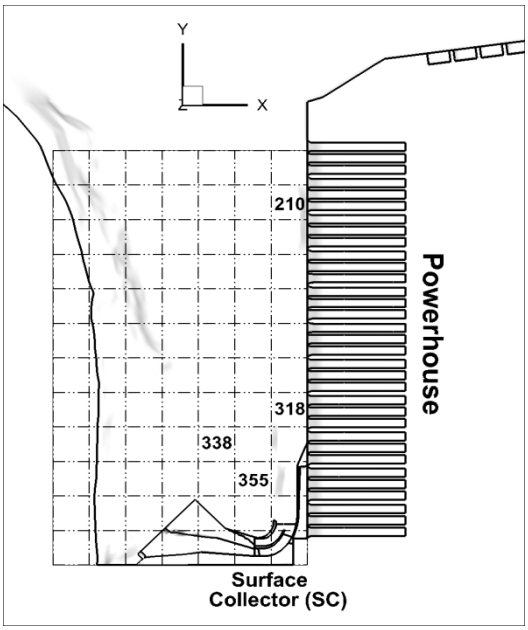

Figure 4.11 Correlation analysis zones. The number shows the zone ID.

Table 4.2 reports the statistical parameters, expressed in SI units, of the flow variables for each of the four zones. Figures 4.12-4.16 show the correlation coefficients between the fish thrust and the flow variables presented in Table 4.1. Coefficients for the zones 210, 318, 338, and 355 were calculated with 8,404, 11,063, 3,398, and 10,501 fish positions, respectively. On average, the magnitude of the flow acceleration for zones 338 and 355 is approximately one order of magnitude smaller than in the zones 210 and 318. As expected, the closest zones to the turbine intakes, 210 and 318, show the highest values of flow acceleration. Fish swimming activity correlates considerably better with the flow variables in zones 210 and 318 than in the other two zones. The present analysis shows that for zones located 25 m or more away from the turbines, correlation coefficients between flow variables and swimming thrust do not vary significantly. For all the flow variables analyzed, the average values of the correlation coefficients are 0.26, 0.24, 0.09, and 0.08 for the zones 210, 318, 338, and 355, respectively. The strongest correlation (0.73) was found between the swimming thrust in the vertical direction and the flow acceleration in the vertical direction in zone 210.

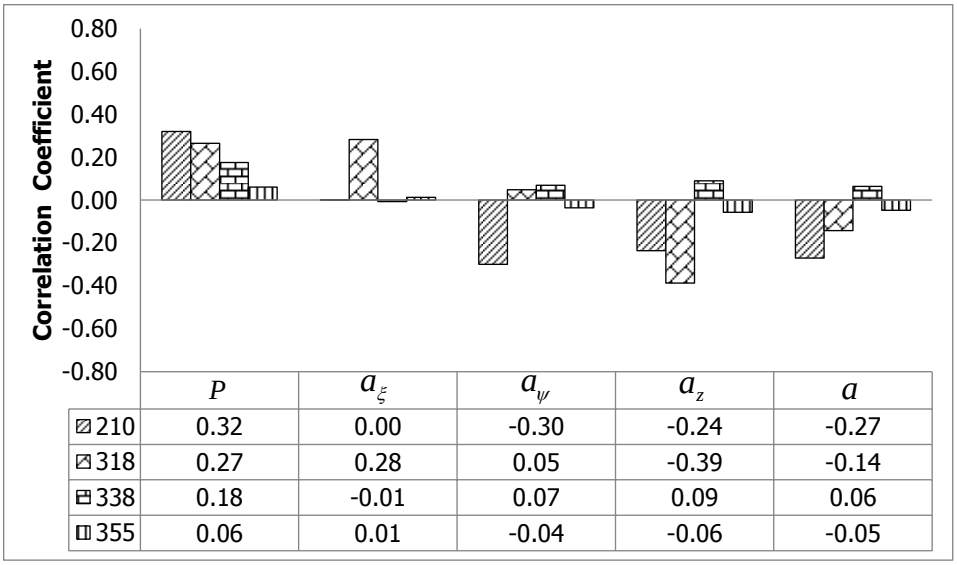

	P	a_ξ	a_ψ	a_z	a
210	0.32	0.00	-0.30	-0.24	-0.27
318	0.27	0.28	0.05	-0.39	-0.14
338	0.18	-0.01	0.07	0.09	0.06
355	0.06	0.01	-0.04	-0.06	-0.05

Figure 4.12 Correlation coefficients. Fish thrust in the flow direction (XY plane).

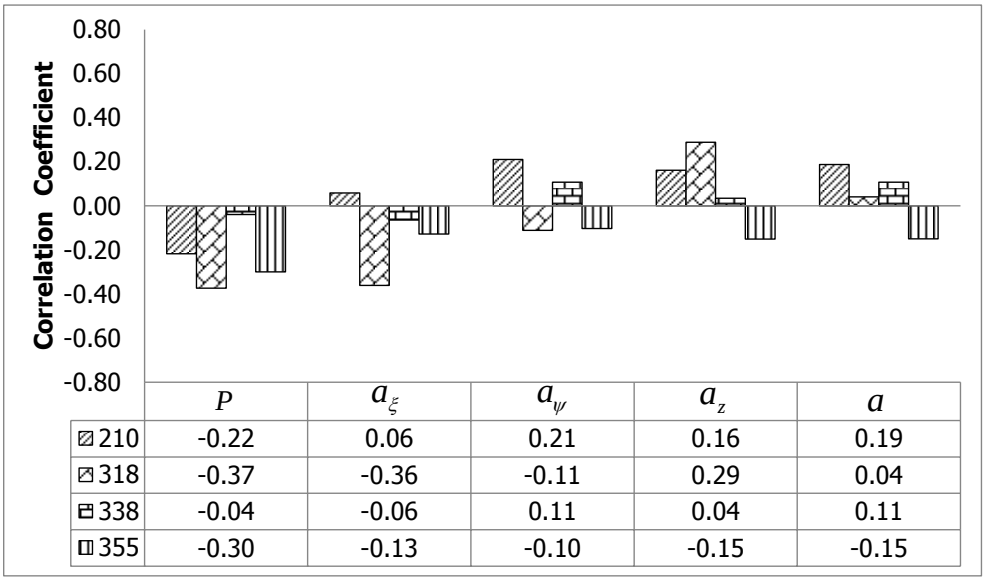

	P	a_ξ	a_ψ	a_z	a
210	-0.22	0.06	0.21	0.16	0.19
318	-0.37	-0.36	-0.11	0.29	0.04
338	-0.04	-0.06	0.11	0.04	0.11
355	-0.30	-0.13	-0.10	-0.15	-0.15

Figure 4.13 Correlation coefficients. Fish thrust normal to the flow direction (XY plane).

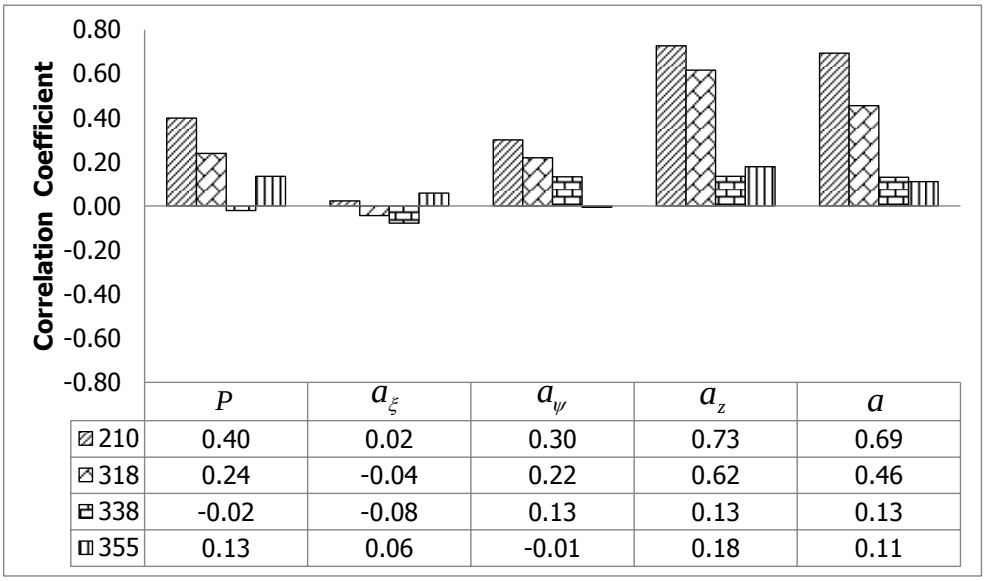

	P	a_ξ	a_ψ	a_z	a
210	0.40	0.02	0.30	0.73	0.69
318	0.24	-0.04	0.22	0.62	0.46
338	-0.02	-0.08	0.13	0.13	0.13
355	0.13	0.06	-0.01	0.18	0.11

Figure 4.14 Correlation coefficients. Fish thrust in the vertical direction.

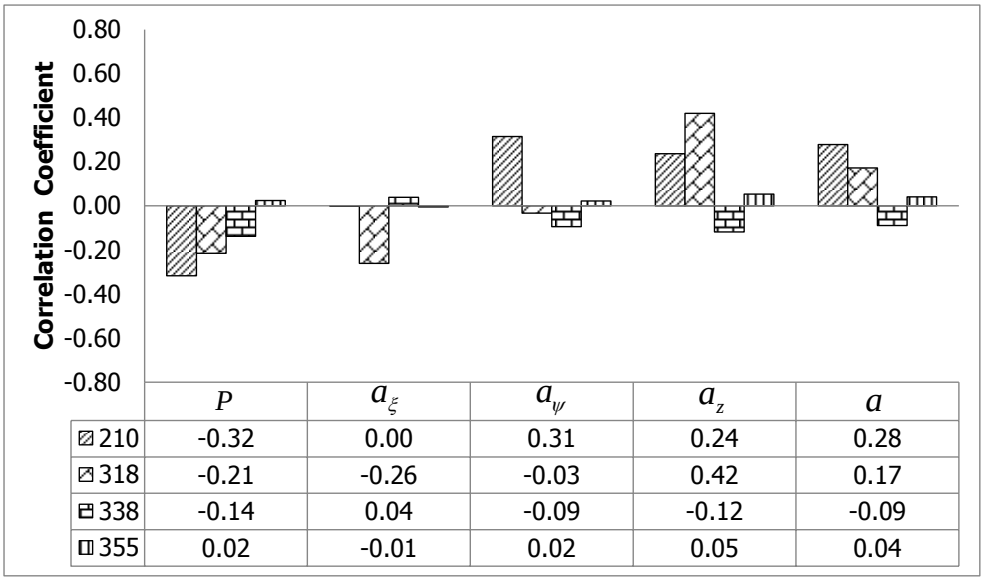

	P	a_ξ	a_ψ	a_z	a
210	-0.32	0.00	0.31	0.24	0.28
318	-0.21	-0.26	-0.03	0.42	0.17
338	-0.14	0.04	-0.09	-0.12	-0.09
355	0.02	-0.01	0.02	0.05	0.04

Figure 4.15 Correlation coefficients. Fish thrust magnitude (XY plane).

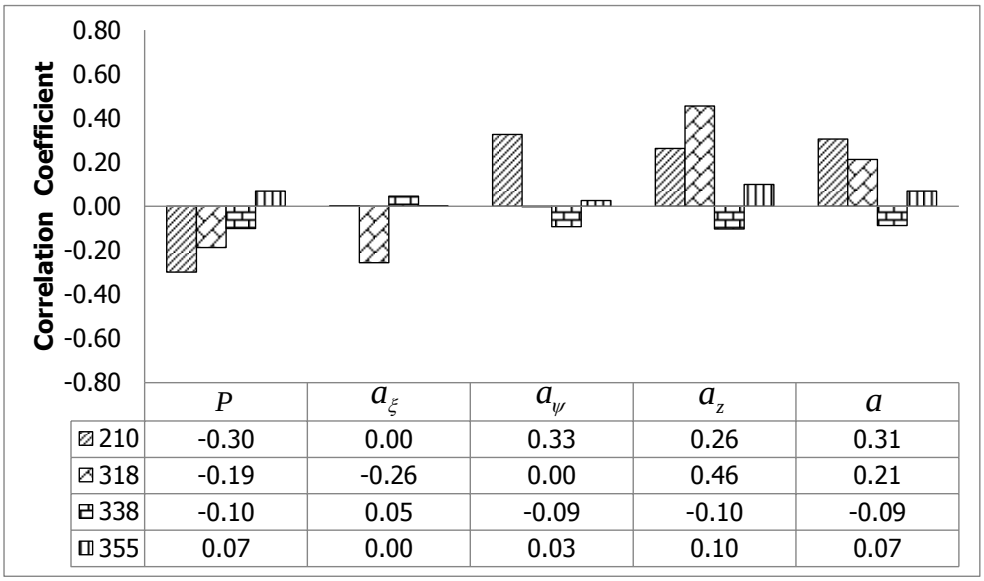

	P	a_ξ	a_ψ	a_z	a
210	-0.30	0.00	0.33	0.26	0.31
318	-0.19	-0.26	0.00	0.46	0.21
338	-0.10	0.05	-0.09	-0.10	-0.09
355	0.07	0.00	0.03	0.10	0.07

Figure 4.16 Correlation coefficients. Fish thrust magnitude.

Table 4.2 Flow variables statistical parameters.

Zone ID			Average	STDEV	Min	Max
	210	a_ξ	-5.57E-05	5.87E-03	-1.02E-01	1.07E-01
		a_ψ	5.26E-03	1.33E-02	-2.67E-02	1.48E-01
		a_z	-1.63E-03	9.90E-03	-8.86E-02	4.37E-01
		a	9.18E-03	1.91E-02	8.19E-04	4.64E-01
	318	a_ξ	1.40E-03	6.61E-03	-7.31E-02	9.50E-02
		a_ψ	3.81E-03	1.21E-02	-6.67E-02	1.26E-01
		a_z	-2.67E-03	5.03E-03	-2.51E-01	1.53E-01
		a	8.83E-03	1.71E-02	6.72E-04	4.26E-01
	338	a_ξ	1.00E-03	5.33E-04	-1.25E-03	2.33E-03
		a_ψ	-2.64E-04	5.33E-04	-2.38E-03	8.90E-04
		a_z	1.47E-04	2.50E-04	-2.09E-04	2.42E-03
		a	1.16E-03	6.36E-04	2.10E-04	3.01E-03
	355	a_ξ	6.24E-04	1.42E-03	-4.53E-02	2.35E-02
		a_ψ	1.47E-04	1.12E-03	-6.46E-02	1.06E-02
		a_z	-1.00E-03	1.22E-03	-1.49E-02	1.51E-04
		a	1.71E-03	1.87E-03	1.46E-04	9.48E-02

For zones 25 m or more away from the turbine intakes, hydrostatic pressure is not well correlated (< 0.30) with fish swimming activity in the vertical direction. In summary, for zones close (< 25 m) to the turbine intakes fish activity is correlated with the flow acceleration, particularly in the vertical direction. Away from the turbine intakes, fish activity does not show a linear relation with the analyzed flow variables.

4.1.5 Statistics

Figures 4.17-4.19 show scatter plots of flow acceleration vs. $\left|\overline{F}_T\right|$, α, and θ. On average, fish thrust tends to increase with flow acceleration. For flow accelerations of $1.0\text{x}10^{-3}$ and $1.0\text{x}10^{-2}$ m/s^2 the average value of the thrust force was $4.6\text{x}10^{-3}$ and $7.9\text{x}10^{-3}$ N, respectively. Figure 4.18 shows a general tendency in fish to migrate downstream tail first. Kemp et al. (2006) reported the majority (70%) of juvenile salmon switching from facing downstream to swimming tail first as they approach high acceleration zones. Results in Fig. 4.18 are in accordance with the Kemp et al. (2006) findings. For flow accelerations below $1.0\text{x}10^{-3}$ m/s^2, Figure 4.19 shows that fish did not have a clear

preference between swimming upwards or downwards. As fish swam in higher flow acceleration zones, fish tended to swim upwards. This tendency disappeared for flow accelerations above $1.0x10^{-2}$ m/s^2. Figures 4.20-4.22 show probability density distributions for $\left|\overline{F}_T\right|$, α, and θ for four different values of flow acceleration. These figures display similar swimming patterns for values of flow acceleration equal to $5.0x10^{-4}$ m/s^2 and $1.0x10^{-3}$ m/s^2. About 15 % of the fish migrated with values of α between -60° and 60°. The rest of the fish swam tail first. For those values of flow acceleration fish did not show a clear tendency to move either upwards or downwards. Figures 4.20-4.22 also show similar swimming patterns for flow accelerations of $5.0x10^{-3}$ m/s^2 and $1.0x10^{-2}$ m/s^2. About 95 % of the fish moved downstream tail first for these flow accelerations. For these values of flow acceleration, the probability density functions of θ show a bias towards values smaller than 90°. Comparison of the probability density functions suggest the existence of an acceleration threshold between $1.0x10^{-3}$ m/s^2 and $1.0x10^{-2}$ m/s^2 that triggers behavioral responses in juvenile Chinook salmon.

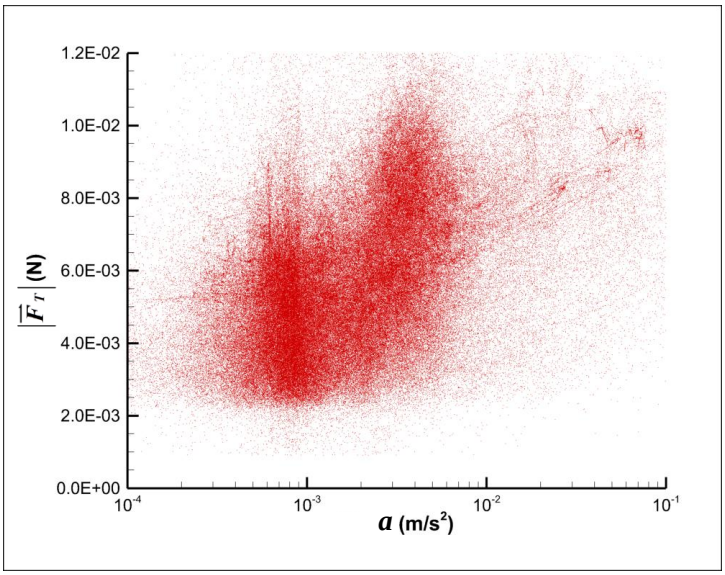

Figure 4.17 Flow acceleration vs. swimming thrust magnitude.

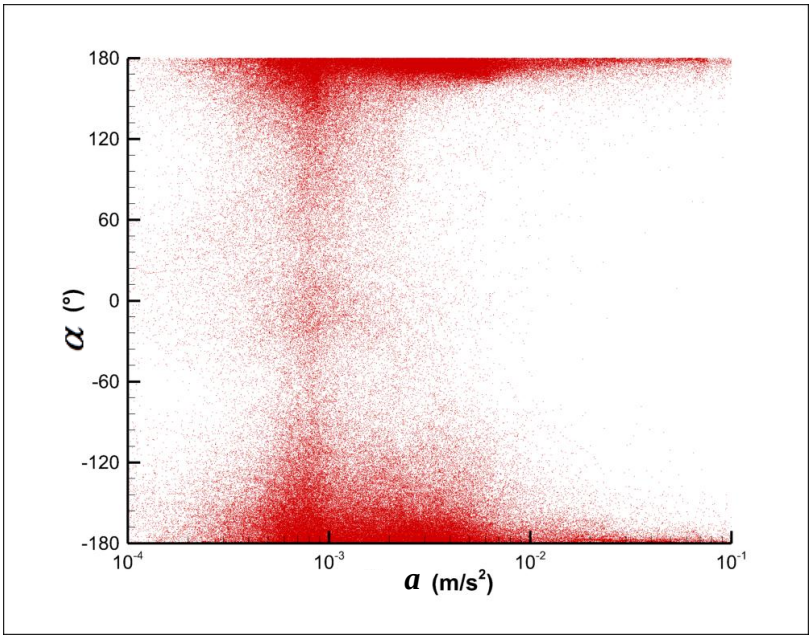

Figure 4.18 Flow acceleration vs. α .

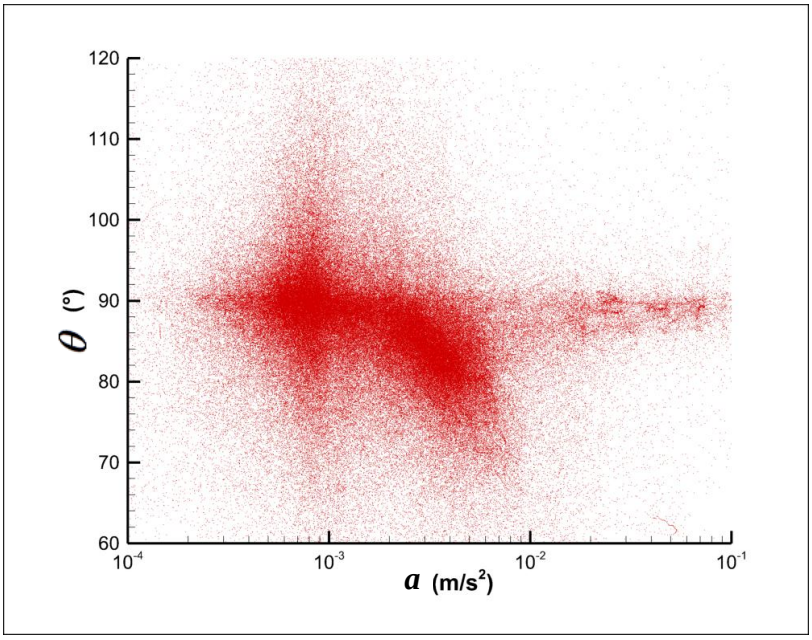

Figure 4.19 Flow acceleration vs. θ .

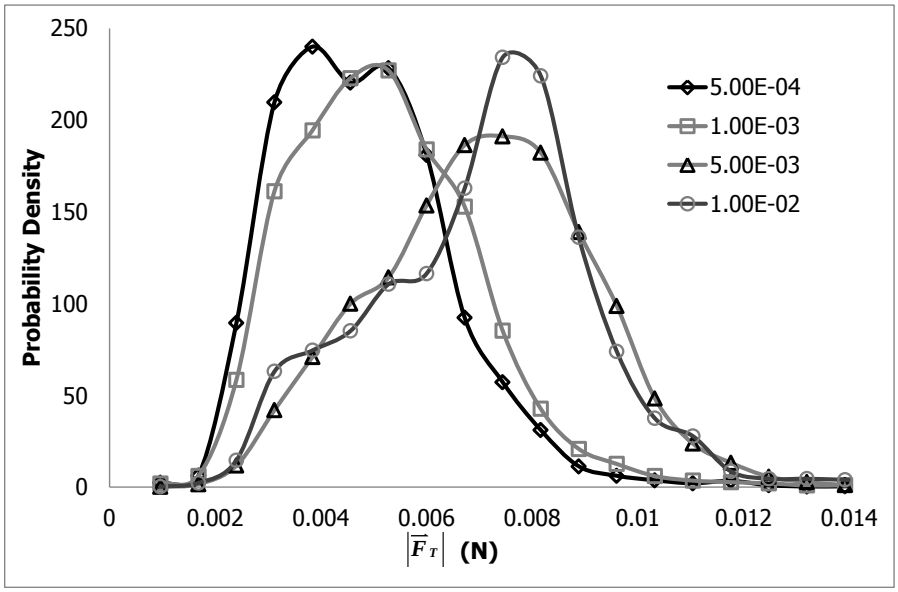

Figure 4.20 Fish thrust probability density. The legend shows values of flow acceleration.

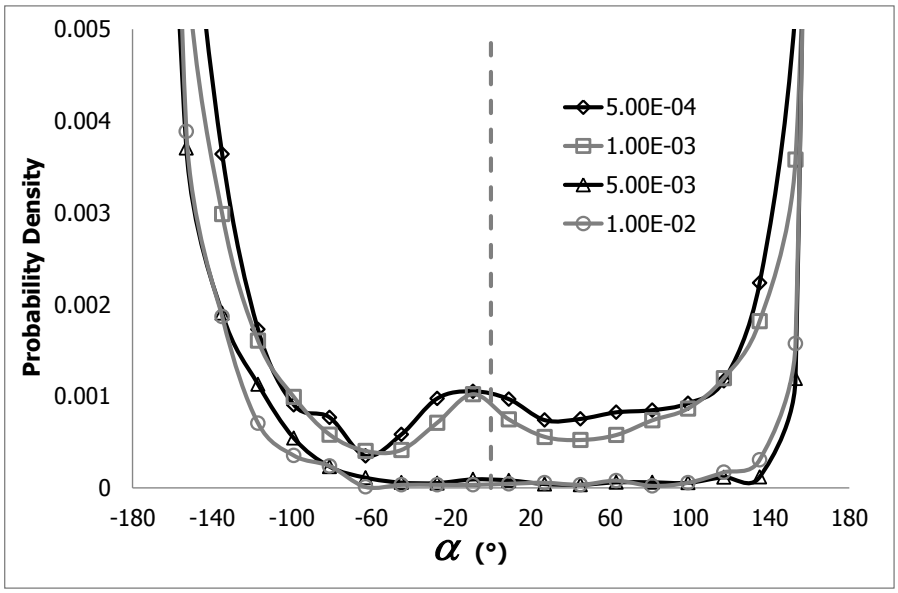

Figure 4.21 α probability density. The legend shows values of flow acceleration.

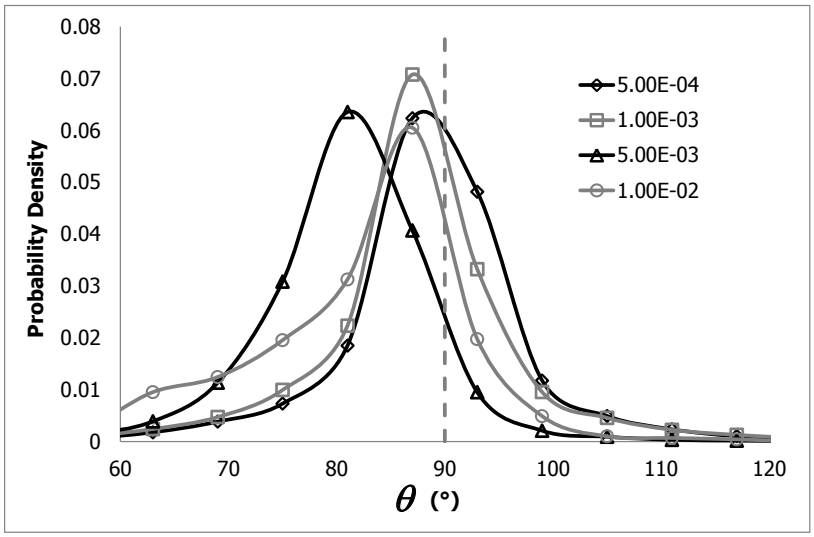

Figure 4.22 θ probability density. The legend shows values of flow acceleration.

In Figure 4.22, the curve for $5.0x10^{-3}$ m/s^2 shows a more marked tendency in fish to swim upwards. This value of flow acceleration is found approximately 10 m away from the turbine intakes (see Figure 3.8). As fish approached the turbines they tried to avoid being trapped by swimming both upwards and away (in the XY plane) from the turbines. The closer the got to the turbines the tendency to swim upwards diminished. The fish tendency to swim upward when exposed to high values of flow accelerations could be a consequence of the Dam 1 configuration and not a natural reaction of the fish. Fish may have swum upward close to the turbines to avoid being trapped by the flow. In Dam 1 forebay most of the high acceleration zones are close to the turbine intakes and for fish swimming in the first 15-20 m of the water column, the flow velocity was directed downward. Fig. 4.23 shows the probability density distribution for θ calculated for fish positions 20 m or more away from the turbines. This figure also shows a bias towards values of θ smaller than 90°. The studied Chinook trajectories show a fish tendency to swim upwards as acceleration increases. This statement is valid for both downward flows and for flows with a negligible vertical component. The fish trajectories and flow

conditions used in this thesis do not show data on fish swimming in high acceleration zones with the flow pointing upwards.

Figure 4.24 presents the probability of gliding and Figure 4.25 shows probability densities of times of active swimming and gliding. As flow acceleration increases, the probability of gliding decreases. The average time fish actively swam was 40 s and the average time of gliding was 18 s. Fish that swam for long periods (>100 s) changed the swimming thrust on average every $\tau = 50s$.

Figure 4.26 shows probability densities of swimming depths for Chinook swimming in the forebays of Dam 1 and Dam 2. Swimming depths for Dam 1 were available for the zone close to the powerhouse. This zone has a shallow bathymetry close to the west bank. Timko et al. (2007) measured approach swimming depths for Chinook swimming 150 m upstream of Dam 2. This information is plotted in Figure 4.26. Chinook swimming in Dam 1 tended to stay closer to the free surface than Chinook swimming in the forebay of Dam 2.

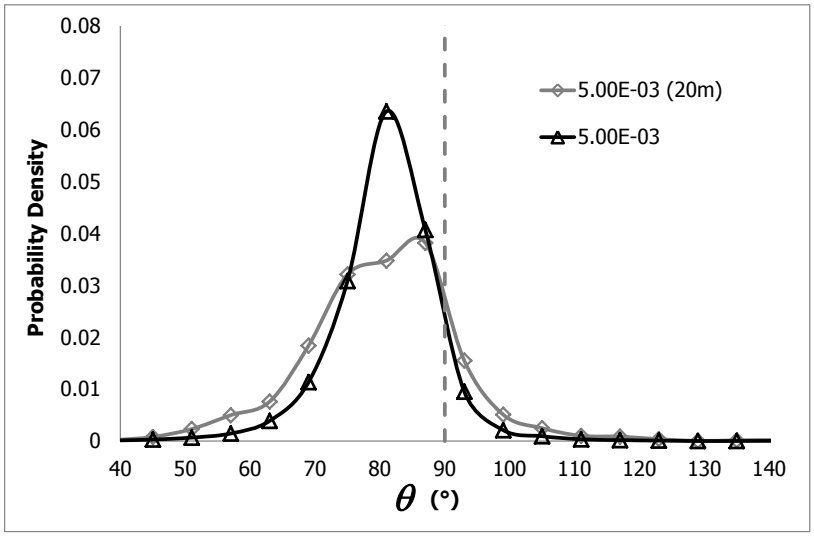

Figure 4.23 θ probability density for fish swimming away from the turbine intakes. The legend shows values of flow acceleration.

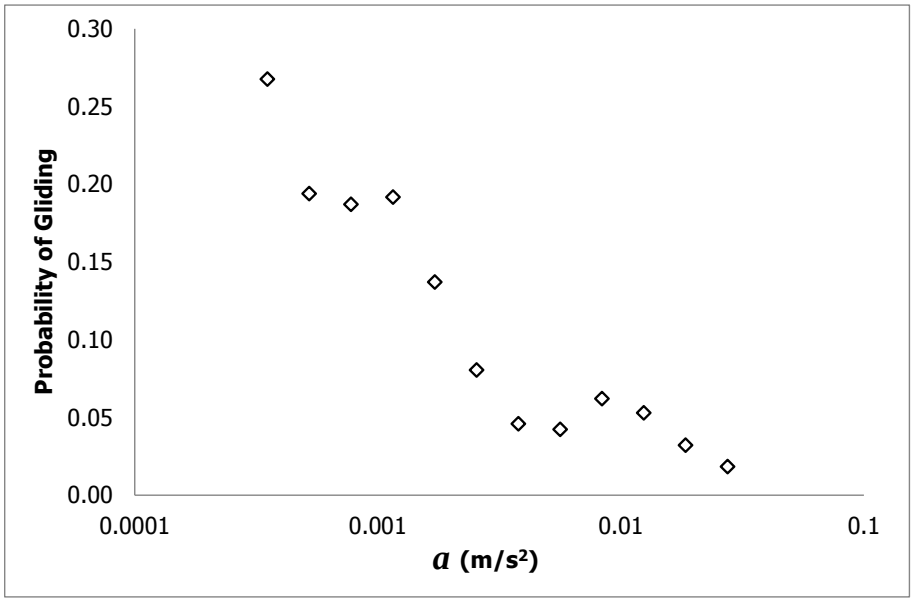

Figure 4.24 Probability of gliding.

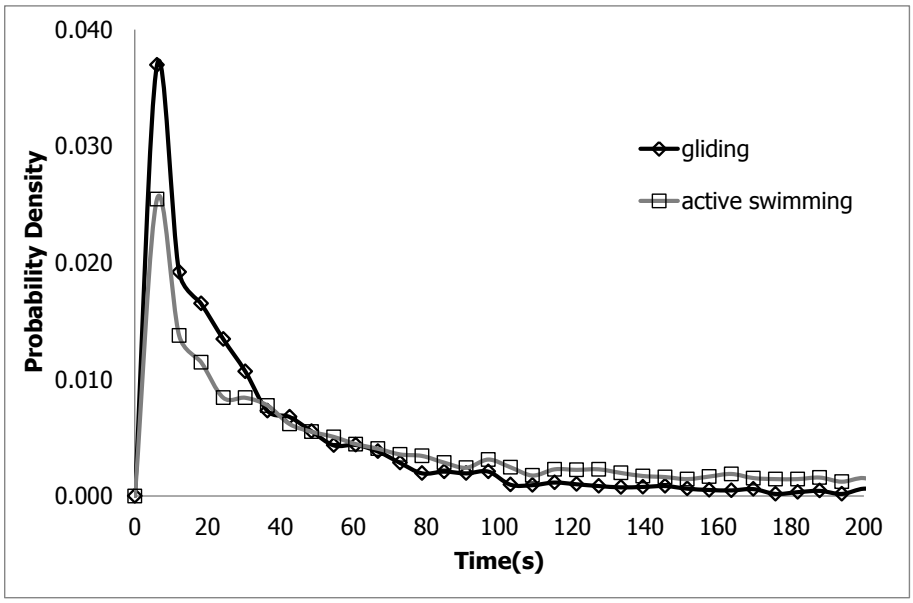

Figure 4.25 Times of active swimming and gliding.

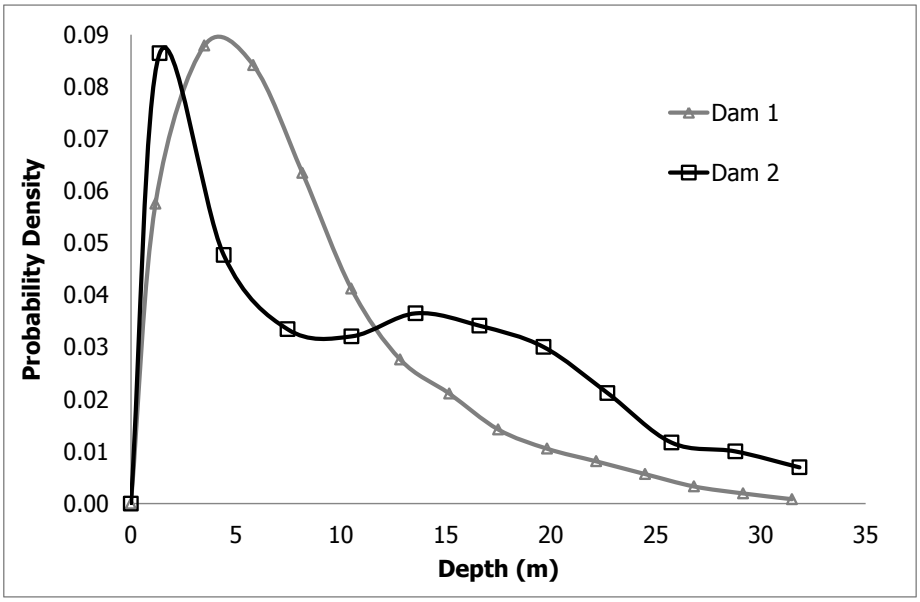

Figure 4.26 Chinook swimming depths.

In Dam 1, 70% of the fish occupied the first 10 meters of the water column whereas in Dam 2 the same percent of fish swam in the first 16 m of the water column.

The curve for Dam 1 was created using the average swimming depths of the 662 fish trajectories. As it was mentioned before, at Dam 1 fish locations were available in the powerhouse zone. The curve for Dam 1 could reflect no only fish natural swimming depth preferences. Close to the West bank, the powerhouse zone of Dam 1 has a shallow bathymetry. Near the turbine intakes the flow velocity point downwards which could trigger fish changes in swimming depth. On the other hand, the curve for Dam 2 was not created with average swimming depth along fish trajectories. The first detection of Chinook entering the hydrophone array was used to create the curve for Dam 2.

4.2 Laboratory Studies on Juvenile Salmon Behavior

Literature reports several laboratory studies on the interplay between flow field variables and downstream migrating juvenile salmon behavioral responses (e.g. Haro et

al. 1998, Kemp et al. 2006, and Enders et al. 2009). Authors report measured flow velocities and velocity gradients together with observed fish behavior. However, values of flow accelerations are rarely mentioned. To determine a_b, two different fish behavior laboratory studies were reproduced using CFD simulations.

4.2.1 Haro et al. (1998)

Haro et al. (1998) investigated the behavior and passage rate of Atlantic salmon ($L \approx$155-240 mm) and juvenile American shad ($L \approx$65-108 mm) passing over a sharp-crested weir.

Experiments were carried out in a flume 3 m wide, 6 m deep, and 38 m long. The total flow over the weir was 2.83 m^3/s. Figure 4.27a displays an overview of the CFD model built to simulate the flow conditions described in Haro et al. (1998). The CFD model spans approximately 8 meters upstream of the weir.

4.2.1.1 Numerical Model and Grids

The Volume of fluid (VOF) model was used to obtain the free surface shape and flow field variables. Mass conservation was achieved using a pressure-velocity coupling PISO algorithm with body force weighted spatial discretization for the pressure. Using a fixed time step size of 0.001 s, statistically converged solutions were achieved after running approximately 50 s. The convergence criterion was the mass flow rate flowing over the weir. A first order upwind scheme was selected for the momentum and $k-\varepsilon$ model equations. A structured grid of about 350,000 nodes was generated using GRIDGEN 15.15, with a typical grid size for the region close the weir of 5 cm, 4 cm, and 7 cm along the *x*, *y*, *z* axes. A 2D view of the grid is shown in Figure 4.27b.

4.2.1.2 Results

Figure 4.27c presents the free surface and velocity isolines predicted by the CFD model of the sharp-crested weir. Results reported by Haro et al. (1998) are also shown in

the same figure. To build the CFD model the width of the weir was estimated from an isometric view presented in Haro et al. (1998), which could explain the discrepancies between the CFD and measured results.

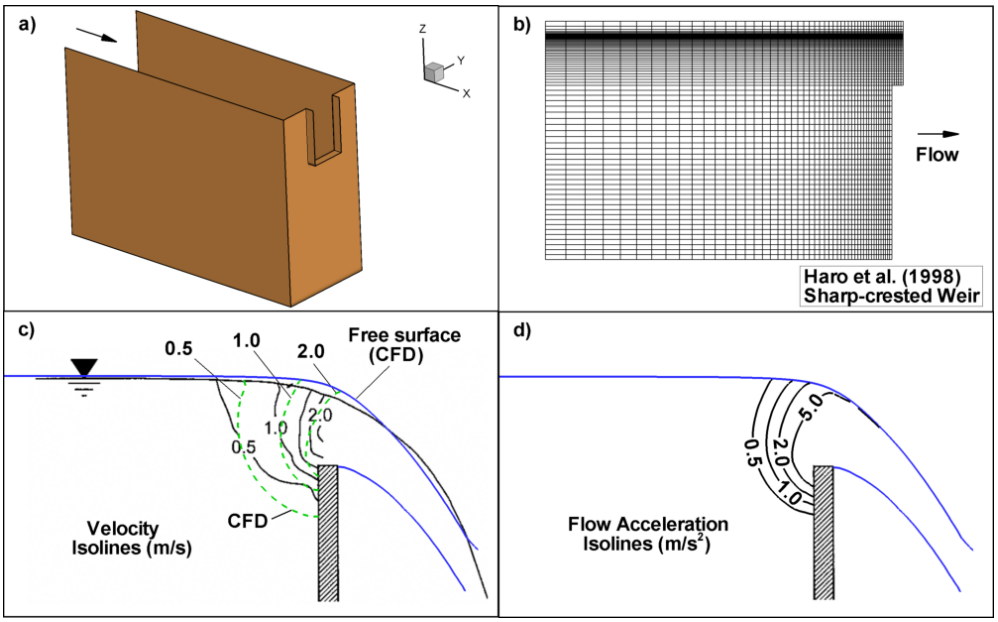

Figure 4.27 Haro et al. (1998). a) CFD model overview, b) Computational mesh, c) Measured and predicted velocity isolines and free surface, and d) Flow acceleration isolines from CFD results.

Flow accelerations in Fig. 4.27d vary from 0.5 m/s^2 to 5.0 m/s^2 over a length of 0.6 m. After 30 and 180 minutes in the flume, 16.7% and 74.3% of Atlantic salmon smolts passed the weir, respectively. Clearly, fish needed time to acclimate to the flow conditions before swimming over the weir. The paper also reported that fish frequently used burst swimming to attempt to escape from velocities above 1 m/s, which corresponds to a flow acceleration of approximately $a_b = 1.6\ m/s^2$, according to the CFD results.

4.2.2 Enders et al. (2009)

Enders et al. (2009) presented the first quantitative study on Chinook salmon ($L \approx 97$ mm) avoidance behavior to rapidly accelerating flows. Movements of fish were recorded when fish were trying to swim through a rectangular orifice. The location at which fish displayed avoidance behavior was reported in the paper. Figures 4.28a and 4.28b show a picture of the experimental setup and the CFD model developed to simulate the flow conditions. The water level was assumed constant (45.8 cm) upstream of the rectangular orifice. The paper did not report the total flow rate through the orifice.

4.2.2.1 Numerical Model and Grids

The VOF model was used to simulate the flow conditions and compute the flow rate through the orifice. To couple pressure and velocity, the SIMPLE algorithm with body force weighted spatial discretization for the pressure was used. After simulating approximately 70 seconds, with a fixed time step size of 0.001 s, statistically converged solutions were achieved. The flow rate at the inlet boundary was modified to achieve the reported water surface elevation. CFD results were obtained with a structured grid of about 530,000 nodes and with grid size close the orifice of 4 mm, 19 mm, and 4 mm along the *x*, *y*, *z* axes. Figure 4.28c presents a view of the grid near the orifice.

4.2.2.2 Results

CFD simulations predicted a flow rate through the orifice of 0.0367 m^3/s. Figure 4.29 displays velocity vectors measured and predicted by the CFD simulation in the test arena. Velocity measurements presented in this figure were taken 2 cm above the bottom of the flume. CFD predicted flow velocities on average 10% higher than the measured value for the region immediately upstream of the orifice.

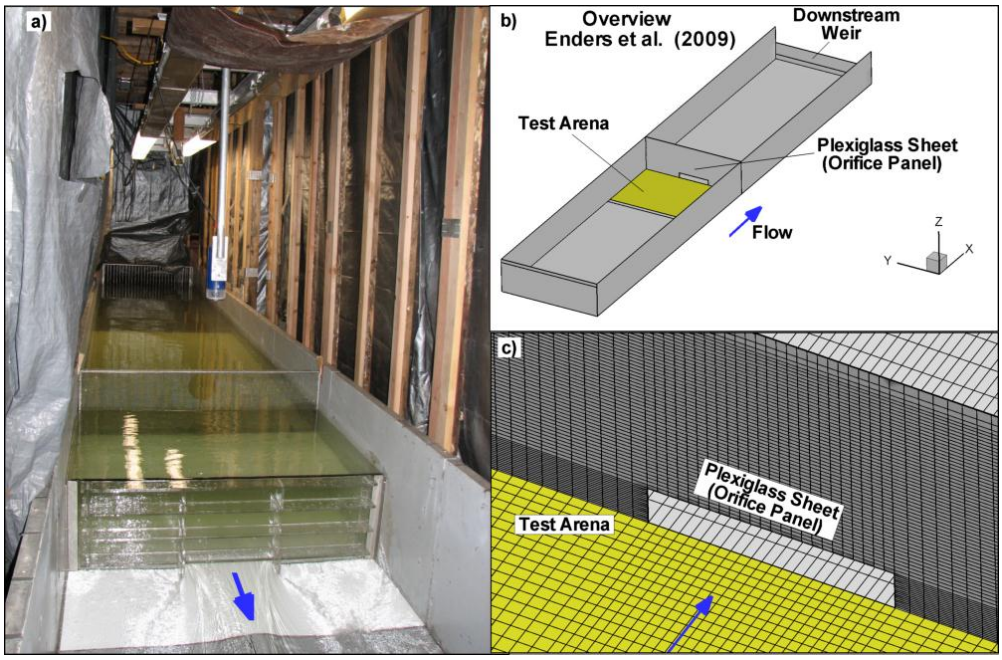

Figure 4.28 Enders et al. (2009). a) Picture of the experimental facility kindly provided by Dr. Eva Enders, b) CFD model overview, and c) Computational mesh.

The CFD model did not account for flume wall's roughness or geometric irregularities in the experimental facility, which could explain the discrepancy between the numerical and experimental results. The paper by Enders et al. (2009) shows plots with the position where Chinook displayed avoidance behavior. Values of a_b, can be determined by superimposing the CFD results on the plots mentioned above. Figure 4.30 displays the recorded positions at the onset of Chinook avoidance behavior together with flow acceleration isolines from CFD results. Arrows represent fish location and arrowheads symbolize the position of the fish head. Figure 4.31 shows the probability density of a_b. The average value of the flow acceleration along the fish length was used to create this figure. For the 68 fish analyzed, the average and standard deviations of a_b were 0.70 and 0.73 m/s^2.

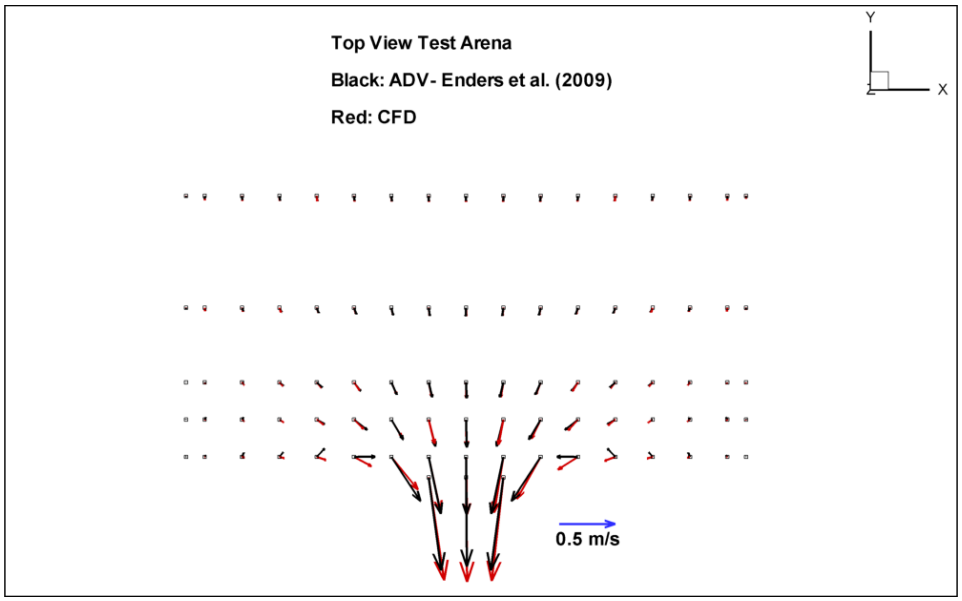

Figure 4.29 Enders et al. (2009). Flow velocity vectors comparison. Acoustic doppler velocimeter data kindly provided by Dr. Eva Enders.

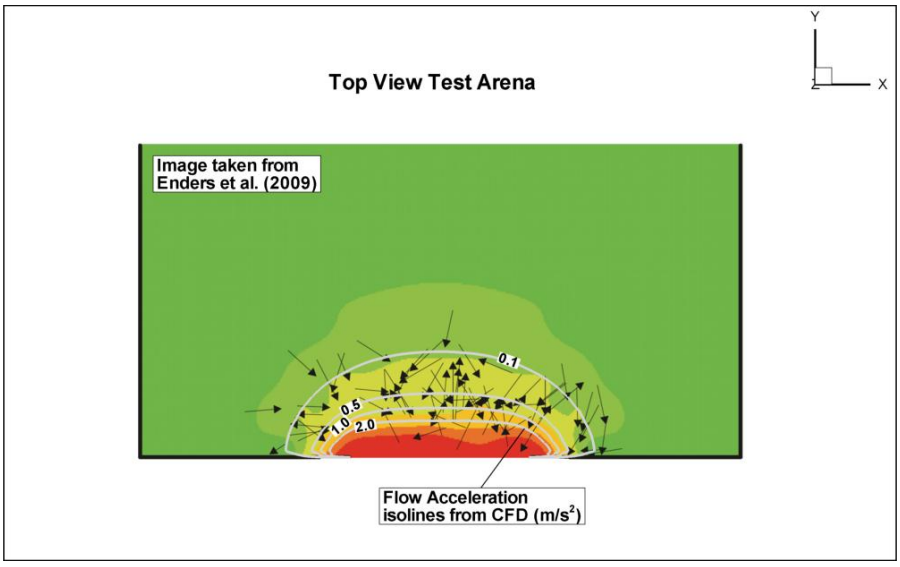

Figure 4.30 Enders et al. (2009). Flow acceleration isolines from CFD. Arrows represent fish location where avoidance behavior was recorded. Arrowheads symbolize fish heads.

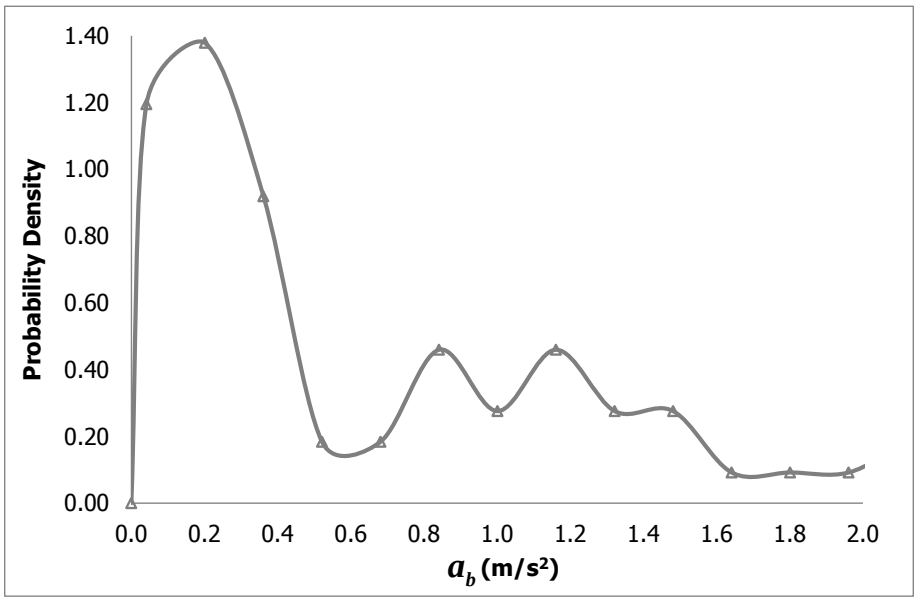

Figure 4.31 Enders et al. (2009). Frequency distribution of averaged flow acceleration that triggered avoidance behavior.

According to the CFD results presented in Chapter III for the simulation 2010_NS and the information displayed in Figure 4.31, juvenile salmon swimming in Dam 1 forebay are likely to start showing avoidance behavior approximately 2 and 1.5 meters upstream of the surface collector entrance and turbine intakes, respectively. At Dam 2, avoidance behavior is likely to begin approximately 4 meters upstream of the top-spill entrance and 9 m upstream of the spillway gates.

CHAPTER V

FMM PARAMETERS

The first part of this chapter presents the linkage between the results discussed in Chapter IV and FMM parameters. Analyzed measured trajectories showed Chinook behavior under a limited range of flow accelerations. No data were available for fish swimming in the low flow acceleration (a <1.0x10^{-4} m/s^2) zone upstream of Dam 1. This chapter shows a parametric study of some variables used to describe fish behavior when swimming in regions with low flow acceleration.

5.1 FMM Parameters

FMM parameters rely, for the most part, on the preceding analyses of juvenile salmon measured trajectories and fish behavior laboratory studies. Table 5.1 shows the relation between the model parameters presented in Table 2.2 and the figures of Chapter IV.

van Netten (2006) derived threshold values of hydrodynamic detection of the fish canal lateral line and line organ. Following van Netten (2006), FMM assumes that the minimum value of flow acceleration detected by juvenile salmon is $a_d = 10^{-4} m/s^2$. Under natural flow conditions, fish do not impact walls even in the absence of light. Fish wall avoidance is most likely achieved by the combination of visual capabilities and flow field variables detection. Changes in the flow field variables near walls should also help fish avoid impacting obstacles. Trying to accurately capture the flow field near walls could lead to computationally expensive simulations when simulating hydrodynamics at hydroelectric facilities scale. Fish obstacle detection and avoidance should not play a major role in deciding final migration route when juvenile salmon are swimming in forebays and tailraces. Juvenile salmon length scale is approximately two orders of magnitude smaller than the length scale of typical hydraulic structures at hydroelectric

facilities. FMM simplifies fish interactions with obstacles by defining d_d and d_a. Values for these parameters that yield model results comparable to observed Chinook trajectories are $d_d = 15L$ and $d_a = 5L$.

The information presented in Figure 4.21 was obtained for Chinook swimming in sustained mode. FMM assumes that when flow acceleration is higher than a_b fish swim in burst mode. Domenici and Blake (1997) reported frequency distributions of fish escape trajectories (away responses) in response to stimuli. Based on this information, FMM randomly selects values of α from the intervals [-180°,-130°] and [130°, 180°] when simulated fish are exposed to flows with accelerations above a_b.

The model parameters a_b and P_m represent characteristics that are different for each simulated fish. At the beginning of every simulation, these two parameters are randomly defined for each simulated fish and remain constant throughout the simulation. On the other hand, t_{as}, t_g, P_g, $\left|\overline{F}_T\right|$, α, and θ change over time as a function of the flow acceleration and obstacle detection.

5.2 Parametric Study

The CFD results presented in chapter III for the case 2005_S were used to carry out the parametric study. FMM results were compared against measured percentages of fish passing through the powerhouse, spillway, and surface collector. Four different parameters were analyzed. Number of simulated fish, initial spatial distribution, α for $a <$ 1.0x10^{-4} m/s^2, and the pressure threshold P_m. Table 5.2 presents the conditions for the eleven simulations used in this parametric study. For all the simulations, the simulated fish were released approximately 850 m upstream of the spillway. A top view of the release cross section AB is presented in Figure 5.1a. 24,000, 12,000, 6,000, and 3,000 simulated fish were released in order to assess the effect of the number of simulated fish on model results statistics. As part of this parametric study, different fish horizontal spatial distributions were tested for the initial condition. Figure 5.1b displays

the distributions. Distribution P1 evenly spreads simulated fish across the river width. Distributions P2, P3, and P4 follow a normal distribution with standard deviation of 150, 100, and 50 m, respectively. Johnson et al. (2000) and Johnson et al. (2006) reported that juvenile salmon roughly follow the bulk of the flow when approaching dams. For $a < a_d$, α was assumed to be uniformly distributed in the [-50°, 50°], [-70°, 70°], and [-90°, 90°] intervals.

Table 5.1 FMM parameters.

Symbol	Meaning	Modeled by
a_d	minimum flow acceleration detected by the fish lateral line	1.0×10^{-4} m/s^2
a_b	flow acceleration threshold for BM	see Figure 4.31
d_a	obstacle avoidance distance	5L
d_d	obstacle detection distance	15L
t_{as}	active swimming time	see Figure 4.25
t_g	gliding time	see Figure 4.25
P_g	probability of gliding	see Figure 4.24 (for a <5.0×10^{-4} m/s^2 the curve was extrapolated)
P_m	pressure threshold	see parametric study
$\lvert\vec{F}_T\rvert$	magnitude of the fish swimming thrust	see Figure 4.20 (for a <5.0×10^{-4} m/s^2 the curve for 5.0×10^{-4} m/s^2 was taken)
α	angle between the fish thrust and flow velocity in the XY plane	see Figure 4.21 (for a <1.0×10^{-4} m/s^2 see parametric study)
θ	swimming inclination from the vertical axis	see Figure 4.22 (for a <5.0×10^{-4} m/s^2 the curve for 5.0×10^{-4} m/s^2 was taken)

Table 5.2 Parametric study simulations.

		Simulations										
		S1	S2	S3	S4	S5	S6	S7	S8	S9	S10	S11
Number of Simulated Fish	24000	⊗										
	12000		⊗									
	6000			⊗								
	3000				⊗	⊗	⊗	⊗	⊗	⊗	⊗	⊗
Initial Spatial Distribution	P1					⊗						
	P2						⊗					
	P3	⊗	⊗	⊗	⊗				⊗	⊗	⊗	⊗
	P4							⊗				
α for $a <$ $1.0\text{x}10^{4}$ m/s^{2}	[-50°,50°]	⊗	⊗	⊗	⊗	⊗	⊗	⊗			⊗	⊗
	[-70°,70°]								⊗			
	[-90°,90°]									⊗		
P_m	No P_m										⊗	
	Dam 1											⊗
	Dam 2	⊗	⊗	⊗	⊗	⊗	⊗	⊗	⊗	⊗		

Three different simulations were run to evaluate the effect of the pressure threshold on FMM predictions. Pressure thresholds given by the swimming depths curves for Dam 1 and Dam 2 were used (see Figure 4.26). A simulation without any pressure threshold was also run.

5.2.1 Number of Simulated Fish

Results are shown in Figure 5.2. For the tested number of simulated fish, model predictions show minor variations. The 24,000 simulation results were used to estimate the relative errors. The maximum errors for predictions for the surface collector, units 1-2, units 3-11, and spillway, were -3.5, 2.7, -2.9, and 5.0%, respectively. The average

relative errors for the simulations with 12,000, 6,000, and 3,000 simulated fish were 1.5, 2.2, and 2.8%, respectively. The CPU time required for the simulations with 24,000, 12,000, 6,000, and 3,000 simulated fish to run the first 2,500 time steps was 504, 253, 175, and 160 minutes, respectively.

5.2.2 Initial Spatial Distribution

Figure 5.3 presents the percentages of fish passed predicted by the model. As the standard deviation of the spatial distribution decreases, FMM tends to predict fewer fish passing through the spillway and surface collector and more fish passing through the units 3-11 and 1-2. The relative differences between the simulations with the distributions P1 and P4 are -4.8, 8.9, 23.9, and -76.7% for percentages of fish passing the surface collector, units 1-2, units 3-11, and spillway, respectively.

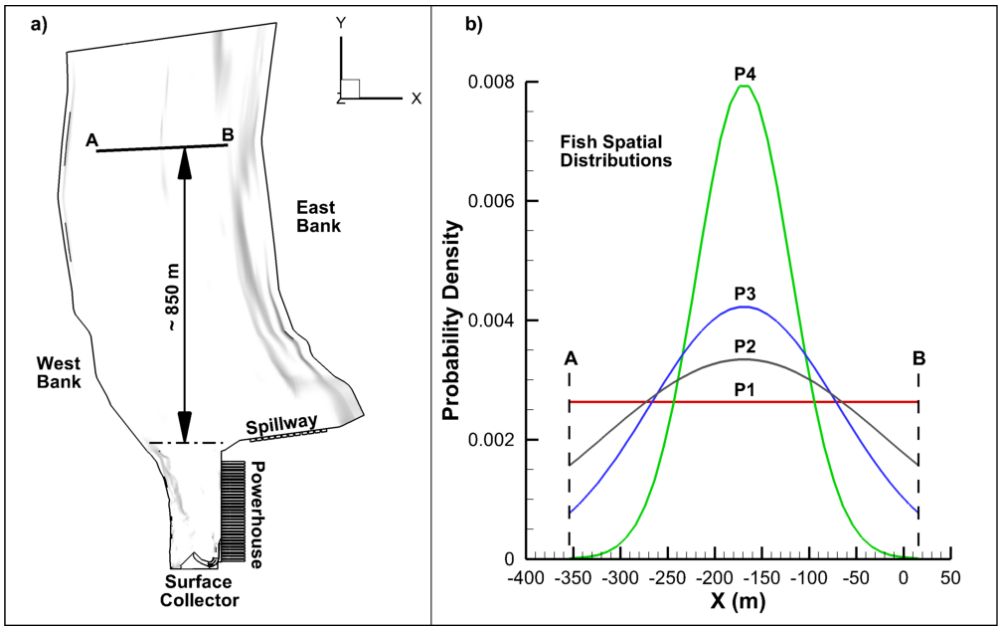

Figure 5.1 Dam 1. Release cross section AB and initial spatial distributions.

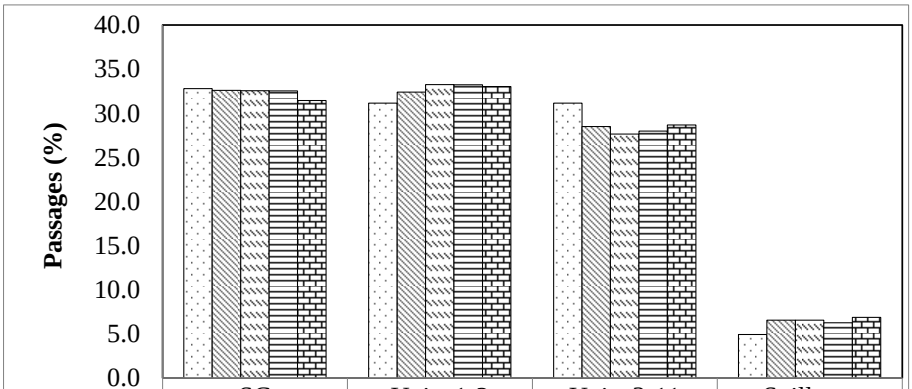

	SC	Units 1-2	Units 3-11	Spillway
Measured	32.8	31.1	31.1	4.9
24000(S1)	32.6	32.4	28.5	6.5
12000(S2)	32.5	33.3	27.6	6.6
6000(S3)	32.5	33.2	28.0	6.3
3000(S4)	31.4	33.0	28.7	6.9

Figure 5.2 FMM predictions for a different number of simulated fish.

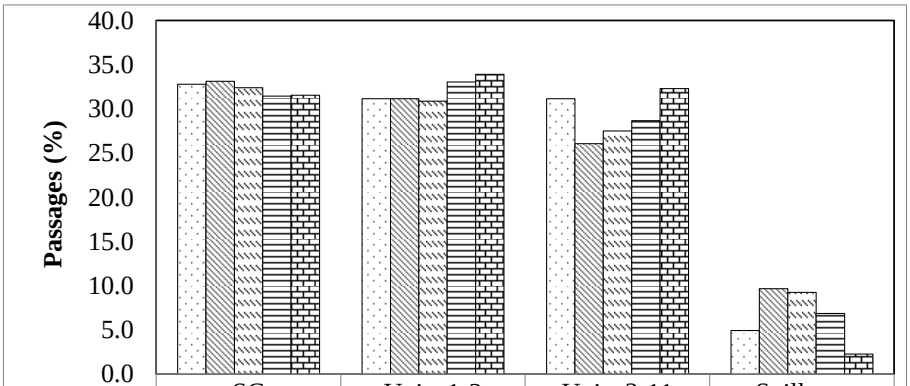

	SC	Units 1-2	Units 3-11	Spillway
Measured	32.8	31.1	31.1	4.9
P1(S5)	33.1	31.2	26.1	9.7
P2(S6)	32.4	30.9	27.5	9.2
P3(S4)	31.4	33.0	28.7	6.9
P4(S7)	31.5	33.9	32.3	2.3

Figure 5.3 FMM predictions for different initial horizontal distributions.

At a distance of approximately 300 m upstream of the dam, most (~90%) of the simulated fish that left the domain through the spillway swam within 200 m from the East bank. The distribution P4 concentrates simulated fish in the center of the forebay and prevents fish that roughly follow the flow from swimming in the spillway region.

Comparing the results of the simulations with distributions P1 and P4, it is possible to conclude that the percent of the simulated fish that did not pass through the spillway ended up passing, for the most part (~83%), through the units 3-11. In the simulation with the distribution P4, more fish entered the powerhouse zone close to the turbine intakes increasing their chances of being trapped by the turbine flow.

The simulation with the distribution P3 yielded the closest results to the measured data. Average relative errors, with respect to the measured data, for the simulations with distributions P1, P2, P3, and P4 are 28.5, 25.4, 14.4, and 17.6%, respectively.

Fish passages predicted for the surface collector were less influenced by the initial horizontal distribution than predictions for the turbines and spillway. The average value of the pressure threshold P_m for the simulated fish that passed through the surface collector corresponds to a depth of 11.8 m. For the simulated conditions at Dam 1, the surface collector is the only possible outlet for fish swimming in the first 12 m of the water column and thus fish swimming close to the free surface are prone to passing downstream through the surface collector.

5.2.3 Swimming Direction in Low Acceleration Flows

Model predictions are presented in Figure 5.4. The effect of allowing simulated fish to deviate from the flow direction is more evident in spillway passages predictions. By using the [-90°, 90°] interval in place of the [-50°, 50°] interval, model predictions for spillway passages increased by about a factor of 1.3.

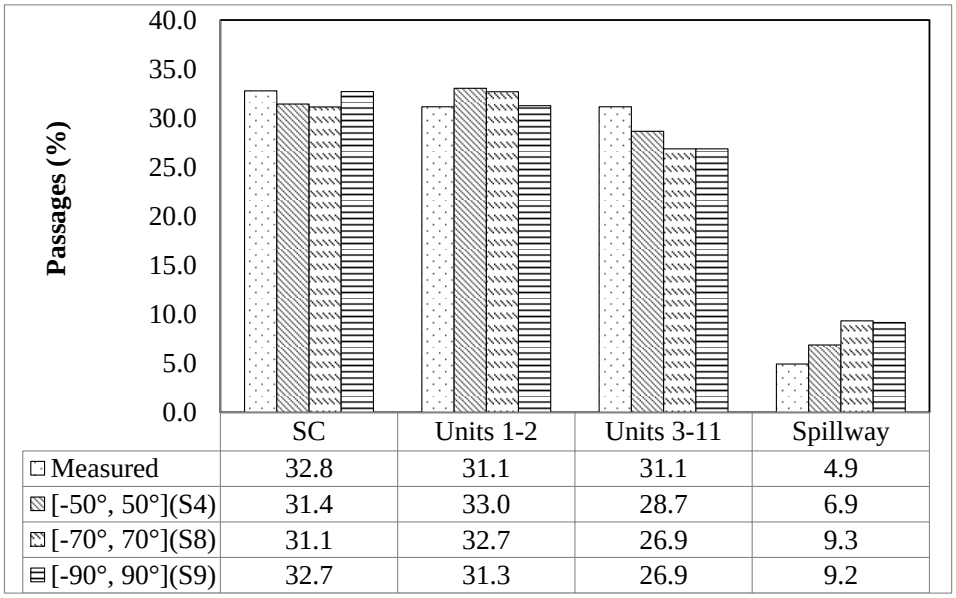

	SC	Units 1-2	Units 3-11	Spillway
Measured	32.8	31.1	31.1	4.9
[-50°, 50°](S4)	31.4	33.0	28.7	6.9
[-70°, 70°](S8)	31.1	32.7	26.9	9.3
[-90°, 90°](S9)	32.7	31.3	26.9	9.2

Figure 5.4 FMM predictions for different distributions of α.

5.2.4 Pressure Threshold

Figure 5.5 shows the model results for the three simulations. According to FMM formulation, the pressure threshold defines the region in the water column that every simulated fish tries to occupy. In a simulation without pressure threshold, simulated fish move up and down following the distribution of θ. With a pressure threshold, a simulated fish also moves up and down following the distribution of θ but if the pressure detected is beyond the pressure threshold, the fish tries to move upwards. The simulation without pressure threshold predicts approximately one third of the measured passages through the surface collector. For this simulation, approximately half of the fish left the domain through the units 3-11. These results demonstrate the need for including a pressure threshold in the model formulation. The simulations with no pressure threshold, and Dam 1 and Dam 2 pressure thresholds have average relative errors of 36.3, 23.5, and 14.4 % when compared against the measured data.

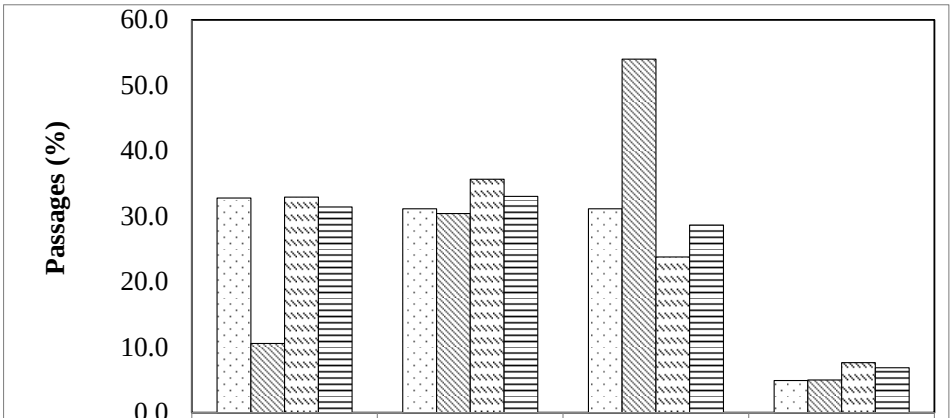

	SC	Units 1-2	Units 3-11	Spillway
Measured	32.8	31.1	31.1	4.9
No Pm(S10)	10.6	30.4	54.0	5.0
Dam 1(S11)	32.9	35.6	23.8	7.6
Dam 2(S4)	31.4	33.0	28.7	6.9

Figure 5.5 FMM predictions for different pressure thresholds.

5.2.5 Conclusions

The results above show that for the 2005_S flow field, the simulation (S4) that better matched measured passages has the following conditions. The pressure threshold following the curve for Dam 2 in Figure 4.26, for $a < a_d$, α was uniformly distributed in the [-50°, 50°] interval, and the initial spatial distribution P3.

FMM results are most affected by changes in the pressure threshold. Assuming that simulated fish do not have a tendency to occupy different parts of the water column yielded relative errors of approximately 70% for the surface collector predictions. Different values of α (in the region of low flow acceleration) and the spatial initial distribution affect, for the most part, FMM predictions for the spillway and units 3-11. FMM predictions for the surface collector are not significantly affected by these two parameters.

CHAPTER VI

FMM APPLICATION TO THE FOREBAY OF TWO HYDROPOWER DAMS

FMM was used to predict juvenile salmon migration route selection in the forebays of Dam 1 and Dam 2. Results were compared against data from acoustically tagged fish and passive particles. Model parameters are presented in Table 5.1. Parameters that yielded best results in the parametric study of the preceding chapter were used.

6.1 Dam 1 Forebay

The performance of FMM was compared against the reported Chinook migration route selection and the recorded fish trajectories. Table 3.1 shows the flow conditions. After simulating approximately 7,000 s, about 3.0% of the simulated fish were trapped in the recirculation zones shown in Figures 3.3a-3.5a and 3.3b-3.5b. Statistics presented below excluded the information from the trapped fish.

6.1.1 Migration Route Selection

Table 6.1 shows percent of Chinook passages through the four recorded migration routes at Dam 1 forebay. Measured data and results from FMM and passive particles are also presented. In Table 6.1, the column error shows the relative error between the measured values and FMM predictions. M and P stand for measured and passive particles, respectively. Figures 6.1, 6.2, and 6.3 show bar diagrams with the information presented in Table 6.1 for the cases 2004_S, 2005_S, and 2010_NS, respectively.

FMM outperformed passive particle predictions under the three conditions simulated except in the predictions of spillway passage and units 1-2 passage for the case 2004_S. In a consistent way with the flow distribution shown in Table 3.1, most of the

passive particles were drawn towards the turbines. Estimation of percent of fish passages through migration routes based solely on the percent of total river flow does not yield good results at Dam 1 forebay. The surface collector drew about 4.5% of the total river flow and attracted approximately 30.0% of the migrants. Behavioral rules are needed to simulate the portion of the fish avoiding being drawn by the turbine intakes.

Table 6.1 Chinook passages at Dam 1.

	2004_S (%)				2005_S (%)				2010_NS (%)			
	M	P	FMM	Error	M	P	FMM	Error	M	P	FMM	Error
SC	29.8	0.0	28.2	-5.3	32.8	0.0	31.4	-4.1	31.8	2.1	30.8	-3.1
Units 1-2	28.4	33.4	37.1	30.6	31.1	34.3	33.0	6.1	32.2	21.8	29.6	-8.2
Units 3-11	24.4	50.5	26.8	9.6	31.1	52.2	28.7	-8.0	36.0	76.2	39.6	10.1
Spillway	17.4	16.2	7.9	-54.4	4.9	13.5	6.9	39.6	0.0	0.0	0.0	0.0

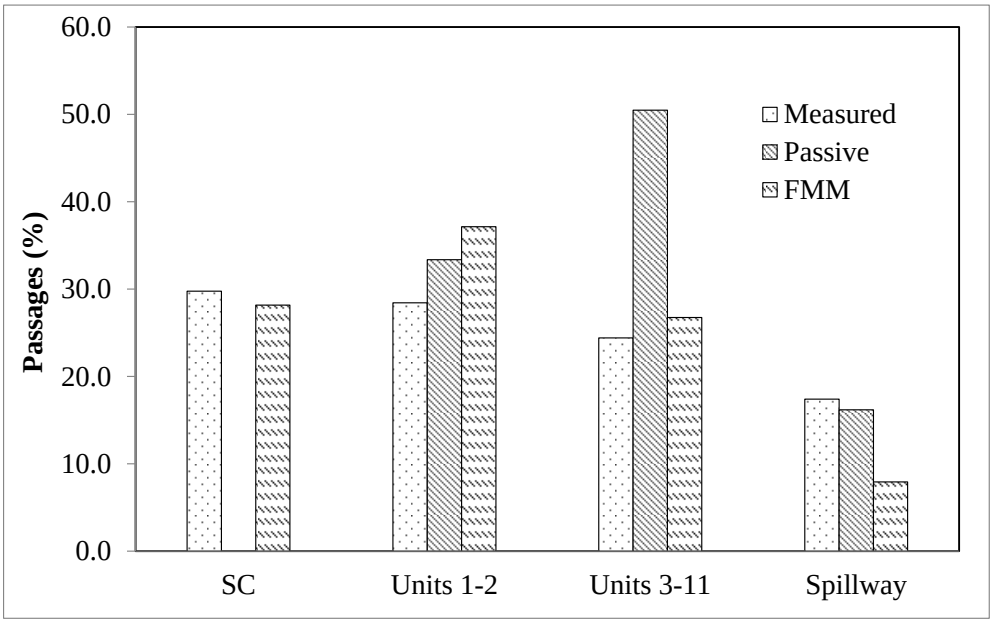

Figure 6.1 Chinook passages. Dam 1. Case: 2004_S.

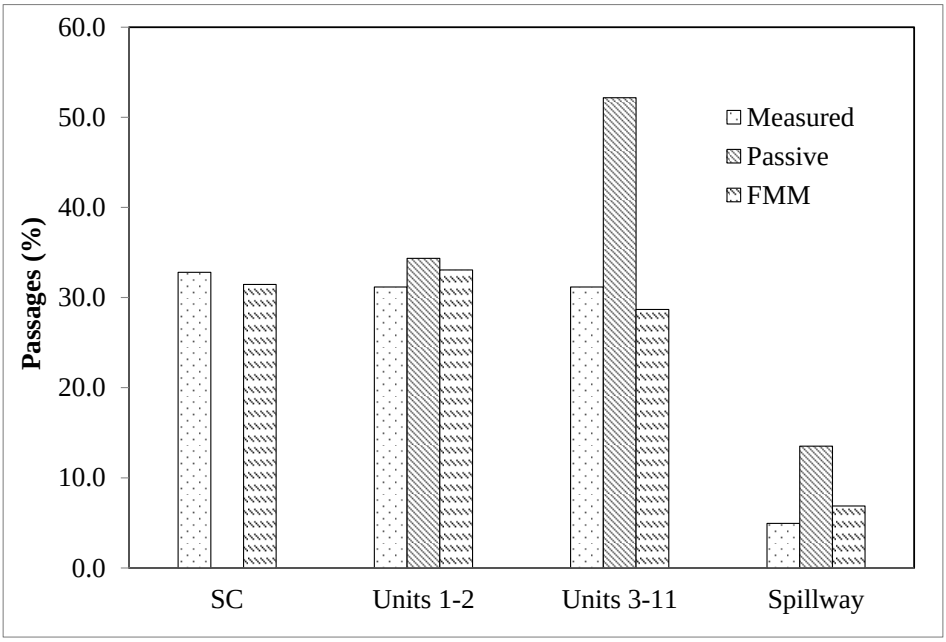

Figure 6.2 Chinook passages. Dam 1. Case: 2005_S.

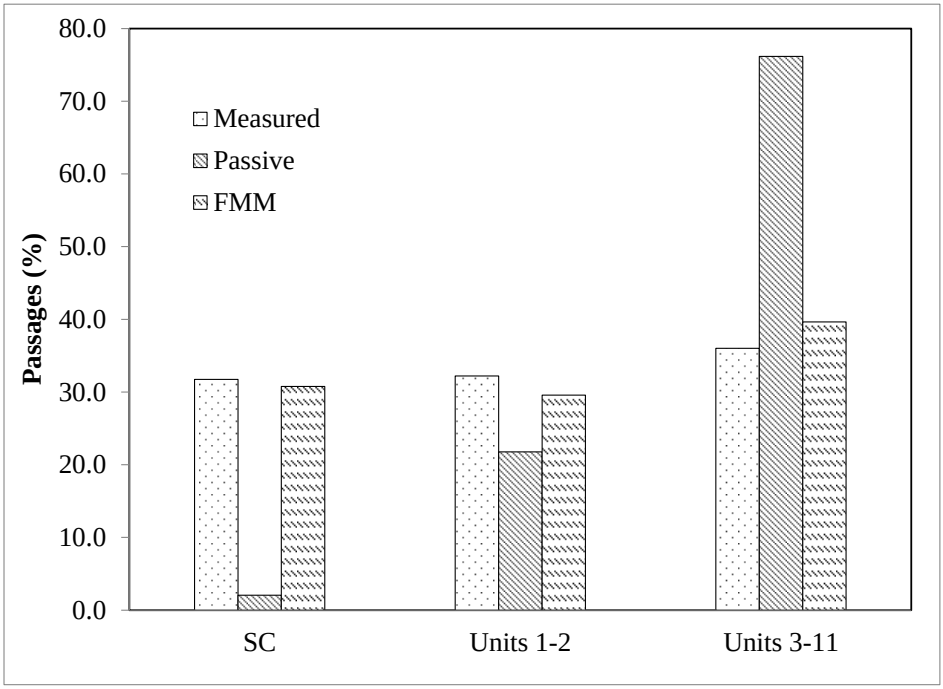

Figure 6.3 Chinook passages. Dam 1. Case: 2010_NS.

Model predictions for the case 2010_NS showed the lowest relative errors. Results for the case 2004_S showed the biggest discrepancies between model predictions and measured data. FMM predictions for the surface collector were the closest to the measured data and spillway passages showed the highest relative errors.

The probability distributions used to represent the model parameters were determined using the flow field of simulation 2010_NS, which could explain the better performance of the model for those flow conditions.

FMM results underpredicted the percent of Chinook passing through the surface collector. However, the overall trend was captured with the highest and lowest percentages predicted for the cases 2005_S and 2004_S, respectively. For the surface collector, relative errors between model predictions and measured values were below 6%.

The total percent of fish passing through the turbines was, on average, overpredicted by about 20% for the case 2004_S. For the cases 2005_S and 2010_NS, errors were within ± 10%. The results presented above show that the proposed model to represent fish swimming trajectories performed well when predicting migration route selection in the powerhouse region of Dam 1 forebay.

FMM underpredicted and overpredicted Chinook passages through the spillway for the cases 2004_S and 2005_S, respectively. However, in a consistent manner with the measured data, higher percent of passage was predicted for 2004_S than for 2005_S.

6.1.2 Trajectories

Figure 6.4a shows a top view of the Dam 1. Simulated fish were released from the line AB. Lines C, D, E, and F are placed at values of the Y coordinate of 1,100, 500, 300, and 100 m, respectively. The travel times predicted by the model between the lines C and D have an average value of 2,177 s and a standard deviation of 598 s. CFD simulations predicted an average fluid velocity of 0.25 m/s for the same segment CD.

The flow acceleration in the segment CD is, for the most part, below a_d and therefore simulated fish swam roughly in the direction of the flow. That explains why simulated fish have, on average, faster migration rates (0.28 m/s) than the flow velocity.

For the 2010_NS conditions, Figure 6.4b displays the residence time probability density for the segment EF for both measured trajectories and simulated fish. For this segment, the average flow velocity was in the order of 0.6 m/s. The vertical dashed line in Figure 6.4b shows the average residence time of an inert particle. Statistics were calculated with 338 and 1,052 measured trajectories and simulated fish, respectively.

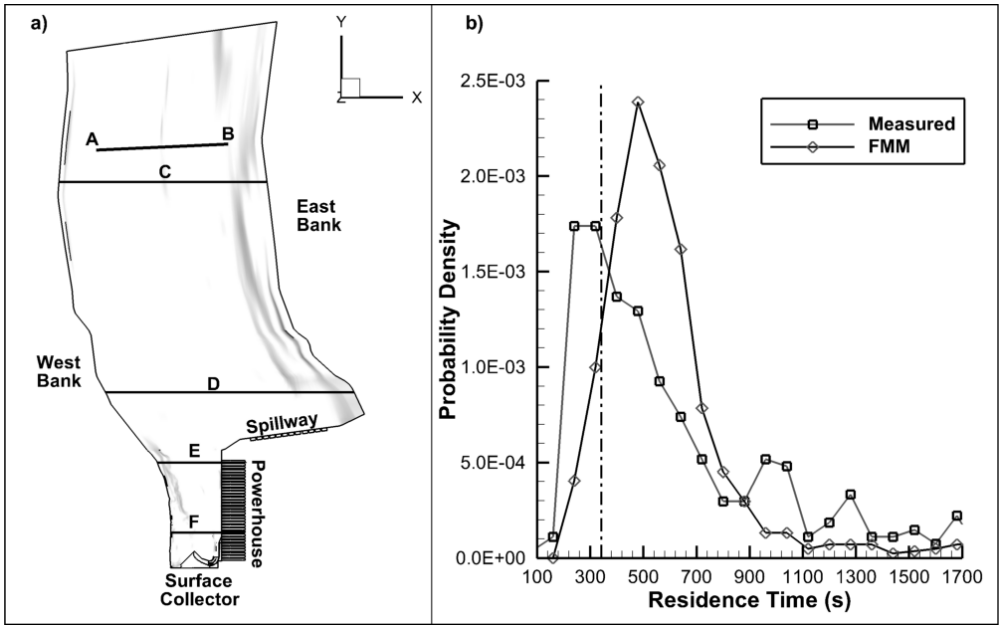

Figure 6.4 Dam 1. Release cross section AB and residence time probability density for the segment EF.

About 15% of the tagged Chinook and 4% of the simulated fish travelled faster than the inert particles. In the segment EF, the average and standard deviation of the residence times were 559 and 204 s for the simulated fish, respectively. The same

parameters were 563 and 324 s for the tagged Chinook, respectively. Average travel times predicted by FMM were in agreement with measured data.

Tiffan et al. (2009) studied migratory behavior of subyearling fall Chinook salmon in different reaches of the Snake River. That study found that fast migrants travelled 1.5 times faster than the average flow velocity. Slow migrants travelled at a rate of 0.6 times the flow velocity. In the segment CD, simulated fish travelled, on average, at a rate 1.1 times the average flow velocity. Average travel times for the segment EF show that simulated fish move downstream at a rate 0.59 times the flow velocity. Migration rates predicted by FMM fall within the interval reported in Tiffan et al. (2009).

Figure 6.5a shows a top view of the powerhouse region of Dam 1. Four different simulated fish trajectories, A, B, C, and D are presented in this figure. Variations in swimming elevations are displayed in Figure 6.5b. The main direction of the fish movement is from top to bottom and left to right in the Figures 6.5a and 6.5b, respectively.

For trajectories A, B, C, and D, Table 6.2 presents the total travel time, the percent of gliding, and the value of the model parameter P_m expressed in meters. Simulated fish detecting pressures higher than P_m try to swim upwards. Trajectory A shows a fish that left the domain through the surface collector whereas fish in trajectories B, C, and D passed downstream through the powerhouse units.

As presented in Table 6.2, fish A and C have similar values of the parameter P_m but FMM predicted different passage routes for those fish. Despite both fish having the tendency to occupy the first 13 m of the water column, fish A passed through the surface collector and fish C through the turbines. Fish A entered the powerhouse zone swimming towards the West bank and kept moving downstream until it found the surface collector. It always swam at distances from the turbine intakes of 18 m or greater.

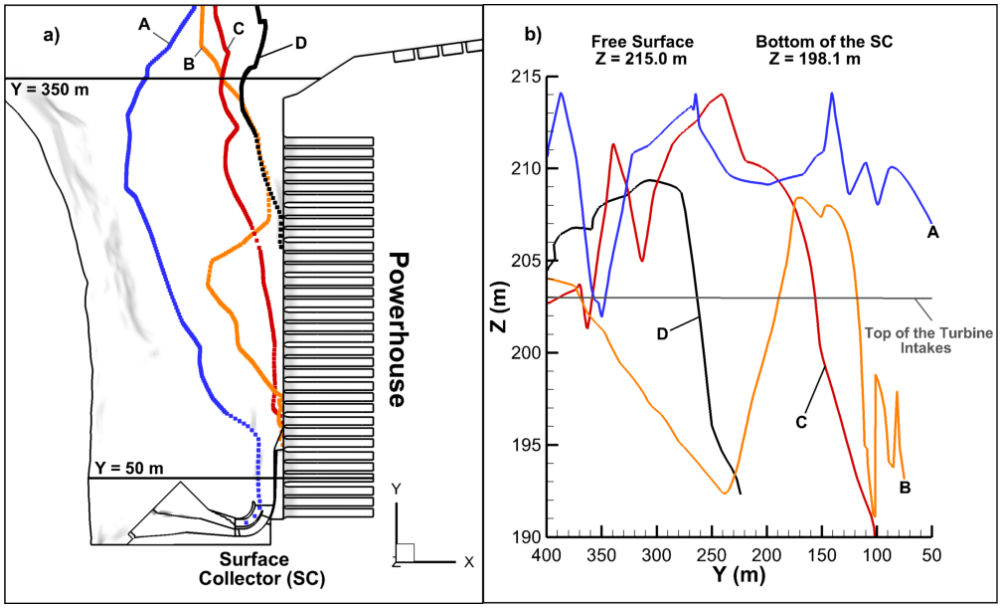

Figure 6.5 Dam 1. Simulated fish trajectories.

Table 6.2 Trajectories in Figure 6.5.

Trajectory	Time (s)	Gliding (%)	P_m (m)
A	3480.0	27.6	13.07
B	4515.0	47.1	19.7
C	3510.0	28.9	13.7
D	3120.0	26.0	26.4

On the other hand, as fish C moved downstream it approached the turbine intakes until it was finally overpowered by the turbine flow. Values of P_m of 19.7 and 26.4 m enabled fish B and D to swim in deeper regions than fish A and C. It is important to clarify that high values P_m do not necessarily mean that simulated fish occupied deep regions. For example, fish D entered the powerhouse region swimming at a depth of about 10.0 m. Fish actual swimming depth is ultimately given by the interaction between P_m, $\left|\overline{F}_T\right|$, θ, and the flow field.

6.2 Dam 2 Forebay

FMM results were compared against the reported fish migration route selection. No measured trajectories were available for Dam 2. Timko et al. (2007) assessed the passage behavior of juvenile salmon at Dam 2 forebay. Acoustic tag receivers were placed as far as 150 m upstream of the dam. Table 3.2 shows the flow conditions. The same model parameters used at Dam 1 were used. 3,000 particles were released 2,000 m upstream of the dam and the standard deviation of the initial spatial distribution P3 (see Figure 5.1) was scaled by the ratio of Dam 1 to Dam 2 forebay widths. After about 8,500 s of simulation time, approximately 2.5% of simulated fish were unable to leave the domain. A top view of Dam 2 forebay and the release cross-section AB are presented in Figure 6.6a. Figure 6.6b displays the horizontal spatial initial distribution.

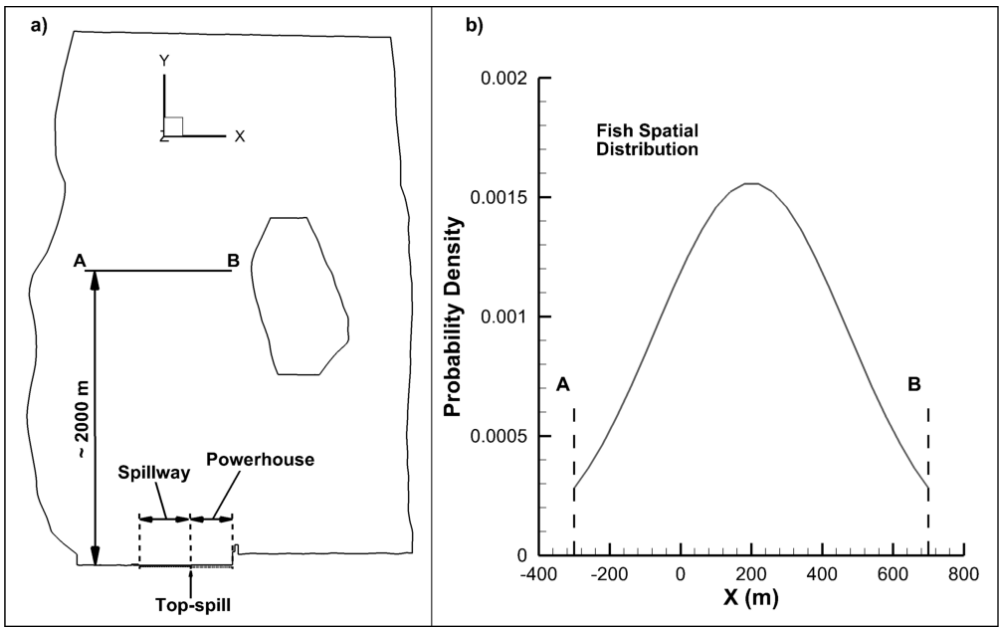

Figure 6.6 Dam 2. Release cross section AB and initial spatial distribution.

6.2.1 Migration Route Selection

Table 6.3 presents percentages of fish passages through the spillway, top-spill, and powerhouse. This table shows results for monitored Chinook, passive particles, and simulated fish. The column Error shows the relative error between measured and FMM predicted passages. M and P stand for measured and passive particles, respectively.

In contrast to Dam 1, at Dam 2 the reported Chinook passages followed the same trend as the distribution of the total river flow. The reported percentages of fish passed were 4.0%, 82.0%, and 14.0% through the top-spill, spillway and powerhouse, respectively. Percent of river flow through these migration routes were 0.6%, 62.8%, and 36.6%.

Table 6.3 Chinook passages at Dam 2.

	2002MOA (%)			
	M	P	FMM	Error
Top-spill (Bay 22)	4.0	0.8	1.6	-58.9
Spillway	82.0	67.7	85.3	4.0
Powerhouse	14.0	31.5	13.1	-6.5

Passive particles showed results consistent with the flow distribution. Percent of passages for the monitored fish, passive particles, and simulated fish are displayed in Figure 6.7. FMM shows better results than passive particles. FMM underpredicted the powerhouse passages with a relative error of -6.5% and overpredicted passages through the spillway with a relative error of 4.0%. FMM predictions for the top-spill have the biggest discrepancies with measured data.

6.2.2 Trajectories

On average, it took longer for simulated fish to pass downstream through the powerhouse than through either the spillway or the top-spill. Average travel times for

simulated fish passing through the top-spill, spillway, and powerhouse were 5,200, 5,328, and 5,507 s, respectively. The fastest simulated fish passed downstream in 3,108 s through the spillway. The slowest selected the powerhouse as its migration route and spent 8,295 s in Dam 2 forebay. Table 6.4 shows the travel time statistical parameters for simulated fish passing downstream through the top-spill, spillway, and powerhouse.

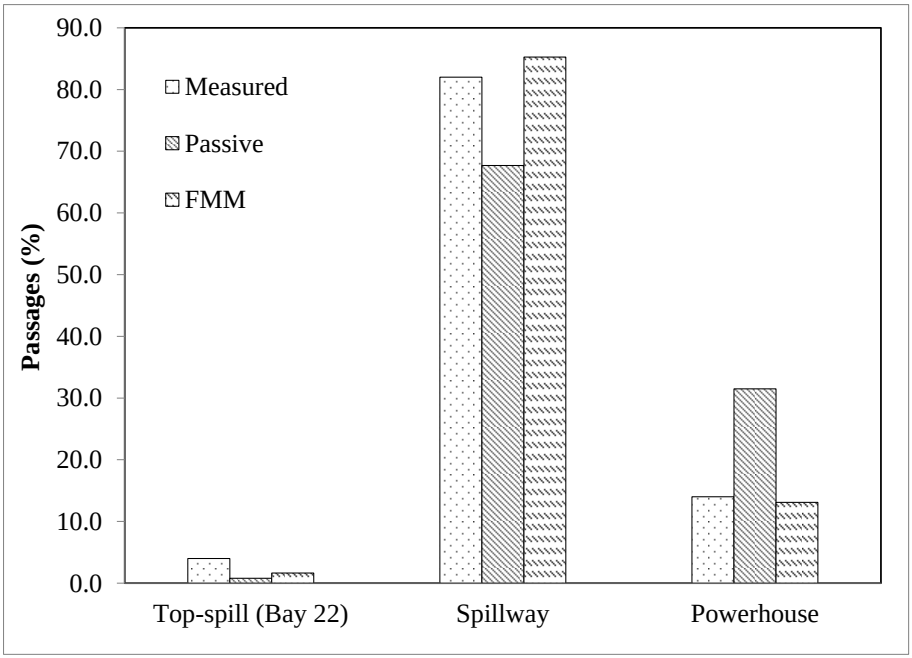

Figure 6.7 Chinook passages. Dam 2. Case: 2002MOA.

Table 6.4 Travel time statistics.

	Travel Times (s)			
	Mean	STDEV	Min	Max
Top-spill (Bay 22)	5200.1	638.0	3830.0	7262.0
Spillway	5328.1	553.9	3108.0	8154.0
Powerhouse	5506.9	639.0	4265.0	8295.0

According to the model assumptions, simulated fish swimming in flows with accelerations below a_d try to roughly follow the flow and α is selected from the [-50°, 50°] interval. Figure 4.21 shows that for values of flow accelerations above a_d fish try to swim tail first which could slow fish migration rate. Figure 6.8 presents average cross-sectional flow velocity and simulated fish velocity at different distances from Dam 2. For distances of 200 m or more, simulated fish migrated faster that the flow velocity. At 300 m upstream of the dam, the ratio between fish velocity and flow velocity was 1.4. For greater distances, the ratio was about 1.6. As mentioned above, Tiffan et al. (2009) reported ratios of 1.5 and 0.6 for fast and slow migrants.

According to Tiffan et al. (2009), FMM tends to overpredict fish velocities for the region upstream (> 300 m) of the dam. It is worth noting that the ratio between fish and flow velocity at Dam 1 was 1.1 for the region with low flow acceleration.

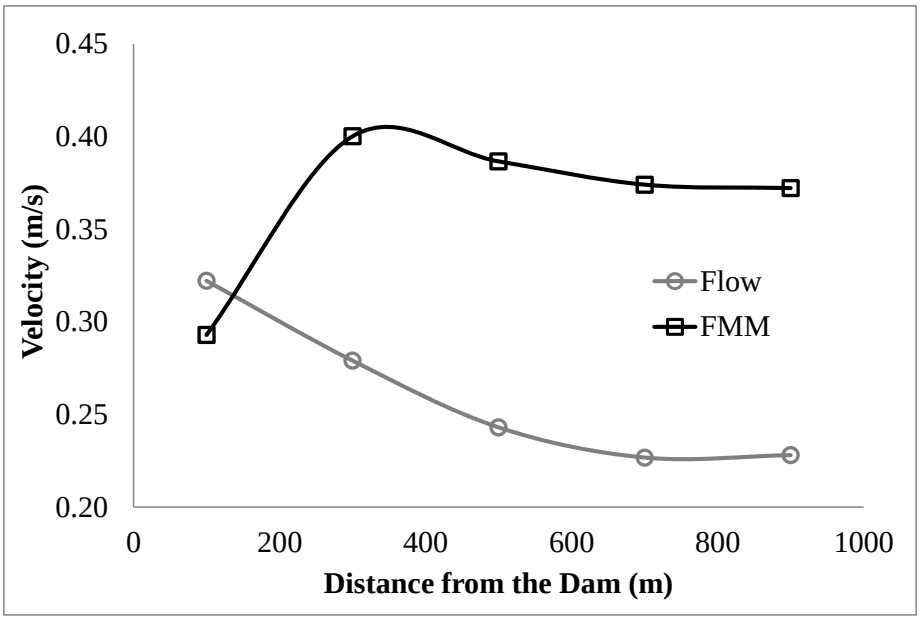

Figure 6.8 Average flow and simulated fish velocities.

In Figure 3.11b, the region with flow accelerations above a_d extends up to approximately 200 m upstream of the dam. In that region the swimming direction of simulated fish is given by the probability distributions in Figures 4.21 and 4.22. As presented in Figure 6.8, within 200 m from the dam, average simulated fish velocity is smaller than the average flow velocity.

The median of the residence times reported for Chinook, for all migration routes, was 1,080 s (Timko et al. 2007). Fish residence times were calculated as the difference between the last and the first fish detections. Information on the location of fish first detection was not given in Timko et al. (2007). A reasonable assumption for tag receiver's detection range is 50-150 m. Under this assumption, the reported Chinook residence times were calculated for fish swimming within 300 m of Dam 2. Figure 6.9 shows the probability densities of residence time for simulated fish swimming within 200 and 300 m of Dam 2. Residence times for the region within 200 m of Dam 2 have an average and standard deviation of 682.9 and 406.2 s, respectively.

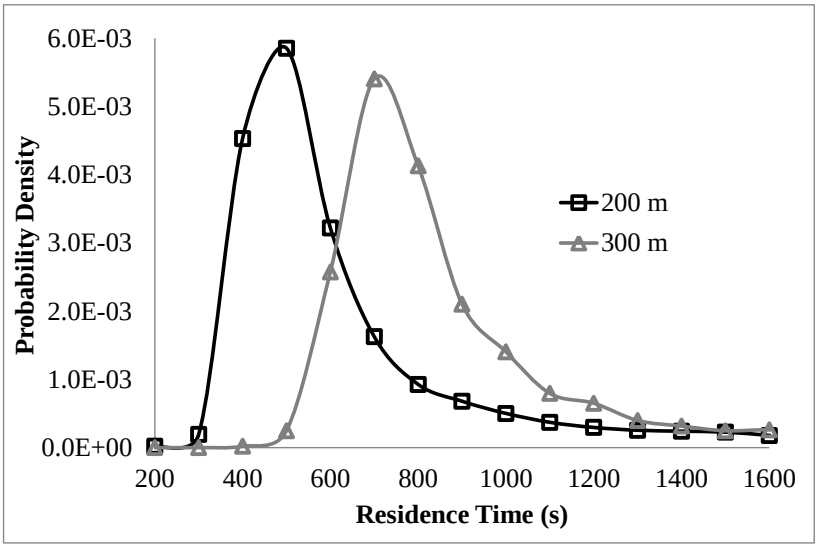

Figure 6.9 Residence time probability densities.

Values of the same statistical parameters are 923.0 and 419.6 s for fish swimming within 300 m of Dam 2. Under the assumptions stated above, FMM predicts Chinook residence times comparable to values reported in Timko et al. (2007).

A top view of four different simulated fish (A, B, C, D) approaching Dam 2 is presented in Figure 6.10a. Variation in swimming elevation for the four trajectories is displayed in Figure 6.10b. The movement of fish in Figures 6.10a and 6.10b is from top to bottom and from left to right, respectively. Table 6.5 shows total travel time, percent of gliding, and the value of P_m for trajectories A, B, C, and D.

After simulating 8,350 s, the fish A could not find an outlet to pass downstream. After approximately 5,000 s of simulation, this fish swam within 10 m of the dam. The value of the coefficient P_m for fish A prevented it from swimming in deeper regions where the spillway flow could have entrained it.

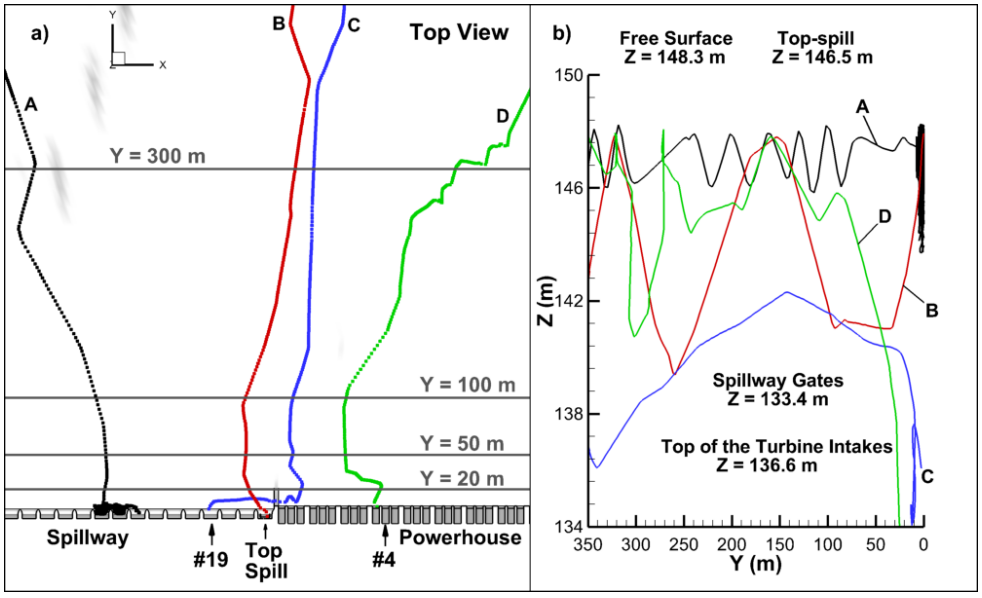

Figure 6.10 Dam 2. Simulated fish trajectories.

Table 6.5 Trajectories in Figure 6.10.

Trajectory	Time (s)	Gliding (%)	P_m (m)
A	8350.0	18.7	2.0
B	5330.0	38.0	15.2
C	5185.0	27.6	13.9
D	6605.0	31.8	30.0

After milling about for approximately one hour, fish A swam close to the spillway #15. Note that FMM does not explicitly contemplate fish milling behavior. The swimming patterns of fish A, in the region within 8 m from the dam, were the result of both wall avoidance and the fish orienting itself with respect to the flow velocity.

As mentioned above, about 2.5% of the simulated fish were in the domain after approximately 8,500 s of simulation. FMM predictions on percent of fish passing through the top-spill could improve, assuming that some of these fish can find the top-spill.

Despite simulated fish B and C's tendency to swim in the first 15 m of the water column, the former left the domain through the top-spill and the latter through spillway bay #19. For these fish, the trajectories in Figure 6.10b show steep changes in swimming elevation at a distance of about 20 m from the dam, which is consistent with the streamlines presented in Figures 3.10c and 3.10d.

At 40 m upstream of the dam, fish D was directed towards the powerhouse unit #3 but after making a turn, ended up passing downstream through unit #4. This fish started a downwards trajectory with a -3/16 slope approximately 80 m upstream of the dam. Table 6.5 shows that Fish D had a value of P_m equal to 30 m and thus could occupy virtually any depth in Dam 2 forebay.

CHAPTER VII

CONCLUSIONS AND FUTURE WORK

7.1 Conclusions

This work developed a mechanistic model to simulate swim paths of downstream migrating juvenile salmon based on the fish swimming thrust. The fish movement model (FMM) integrates information on juvenile salmon behavior at both field and laboratory scale and literature on juvenile salmon swimming capabilities. FMM was implemented in the particle tracking algorithm of ANSYS FLUENT 12.0 and tested at the forebay of two hydropower dams. Good agreement was found between model results and measured data.

This thesis developed a comprehensive analysis of juvenile Chinook salmon swim paths measured in the forebay of a hydropower dam. The flow variables at the fish location were obtained from CFD simulations. Fish swimming thrust was found from solving Newton's Second Law. Results showed that fish thrust is correlated with flow acceleration. The methodology presented to analyze fish measured swim paths is an important contribution of this thesis.

Since Chinook responses to hydrodynamics greatly vary among different individuals, probability distributions of fish swimming variables were generated for different values of flow acceleration. The results of this thesis show that as flow acceleration increases the magnitude of the fish average thrust increases and the probability of fish coasting with the flow decreases. The analyzed data also show that as flow acceleration increases, juvenile Chinook salmon tend to migrate tail first. For a flow acceleration of $5x10^{-4}$ m/s^2, approximately 85% of the analyzed fish travelled tail first, whereas for an acceleration of $1x10^{-2}$ m/s^2 approximately 95% showed this behavior. For most (~99%) of the analyzed fish, the magnitude of the thrust did not exceed fish

sustained mode swimming capacities and thus Chinook salmon migrating tail first should not necessarily be assumed as an indication of fish desire to move upstream.

For the analyzed fish, probability distributions of the vertical swimming direction have a close to Gaussian shape. Chinook salmon did not show a clear preference between swimming upwards or downwards for flow accelerations below $1x10^{-3}$ m/s^2. For flow accelerations above $5x10^{-3}$ m/s^2, Chinook showed a tendency to swim upwards. The presented analysis of measured juvenile salmon swimming patterns had not been developed before.

The laboratory experiment presented in Enders et al. (2009) reported the flow velocity and velocity gradient at the onset of Chinook avoidance behavior. This thesis built a CFD model to reproduce the flow conditions described in Enders et al. (2009) to determine the flow acceleration that triggered avoidance behavior in Chinook salmon smolts. Values of acceleration were determined for 68 Chinook salmon. The average and standard deviation were 0.70 and 0.73 m/s^2, respectively.

The flow field information at Dam 1 for the year 2010 and measured fish swim paths were used to determine the probability distributions of fish swimming variables. FMM performance was tested with two additional flow conditions at Dam 1 and one flow condition at Dam 2.

7.1.1 Dam 1

A parametric study tested the effect of modifying the pressure threshold P_m, α in the region of low flow acceleration (< $1.0x10^{-4}$ m/s^2), and the fish initial spatial distribution. Best results were obtained for the following conditions. 1) P_m follows the distribution in Figure 4.26 for Dam 2. 2) In the region of low flow acceleration, α is uniformly distributed in the [-50°, 50°] interval. 3) At the beginning of the simulation fish are normally distributed across the width of the forebay.

The capacity of FMM to predict fish migration route selection was compared against measured data. Three different dam operating conditions were simulated. Flows through units 1-2, units 3-11, and the surface collector were approximately 21%, 65%, and 5% of the total river flow. Measured percent of fish passing through each of these three outlets was about 30%. Since the percent of fish passing through the three possible outlets does not follow the river flow distribution, behavioral rules are needed to predict percent of fish passages.

Overall, simulated fish outperformed passive particles. The average relative error was higher for the cases with the spillway operating. On average, cases with spillway gave a relative error of 20%, whereas the average error for the case without spillway was 7%. The biggest discrepancy was found in the prediction of fish passing through the spillway in 2004 (relative error: -54.4%). FMM predictions for the surface collector were in good agreement with measured data and had relative errors in the order of 4%. Model results for the surface collector for the case without spillway have the smallest relative error (-3.1 %).

FMM predicted well the residence times in the powerhouse region of Dam 1. In an area that spans 200 m, simulated fish and tagged Chinook had an average residence time of 559 and 563 s, respectively. The migration rates predicted by FMM for simulated fish fall within the interval reported in Tiffan et al. (2009). The ratio between the fish velocity and the flow velocity was approximately 1.1 and 0.6 for the region upstream of the spillway and the powerhouse zone, respectively.

7.1.2 Dam 2

For the simulated condition at Dam 2 forebay, the reported fish passages showed a similar trend to the total river flow distribution. The percent of river flow through the top-spill, spillway, and powerhouse were 0.6%, 62.8%, and 36.6%, respectively. The fish passages were 4%, 82%, and 14%, respectively. FMM performed better than the passive

particles at predicting fish passages. FMM predictions for the top-spill, spillway, and powerhouse gave relative errors of -58.9, 4.0, and -6.5%, respectively.

CFD results showed that the powerhouse region of Dam 1 and the zone within 250 m of Dam 2 have values of flow acceleration above $1x10^{-4}$ m/s^2. Therefore, in both zones, simulated fish swimming patterns followed the probability distributions developed in Chapter IV. For the region within 300 from Dam 2, residence times predicted by FMM were comparable with measured values. This could be an indication that Chinook approaching Dam 2 behave similarly to Chinook in the powerhouse region of Dam 1 and therefore the use of parameters obtained with Dam 1 data is valid.

In the region upstream of Dam 2 (> 300 m) FMM overpredicted fish velocities. The ratio between simulated fish velocity and flow velocity was approximately 1.6. This value is slightly above the upper limit defined by Tiffan et al. (2009) for fast migrants.

7.2 Future Work

To study juvenile salmon responses to hydrodynamics, this thesis analyzed Chinook trajectories measured in the powerhouse region of Dam 1 in the year 2010. No Chinook measured trajectory was available in the low flow acceleration region upstream of the dam. Behavior of fish represented by these trajectories could be affected by specific conditions at Dam 1. Several dams have carried out fish survival and fish migration studies using hydroacoustic telemetry. These data can be used to replicate the analysis presented in this thesis. Information on juvenile salmon behavior in zones of low flow acceleration is of particular interest. Having probability distributions obtained with a larger set of data can extend the validity of the model. A larger set of data could also assist in the development of species-specific probability distributions.

FMM simulates fish behavior assuming that fish react mainly to flow acceleration and pressure. Provided that information is available, other important variables that

influence fish migratory behavior can be included in the formulation of the model, such as temperature gradients, time of the day, food availability, and predator abundance.

The model presented in this thesis assigns two of the model parameters to every simulated individual, a_b and P_m. The other model parameters are randomly selected throughout the simulations from probability distributions obtained with the entire population of analyzed Chinook. With this approach, a simulated fish does not have a distinct set of swimming characteristics. A simulated fish could behave as a fast migrant for some period of time and then behave as a slow migrant. A different way to simulate fish movements could be to assign a set of swimming patterns, which remain constant throughout the simulation, to every simulated individual. The swimming patterns can be obtained from analyzing measured trajectories of fish that behave similarly.

Juvenile salmon have been observed meandering near the free surface in the vicinity of some hydraulic structures. In its current state, FMM assumes that a fish selects mostly a swimming direction with reference to the flow velocity and this meandering behavior is not explicitly included in the model. This behavior affects residence times and migration route selection. Juvenile salmon measured trajectories can be used to study the conditions that trigger this behavior and develop a mathematical representation of it that can be included in FMM.

Khan et al. (2011) and Johnson et al. (2009) observed juvenile salmon schooling behavior when fish were swimming close to hydropower dams. These studies report that individual fish exhibit different swimming patterns than fish swimming in schools. Schools of fish were more likely to swim against the flow and schooling behavior was more prevalent during day than night. In its current state, FMM does not account for juvenile salmon schooling behavior. The methodology presented in this thesis can also be applied to study behavior of fish swimming in schools by analyzing the school of fish as an individual.

The flow conditions used in this thesis come from averaging powerhouse and spillway operating conditions over several consecutive days. Juvenile salmon responses to hydrodynamics could be triggered by instantaneous changes in spillway and powerhouse discharges. Provided that the rigid-lid assumption is still valid, CFD simulations can be easily run to simulate the dam operating conditions approximately every hour. This could lead to a more accurate representation of juvenile salmon responses to hydrodynamics.

Studies have shown that intensity of fear to stimuli in animals is not constant (Kamin et al. 1963; Starr and Mineka 1977). Post and von der Emde (1999) studied fish electromotor behavior triggered by novel sensory stimuli in the electrogenic teleost. Habituation of fish to acoustic, visual and electrical stimuli was represented by curves of fish response vs. number of stimuli. Millot et al. (2009) investigated changes over time in risk-taking behavior in sea bass by offering them the choice between a safe zone and a risky zone. During the first test 23% of the fish entered in the risky zone. For the second experiment the percent of fish that visited the risky zone increased to approximately 90%.

The literature mentioned above can be used to develop a model of juvenile salmon habituation to high flow accelerations which will allow fish simulated with FMM to modify their value of a_b over time.

Forces considered in this thesis to analyze fish measured swim paths were thrust and drag. Additional forces could be included when solving Newton's Second Law. An accelerating or decelerating fish must move some volume of surrounding fluid. This increases the inertia of the system and thus has an effect in the fish swimming thrust. The phenomenon described above is known as virtual or added mass. Rough estimations indicate that considering the virtual mass force could change results for fish thrust by a factor of up to 1.2.

REFERENCES

Altringham, J. D., and Ian A. Johnston. 1990. Modelling muscle power output in a swimming fish. *Journal of Experimental Biology*.

Beecher, Hal A., Brad A. Caldwell, and S. B. DeMond. 2002. Evaluation of depth and velocity preferences of juvenile coho salmon in washington streams. *North American Journal of Fisheries Management* 22 (3) (08/01; 2011/11): 785-95.

Beeman, J. W., and Alec G. Maule. 2006. Migration depths of juvenile chinook salmon and steelhead relative to total dissolved gas supersaturation in a columbia river reservoir. *Transactions of the American Fisheries Society* 135 (3): 584.

Blake, Robert W. *Fish locomotion*. 1983: Cambridge Univ. Press, Cambridge.

Brett, J. R. 1967. Swimming performance of sockeye salmon (oncorhynchus nerka) in relation to fatigue time and temperature. J. Fish. Res. Bd Can.

Brett, J. R. 1965. The swimming energetics of salmon. Sci. Am. 213:80-85.

Coombs, Sheryl, and Sietse Van Netten. 2005. The hydrodynamics and structural mechanics of the lateral line system. In *Fish physiology.* Vol. Volume 23, 103-139. Academic Press.

Coutant, Charles C., Oak Ridge National Laboratory. Environmental Sciences Division., United States. Dept. of Energy., and Lockheed Martin Energy Research Corp. 1998. *Turbulent attraction flows for juvenile salmonid passage at dams*. Oak Ridge, Tenn.: Environmental Sciences Division, Oak Ridge National Laboratory.

Crittenden, Robert N. 1994. A diffusion model for the downstream migration of sockeye salmon smolts. *Ecological Modelling* 71 (1-3) (/1): 69-84.

Dauble, D., S. Anglea, and G. Johnston. 1999. *Surface flow bypass development in the columbia and snake rivers and implications to lower granite dam.* Walla Walla District, Richland, Washington: Corps of Engineers.

Davidsen, Jan, Martin-A Svenning, Panu Orell, Nigel Yoccoz, J. Brian Dempson, Eero Niemelä, Anders Klemetsen, Anders Lamberg, and Jaakko Erkinaro. 2005. Spatial and temporal migration of wild atlantic salmon smolts determined from a video camera array in the sub-arctic river tana. *Fisheries Research* 74 (1-3) (8): 210-22.

Denton, E. J., and John Gray. 1989. Some observation of the forces acting on neuromasts in fish lateral line canal. *Neurobiology and Evolution*: pp. 229-246.

Denton, E. J., and John Gray. 1988. Mechanical factors in the excitation of the lateral lines of fishes. *Sensory Biology of Aquatic Animals*: pp. 596-617.

Denton, E. J., and John Gray. 1983. Mechanical factors in the excitation of clupeid lateral lines. *Proceedings of the Royal Society of London.Series B, Biological Sciences* 218 (1210) (Apr. 22): pp. 1-26.

Domenici, P., and R. Blake. 1997. The kinematics and performance of fish fast-start swimming. *Journal of Experimental Biology* 200 (8) (April 01): 1165-78.

EIA. 2010. International energy outlook 2010.

Enders, Eva C., Daniel Boisclair, and Andre G. Roy. 2003. The effect of turbulence on the cost of swimming for juvenile atlantic salmon (salmo salar). *Canadian Journal of Fisheries and Aquatic Sciences* 60 (9) (09/01; 2011/11): 1149-60.

Enders, Eva C., Michael H. Gessel, and John G. Williams. 2009. Development of successful fish passage structures for downstream migrants requires knowledge of their behavioural response to accelerating flow. *Canadian Journal of Fisheries and Aquatic Sciences* 66 (12) (12/01; 2011/06): 2109-17.

Evans, Scott D., Noah S. Adams, Dennis W. Rondorf, John M. Plumb, and Blaine D. Ebberts. 2008. Performance of a prototype surface collector for juvenile salmonids at bonneville dam's first powerhouse on the columbia river, oregon. *River Research and Applications* 24 (7): 960-74.

Faber, D. M., M. A. Weiland, R. Moursund, T. J. Carlson, N. Adams, and D. Rhondorf. 2001. Evaluation of the fish passage effectiveness of the bonneville I prototype surface collector using three-dimensional ultrasonic fish tracking. Richland, WA.: Pacific Northwest National Laboratory.

Flagg, Thomas A., Earl F. Prentice, and Lynwood S. Smith. 1983. Swimming stamina and survival following direct seawater entry during parr-smolt transformation of coho salmon (oncorhynchus kisutch). *Aquaculture* 32 (3-4) (5): 383-96.

Foreman, MB, and RC Eaton. 1993. The direction change concept for reticulospinal control of goldfish escape. *The Journal of Neuroscience* 13 (10) (October 01): 4101-13.

Goodwin, R. A. 2004. Hydrodynamics and juvenile salmon movement behavior at lower granite dam: Decoding the relationship using 3-D space-time (CEL agent IBM) simulation. Dissertation, Cornell University.

Goodwin, R. Andrew, John M. Nestler, James J. Anderson, Larry J. Weber, and Daniel P. Loucks. 2006. Forecasting 3-D fish movement behavior using a Eulerian–Lagrangian–agent method (ELAM). Ecological Modelling 192 (1-2) (2/15): 197-223.

Haefner, James W., and Mark D. Bowen. 2002. Physical-based model of fish movement in fish extraction facilities. *Ecological Modelling* 152 (2-3) (7/1): 227-45.

Haider, A., and O. Levenspiel. 1989. Drag coefficient and terminal velocity of spherical and nonspherical particles. *Powder Technology* 58 (1): 63.

Haro, Alex, Mufeed Odeh, John Noreika, and Theodore Castro-Santos. 1998. Effect of water acceleration on downstream migratory behavior and passage of atlantic salmon smolts and juvenile american shad at surface bypasses. *Transactions of the American Fisheries Society* 127 (1) (01/01; 2011/06): 118-27.

Johnson, G. E., F. Khan, M. C. Richmond, R. P. Mueller, J. B. Hedgepeth, C. L. Rakowski, G.R. Ploskey, N.K. Sather, M.G. Anderson, J. A. Serkowski, Z. Deng, and J. R. Steinbeck. 2009. *Smolt Responses to Hydrodynamic Conditions in Forebay Flow Nets of Surface Flow Outlets, 2007.* PNNL. Prepared for U.S. Army Corps of Engineers.

Johnson, G. E., F. Khan, J. B. Hedgepeth, R. P. Mueller, C. L. Rakowski, M. C. Richmond, J. A. Serkowski, and J. R. Skalski. 2006. *Hydroacoustic evaluation of juvenile salmonid at the dalles dam sluiceway, 2005.* PNNL: Prepared for U.S. Army Corps of Engineers.

Johnson, Gary E., Noah S. Adams, Robert L. Johnson, Dennis W. Rondorf, Dennis D. Dauble, and Theresa Y. Barila. 2000. Evaluation of the prototype surface bypass for salmonid smolts in spring 1996 and 1997 at lower granite dam on the snake river, washington. *Transactions of the American Fisheries Society* 129 (2) (03/01; 2011/11): 381-97.

Kemp, Paul S., Michael H. Gessel, and John G. Williams. 2005. Fine-Scale Behavioral Responses of Pacific Salmonid Smolts as They Encounter Divergence and Acceleration Flow. *Transactions of the American Fisheries Society.* 134:390-398.

Kemp, Paul S., Michael H. Gessel, Benjamin P. Sandford, and John G. Williams. 2006. The behaviour of pacific salmonid smolts during passage over two experimental weirs under light and dark conditions. *River Research and Applications* 22 (4): 429-40.

Kemp, Paul S., and John G. Williams. 2008. Response of migrating chinook salmon (ONCORHYNCHUS TSHAWYTSCHA) smolts to in-stream structure associated with culverts. *River Research and Applications* 24 (5): 571-9.

Khan, F., G. E. Johnson, I. M. Royer, N. R. Phillips, J. S. Hughes, E. S. Fischer, and G. R. Ploskey. 2011. *Acoustic imaging evaluation of juvenile salmonid behavior in the immediate forebay of the water temperature control tower at cougar dam* Portland, Oregon: U.S. Army Corps of Engineers.

Lighthill, M. J. 1971. Large-amplitude elongated-body theory of fish locomotion. *Proceedings of the Royal Society of London. Series B, Biological Sciences* 179 (1055) (Nov. 16): pp. 125-138.

Matuda, K., and N. Sannomiya. 1985. Computer simulation of fish behavior in relation to a trap model. *Bulletin of the Japanese Society of Scientific Fisheries* 51 : 33-9.

Matuda, K., and N. Sannomiya. 1980. Computer simulation of fish behavior in relation to fishing gear. I. mathematical model of fish behavior. *Bull.Japan.Soc.Sci.Fish.* 46 : 689-697.

McHenry, Matthew, James Strother, and Sietse van Netten. 2008. Mechanical filtering by the boundary layer and fluid–structure interaction in the superficial neuromast of the fish lateral line system. *Journal of Comparative Physiology A: Neuroethology, Sensory, Neural, and Behavioral Physiology* 194 (9): 795-810.

Meager, Justin J., Paolo Domenici, Alex Shingles, and Anne Christine Utne-Palm. 2006. Escape responses in juvenile atlantic cod gadus morhua L.: The effects of turbidity and predator speed. *Journal of Experimental Biology* 209 (20) (October 15): 4174-84.

Montgomery, John C., Cindy F. Baker, and Alexander G. Carton. 1997. The lateral line can mediate rheotaxis in fish. *Nature* 389 (6654) (10/30): 960-3.

Montgomery, John, Guy Carton, Rainer Voigt, Cindy Baker, and Carol Diebel. 2000. Sensory processing of water currents by fishes. *Philosophical Transactions: Biological Sciences* 355 (1401, Sensory Processing of the Aquatic Environment) (Sep. 29): pp. 1325-1327.

Montgomery, John, Sheryl Coombs, and Matthew Halstead. 1995. Biology of the mechanosensory lateral line in fishes. *Reviews in Fish Biology and Fisheries* 5 (4): 399-416.

Muir, W. D., S. G. Smith, J. G. Williams, and B. P. Sandford. 2001. Survival of juvenile salmonids passing through bypass systems, turbines, and spillways with and without flow deflectors at snake river dams. *North American Journal of Fisheries Management* 21 : 135-146.

Ni, X., H. Jian, and A. Fitch. 2003. Evaluation of turbulent integral length scale in an oscillatory baffled column using large eddy simulation and digital particle image velocimetry. *Chemical Engineering Research and Design* 81 (8): 842.

Office of Technology Assessment (OTA). 1995. *Fish passage technologies: Protection at hydroelectric facilities.* Washington DC.: OTA-ENV, 641.

Peake, S., and R. S. McKinley. 1998. A re-evaluation of swimming performance in juvenile salmonids relative to downstream migration. *Canadian Journal of Fisheries and Aquatic Sciences* 55 (3) (03/01; 2011/06): 682-7.

Sannomiya, N., and K. Matuda. 1987. Least squares parameter estimation in fish behavior model. *Nippon Suisan. Gakkaishi.* 53 (11): 1951-1957.

Scheibe, Timothy D., and Marshall C. Richmond. 2002. Fish individual-based numerical simulator (FINS): A particle-based model of juvenile salmonid movement and dissolved gas exposure history in the columbia river basin. *Ecological Modelling* 147 (3) (1/30): 233-52.

Scruton, D., C. Pennell, C. Bourgeois, R. Goosney, T. Porter, and K. Clarke. 2007. Assessment of a retrofitted downstream fish bypass system for wild atlantic salmon (*salmo salar*) smolts and kelts at a hydroelectric facility on the exploits river, newfoundland, canada. *Hydrobiologia* 582 (1): 155-69.

Scruton, D. A., L. M. N. Ollerhead, K. D. Clarke, C. Pennell, K. Alfredsen, A. Harby, and D. Kelley. 2003. The behavioural response of juvenile atlantic salmon (salmo salar) and brook trout (salvelinus fontinalis) to experimental hydropeaking on a newfoundland (canada) river. *River Research and Applications* 19 (5-6): 577-87.

Sichert, A. B., R. Bamler, and J. L. Van Hemmen. 2009. Hydrodynamic object recognition: When multipoles count. *Physical Review Letters* 102 (5).

Smith, Lynwood S. 1982. Decreased swimming performance as a necessary component of the smolt migration in salmon in the columbia river. *Aquaculture* 28 (1-2) (6): 153-61.

Steig, T. W., and S. V. Johnston. 2010. Behavioral results from acoustically tagged fish using innovative techniques for analyzing three-dimensional data. Paper presented at OCEANS 2010.

Svendsen, J. C., A. O. Eskesen, K. Aarestrup, A. Koed, and A. D. Jordan. 2007. Evidence for non-random spatial positioning of migrating smolts (salmonidae) in a small lowland stream. *Freshwater Biology* 52 (6): 1147-58.

Tang, J., and C. S. Wardle. 1992. Power output of two sizes of atlantic salmon (salmo salar) at their maximum sustained swimming speeds. *Journal of Experimental Biology* 166 (1): 33.

Thorpe, J. E., and R. I. G. Morgan. 1978. Periodicity in atlantic salmon salmo salar L. smolt migration. *Journal of Fish Biology* 12 (6): 541-8.

Tiffan, Kenneth F., Tobias J. Kock, Craig A. Haskell, William P. Connor, and R. K. Steinhorst. 2009. Water velocity, turbulence, and migration rate of subyearling fall chinook salmon in the free-flowing and impounded snake river. *Transactions of the American Fisheries Society* 138 (2) (03/01; 2011/11): 373-84.

Timko, M. A., L. S. Brown, C. D. Wright, R. R. O'Connor, C. A. Fitzgerald, M. L. Meager, S. E. Rizor, P. A. Nealson, and S. V. Johnston. 2007. *Analysis of juvenile chinook, steelhead, and sockeye salmon behavior using acoustic tags at wanapum and priest rapids dams,2006.* Seattle, WA: Hydroacoustic Technology.

van Netten, Sietse. 2006. Hydrodynamic detection by cupulae in a lateral line canal: Functional relations between physics and physiology. *Biological Cybernetics* 94 (1): 67-85.

Videler, J. J., and D. Weihs. 1982. Energetic advantages of burst-and-coast swimming of fish at high speeds. *Journal of Experimental Biology*(97): 169-78.

Virtanen, Erkki, and Leena Forsman. 1987. Physiological responses to continuous swimming in wild salmon (*salmo salar* L.) parr and smolt. *Fish Physiology and Biochemistry* 4 (3): 157-63.

Webb, P. W. 1978. Fast-start performance and body form in seven species of teleost fish. *The Journal of Experimental Biology* 74 (1) (June 01): 211-26.

Webb, P. W. 1977. Effects of median-fin amputation on fast-start performance of rainbow trout (salmo gairdneri). *The Journal of Experimental Biology* 68 (1) (June 01): 123-35.

Webb, P. W. 1976. The effect of size on the fast-start performance of rainbow trout salmo cairdneri, and a consideration of piscivorous predator-prey interactions. *Journal of Experimental Biology* 65 (1) (August 01): 157-77.

Webb, P. W. 1975. Acceleration performance of rainbow trout salmo gairdneri and green sunfish lepomis cyanellus. *The Journal of Experimental Biology* 63 (2) (October 01): 451-65.

Webb, P. W. 1971. The swimming energetics of trout. *Journal of Experimental Biology* 55 (2): 489.

Webb, P. W., and J. R. Brett. 1973. Effects of sublethal concentrations of sodium pentachlorophenate on growth rate, food conversion efficiency, and swimming performance in underyearling sockeye salmon (oncorhynchus nerka). *Journal of the Fisheries Research Board of Canada* 30 (4) (04/01; 2011/11): 499-507.

Webb, P. W., P. T. Kostecki, and E. Don Stevens. 1984. The effect of size and swimming speed on locomotor kinematics of rainbow trout. *Journal of Experimental Biology* 109 (1): 77.

Weihs, D. 1974. Energetic advantages of burst swimming of fish. *Journal of Theoretical Biology*(48): 215-29.

Weihs, D. 1973. The mechanism of rapid starting of slender fish. *Biorheology* 10 (3) (09): 343-50.

Williams, J. G., and Michael H. Gessel. 1993. Fish diversion and screening devices: Is there a relationship to fish behavior? In Proceedings of the Symposium on Fish Passage Policy and Technology, 135-140.

Williams, John. 2008. Mitigating the effects of high-head dams on the columbia river, USA: Experience from the trenches. *Hydrobiologia* 609 (1): 241-51.

Wu, Guanhao, Yan Yang, and Lijiang Zeng. 2007. Kinematics, hydrodynamics and energetic advantages of burst-and-coast swimming of koi carps (cyprinus carpio koi). *Journal of Experimental Biology* 210 (12) (June 15): 2181-91.

Yates, G. T. 1983. Hydromechanics of body and caudal fin propulsion. *Fish Biomechanics*: pp. 177-213.

Yuksel, I. 2010. As a renewable energy hydropower for sustainable development in turkey. *Renewable and Sustainable Energy Reviews* 14 (9) (12): 3213-9.

Zabel, R. W., and J. J. Anderson. 1997. A model of the travel time of migrating juvenile salmon, with an application to snake river spring chinook. *North American Journal of Fisheries Management*(17): 93-100.

Zabel, R. W. 1994. Spatial and Temporal Models of Migrating Juvenile Salmon with Applications. Dissertation, University of Washington.